



## 저작자표시-비영리-변경금지 2.0 대한민국

이용자는 아래의 조건을 따르는 경우에 한하여 자유롭게

- 이 저작물을 복제, 배포, 전송, 전시, 공연 및 방송할 수 있습니다.

다음과 같은 조건을 따라야 합니다:



저작자표시. 귀하는 원저작자를 표시하여야 합니다.



비영리. 귀하는 이 저작물을 영리 목적으로 이용할 수 없습니다.



변경금지. 귀하는 이 저작물을 개작, 변형 또는 가공할 수 없습니다.

- 귀하는, 이 저작물의 재이용이나 배포의 경우, 이 저작물에 적용된 이용허락조건을 명확하게 나타내어야 합니다.
- 저작권자로부터 별도의 허가를 받으면 이러한 조건들은 적용되지 않습니다.

저작권법에 따른 이용자의 권리는 위의 내용에 의하여 영향을 받지 않습니다.

이것은 [이용허락규약\(Legal Code\)](#)을 이해하기 쉽게 요약한 것입니다.

[Disclaimer](#)

Doctoral Thesis

# Integrative multi-omics analysis for the effect of genetic alterations in cancer xenograft and organoid models

Hyeongsun Jeong

Department of Biomedical Engineering

Ulsan National Institute of Science and Technology

2023

# Integrative multi-omics analysis for the effect of genetic alterations in cancer xenograft and organoid models

Hyeongsun Jeong

Department of Biomedical Engineering

Ulsan National Institute of Science and Technology

# Integrative multi-omics analysis for the effect of genetic alterations in cancer xenograft and organoid models

A dissertation submitted to  
Ulsan National Institute of Science and Technology  
in partial fulfillment of the  
requirements for the degree of  
Doctor of Philosophy

Hyeongsun Jeong

12.13.2022 of submission

Approved by

  
\_\_\_\_\_  
Advisor

Taejoon Kwon

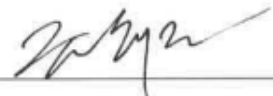
# Integrative multi-omics analysis for the effect of genetic alterations in cancer xenograft and organoid models

Hyeongsun Jeong

This certifies that the dissertation of Hyeongsun Jeong is approved.

12.15.2022 of submission

Signature



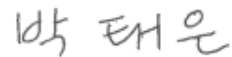
Advisor: Taejoon Kwon

Signature



Kyungjae Myung

Signature



Tae-Eun Park

Signature



Tae Joo Park

Signature



Byung Gyu Kim

## Abstract

DNA damage is a well-recognized factor in the development and progression of cancer. Numerous studies on genetic changes associated with cancer or the DNA repair pathway have been conducted, however, there is still a need for additional research on their function. The establishment of patient-derived xenografts or organoids for the purpose of testing functional genomic approaches is the subject of ongoing research. According to model-specific characteristics, it is not fully understood how these attempts to simulate patient cancer differ from original cancer. To comprehend the distinction between genuine patient cancer and these patient-derived disease models in more depth, multi-omics analysis is required to comprehend the overall genotypes, phenotypes, and environmental variables. Depending on the characteristics of each disease model, distinct omics analysis approaches and factors must be considered. In addition, care must be taken to avoid technical errors when integrating omics data generated by different sequencing equipment. There is currently no golden rule for data integration, but several approaches are being developed.

It is crucial to determine the function of genes linked with the DNA repair pathway because these genes contribute to the induction or prevention of cancer. In chapter 1, I identified the interaction between MRE11 and TRIP13 through proximity labeling combined with the SILAC method which is quantitative proteomics using metabolic labeling. TRIP13 depletion doesn't affect the nuclease activity and conformation of the MRN complex but directly inhibits the interaction of MDC1 with MRN complex and MDC1 recruitment on the DNA damage site. TRIP13 degradation with mirin treatment shows additive effects on ATM signaling activation. In conclusion, TRIP13 regulates immediate-early DNA damage sensing through MRE11 and ATM signaling independently of mirin.

When assessing the functional genomic approach using patient-derived disease models, it is essential to determine which aspects of the models' correlation to actual cancer should be properly considered. In chapter 2, I found there are a few overlapped deleterious somatic mutations of the PDX model and their original tumor. I suspected novel mutagen exposure during PDX establishment or sample contamination. However, germline mutations of PDX models are well conserved from original tumors, and their mutational signatures of PDX also mimic that of their tumor. Though the number of overlapped mutations between the PDX model and their tumor was few, brain tumor-specific mutations are found in PDX samples. Especially, histone methylation- and cilia-related gene mutations are enriched in PDX samples. While it suggested these mutated genes are needed for maintaining the stemness of brain tumor PDX model or PDX model would be more appropriate for the samples with high heterogeneity, I have presented precautions and considerations in PDX model genome analysis.

Multi-omics analysis that takes into consideration genetic, expressive, and clinical aspects can

provide important information for the study of diseases with complicated etiologies, such as cancer, and can contribute to the development of diagnosis and treatment. To utilize colorectal cancer organoids for Companion Diagnostics (CDx), in chapter 3, I characterized patient-derived colorectal cancer (CRC) organoids through well-known genomic markers such as Tumor mutation burden (TMB), Microsatellite instability (MSI) and propose a novel grouping method using sharing same mutation site. The classification of CRC patients was more detailed combined with consensus molecular subtype (CMS) classifications. Additionally, I extract the expression features of the patients who experience recurrence or metastasis after first-line chemotherapy treatment with reference to clinical data. Drug response of CRC organoids by patient group and knockdown of the extracted features in the selected organoids would be validated in further study.

In summary, with this dissertation, I conducted functional research on the DNA repair pathway of cancer-related genes, as well as the genetic analysis between patient-derived xenograft and original tumors, and introduced a novel perspective on the diagnosis and treatment of colorectal cancer patients using patient-derived organoids through multi-omics analysis.

## Contents

Abstract.....	5
Contents .....	7
Lists of Figures.....	10
Lists of Tables .....	11
Technical Terms and Abbreviation .....	12
Introduction.....	14
1. TRIP13 participates in immediate-early sensing of DNA strand breaks and ATM signaling amplification through MRE11 .....	16
1.1. Introduction .....	16
1.2. Materials & Methods .....	18
1.2.1. Cell culture.....	18
1.2.2. Sister Chromatid Exchange.....	18
1.2.3. Plasmids.....	18
1.2.4. siRNA knockdown .....	19
1.2.5. Antibodies .....	19
1.2.6. Regulation of MRE11 exonuclease activity and TRIP13 expression .....	20
1.2.7. DSB induction.....	20
1.2.8. Immunofluorescence imaging.....	20
1.2.9. Proteomics experiments with SILAC .....	21
1.2.10. Western blot analysis .....	21
1.2.11. <i>In vitro</i> pulldown assay.....	21
1.2.12. Colony formation assay .....	21
1.2.13. DNA end resection assay .....	22
1.2.14. MRN endonuclease activity assay.....	24
1.3. Results.....	25
1.3.1. TRIP13 participates in the DNA damage response .....	25
1.3.2. MRE11 is a novel TRIP13 interaction partner, however this connection is independent of the MRN complex's conformation and nuclease activity. ....	27
1.3.3. TRIP13 depletion inhibits the physical interaction of MDC1 with MRE11 and reduces the recruitment of MDC1 to DNA damage sites.....	30



1.3.4. TRIP13 promotes DNA resection and homologous recombination via modulating ATM-mediated downstream signaling. ....	32
1.4. Discussion .....	34
2. Enrichment of deleterious mutated genes involved in ciliary function and histone modification in brain cancer patient-derived xenograft models .....	36
2.1. Introduction .....	36
2.2. Materials and methods .....	37
2.2.1. Tumor samples from patients with brain tumors.....	38
2.2.2. Establishment of brain tumor-PDX models. ....	38
2.2.3. Histopathological analysis. ....	39
2.2.4. Mutational analysis.....	39
2.2.5. Mutational signature analysis.....	39
2.2.6. Gene Ontology (GO) term enrichment analysis.....	39
2.3. Results.....	40
2.3.1. Deleterious somatic mutations are discordant between original tumors and xenograft tissues. ....	40
2.3.2. Both primary cancers and xenograft tissues share identical germline mutations. ....	44
2.3.3. Mutational signatures are highly preserved between tumors and xenografts, and they reveal the mutational origin.....	46
2.3.4. Mutations related with brain tumors are enriched in PDX samples. ....	48
2.3.5. Gene mutations associated with histone methylation and cilium are likely enriched in PDX samples. ....	51
2.4. Discussion .....	55
3. Characterization and integrative omics analysis of patient-derived colorectal cancer organoids .....	58
3.1. Introduction .....	58
3.2. Materials and methods .....	60
3.2.1. Organoid culture.....	60
3.2.2. Whole Genome Sequencing (WGS).....	62
3.2.3. Mutational signature analysis.....	62
3.2.4. RNA-seq .....	62
3.2.5. CMS classification .....	62
3.3. Results.....	63
3.3.1. Four of colorectal cancer organoids shows high tumor mutational burden .....	63

3.3.2. COSMIC SBS mutational signature analysis reveals POLE exonuclease domain mutation in CC-50.	68
3.3.3. CRC tumor organoids and CRC cell lines were subdivided by shared deleterious mutations.	69
3.3.4. Colorectal cancer organoid classification with gene expression.	71
3.3.5. Feature selection in the fold change of expression compared to normal reveals C1orf115, MKRN2.	74
3.4. Discussion	76
Conclusion	78
4. References	80

## Lists of Figures

Figure 1.1. TRIP13 is necessary for DSB maintenance.

Figure 1.2. MRE11 is a new TRIP13 interaction partner.

Figure 1.3. TRIP13 depletion affects MDC1 recruitment to DNA damage sites via reducing the MRN complex's physical contact with MDC1.

Figure 1.4. Independent of MRE11 exonuclease activity, TRIP13 promotes HR by modulating ATM downstream signaling and DNA end resection.

Figure 2.1. Histological analysis of brain tumor-PDX tissue sources and origins.

Figure 2.2. Genes containing deleterious mutations are present in both primary and PDX tumor model.

Supplementary Figure 2.1. Overlap deleterious mutations in both original tumor tissues and PDX.

Figure 2.3. Heatmap showing prevalent germline homozygous variations.

Figure 2.4. SBS mutational signature analysis.

Figure 2.5. Mutation profile of previously known genes linked to the development of brain tumors.

Figure 2.6. The 30 most often mutated genes found in tumors and PDX samples. We only examined harmful mutations with a significant effect on protein function modification.

Figure 2.7. Genes associated with histone methylation and cilia are abundant in PDX samples.

Supplementary Figure 3.1. The overlap proportion of germline mutations between normal organoids and tumor organoids.

Figure 3.1. Top-ranked genes with high mutational frequency among our CRC organoid samples.

Figure 3.2. Representative SBS mutational patterns in CRC tumor organoids.

Figure 3.3. A novel CRC organoids classification using shared deleterious mutations.

Figure 3.4. CMS classification and feature extraction using gene expression of CRC organoids.

Supplementary Figure 3.2. Heatmap shows the gene expression profiles of normal and CRC organoids.

## **Lists of Tables**

Table 2.1. COSMIC database annotated mutations in primary tumor and PDX model.

Table 2.2. TP53 and EGFR status in original tumor and PDX model.

Table 3.1. The elements list of organoid culture media.

Table 3.3. The number of somatic mutations represent high tumor mutation burden (TMB-H).

## Technical Terms and Abbreviation

Adenosine Triphosphate (ATP)

Auxin-Inducible Degron (AID)

Brain Tumor-Initiating Cell (BTIC)

Camptothecin (CPT)

Central Nervous System (CNS)

Colony Forming Assay (CFA)

Colorectal cancer (CRC)

ColoRectal Cancer (CRC)

Colorectal Normal Organoids (CNOs)

Colorectal Tumor Organoids (CTOs)

Companion Diagnostics (CDx)

Consensus Molecular Subtype (CMS)

Consensus molecular subtypes (CMS)

Double Base Substitution (DBS)

Double Strand Break (DSB)

Gene Ontology (GO)

Glioblastoma multiforme (GBM)

Green Fluorescence Protein (GFP)

Homologous Recombination (HR)

Homology-Directed Repair (HDR)

Hydroxyurea (HU)

Indole-3-Acetic Acid (IAA)

Insertion-Deletion (ID)

Ionizing Radiation (IR)

Mass Spectrometry (MS)

MicroSatellite Instability (MSI)

MRE11-RAD50-NBS1 (MRN)

Next Generation Sequencing (NGS)

Non-Homologous End-Joining (NHEJ)

Patient-Derived Colon Organoids (PDCOs)

Patient-Derived Xenograft (PDX)

Single-Strand Annealing (SSA)

Single Base Substitution (SBS)

Sister Chromatid Exchange (SCE)

Stable Isotope Labeling by Amino acids in Cell culture (SILAC)

Temozolomide (TMZ)

Tumor MicroEnvironment (TME)

Tumor Mutation Burden (TMB)

Variant Effect Predictor (VEP)

Whole exome Sequencing (WES)

Whole Genome Sequencing (WGS)

World Health Organization (WHO)

## Introduction

DNA damage causes mutations, which, when they accumulate, become malignant tumors. Genomics has been extensively applied to the study of cancer, but the function of the mutations is still unknown. Attempts are being made to conduct this type of research using patient-derived disease model such as xenografts or organoids. However, it is unknown how this environment affects cancer in actual patients. Using the multi-omics method in conjunction with other omics data in addition to genomics, it will be able to distinguish between real patient cancer and this model in deeper level. After the Human Genome Project (HGP) in 2003, large-scale consortiums emerged to provide a huge amount of data, build a database of accumulated information, and develop necessary analysis tools. Large-scale sequencing data was available in less time and at lower cost with the advent of next-generation sequencing in 2008, and omics analysis began to be applied to clinical practice. Advances in omics technologies such as genomics, epigenomics, transcriptomics, proteomics, and metabolomics have made patient-specific medicine possible at a molecular level. While a single '-omics' analysis technology has limited information to access the problem from one side, multi-omics analysis is a large number of '-body' information, so there is much more information to be gained. These integrated omics studies provide important information for the study of complicated causes such as cancer and can contribute more to the development of diagnosis or treatment. An important task given to us now is to apply multi-omics in clinical practice through medical and hospital systems. It is to predict and prevent patients' diseases based on vast and complex omics data, increase the treatment rate by early detection, or provide the most suitable treatment for patients for diseases found.

For multi-omics analysis, it is also important to select a disease model according to the characteristics of each disease model. In the study of diseases such as cancer, access to human samples is very limited, and samples with sufficient quantity and quality required for multi-omics analysis are not common. To overcome these limitations, an analysis of animal models is suggested as an alternative. The multi-omics data obtained through accurately controlled and repeated experiments in animal models can be compared and analyzed with data from limited human samples, providing broader and more accurate research results. Animal testing models differ in terms of human body, genetic, and biological characteristics, so the reliability of drug test responses is limited. Alternatively, patient-derived disease models such as xenograft and organoid have been used in cancer research. In the 2D cell line culture method, it is difficult to reproduce the inherent properties of the cell-derived location and the characteristics of the tissue unit. A patient-derived xenograft derived from cancer patients could be used, but it is not suitable for large-scale drug screening.

Recently, organoids have attracted attention as a new drug screening platform to supplement existing problems. Organoid technology shows a variety of potential applications, including patient organoid bio-banking, various disease modeling, regeneration therapy through fusion of genomic correction technologies, customized therapy and precision therapy linked to patient genomic information.

With interest in the function of gene in DNA damage repair pathways, I discovered the novel role of TRIP13 in DNA double strand breaks sensing and ATM signaling pathway through identifying MRE11 as a novel interacting partner of TRIP13 using quantitative proteomics in 2D cell culture. TRIP13 is an enzyme that uses ATP to cause structural changes in the substrate, so it is difficult to find new interaction partners with traditional immunoprecipitation or affinity precipitation because it does not maintain strong bonds with the substrate. I labeled the candidate substrates of TRIP13 using proximity labeling and discovered novel candidate substrates of TRIP13 using quantitative proteomics through metabolic labeling. Next, I analyzed the mutations in the xenograft model derived from brain cancer patients. I found that there are PDX model-specific mutations through whole exome sequencing analysis comparing brain tumor patient-derived xenograft models with their original tumor samples, even though there are few of the overlapped mutations. and giving caution in the analysis of the results. Based on the experience of this omics analysis, I performed the multi-omics analysis that comprehensively analyzes and integrate whole genome sequencing, RNAseq, and clinical information in patient-derived colorectal cancer organoids. I suggested a novel classifying method of colorectal cancer organoids and separating patient group by genomic, transcriptomic and clinical characteristics. Additionally, I extracted the expression features of the patients related to recurrence and metastasis to validated in further study.



# **1. TRIP13 participates in immediate-early sensing of DNA strand breaks and ATM signaling amplification through MRE11**

## **1.1. Introduction**

Initially, the HORMA domain was recognized as a highly conserved peptide sequence present in three yeast proteins that maintain genome stability through distinct processes: Hop1 (HORMAD1 in humans) is involved in meiotic recombination and chromosomal segregation, Rev7 (MAD2L2) is involved in recombination choice during DNA double-strand break (DSB) repair, and MAD2 is involved in the spindle assembly checkpoint<sup>1-3</sup>. Recent investigations have discovered this domain in proteins that serve as signal mediators, such as MAD2L1BP (also known as p31(comet)) for spindle assembly complex signaling and ATG13 and ATG101 for autophagy signaling<sup>2</sup>. To modulate signaling pathways, these proteins generate physical protein-protein interactions via their HORMA domain; consequently, it is crucial to comprehend their protein interaction partners.

Thyroid hormone receptor-interacting protein 13 (TRIP13, also known as Pch2 in yeast), a typical AAA+ ATPase, is a multiple-context binding partner of members of the HORMA domain protein family. TRIP13 is concentrated in the nucleolus and actively participates in the removal of HORMAD1 from yeast and mammalian chromosomes during meiotic G2/prophase<sup>4</sup>. Moreover, TRIP13, in conjunction with the MAD2-binding protein MAD2L1BP, promotes the deactivation of the spindle assembly checkpoint by dismantling the mitotic checkpoint complex<sup>5</sup>. This checkpoint system guarantees accurate chromosomal segregation by delaying anaphase until the correct bipolar attachment of chromatids to the mitotic spindle has occurred. Due to its crucial function in genomic stability, TRIP13 mutations are strongly linked to malignancies like Wilms tumor<sup>6</sup>, glioblastoma<sup>7</sup>, and head and neck cancer<sup>8</sup>.

TRIP13 plays a function in double-strand break (DSB) repair by selecting between the homology-directed repair (HDR) and nonhomologous end-joining (NHEJ) pathways<sup>3,9</sup>. MAD2L2 (Rev7) is a component of the Shieldin complex that shields double-strand breaks and promotes their end-joining. As a component of the Pol- complex, it is also involved in DNA translesion synthesis. Using a high-throughput yeast two-hybrid screen, researchers previously reported the interaction between TRIP13 and MAD2L2 (Rev7). In addition, according to two studies, this interaction modifies the conformation of MAD2L2 (Rev7), which influences the DNA repair route used<sup>3,9</sup>.

Despite the fact that TRIP13 interacts with proteins that include a HORMA domain, it has also been reported to interact with proteins that lack this domain<sup>10,11</sup>. According to a yeast two-hybrid assay, the TRIP13 homologue in *S. cerevisiae*, Pch2, interacts with Xrs2 (the ortholog of human NBS1)<sup>10</sup>. Interaction disruption between Pch2 and Xrs2 results in checkpoint and recombination problems comparable to those observed in Pch2-deficient cells<sup>10</sup>. Pch2 and Xrs2 are both conserved in mammals, although the interaction between their human orthologs TRIP13 and NBS1 has not been reported.

A proximity labeling-based quantitative proteomics technique was utilized to identify 279 proteins as TRIP13 interaction partners. Numerous of these proteins, such as MRE11 of the MRN complex, were associated with the DNA damage response. This prompted us to hypothesize that TRIP13 and other HORMA domain-containing proteins play a function in the DNA damage response. TRIP13 contributes to the detection of immediate-early DNA damage and modulates ATM signaling independently of the MRN complex.

## **1.2. Materials & Methods**

### **1.2.1. Cell culture**

The fluorescent microscope was used to acquire images (BX53; Olympus). At least 35 metaphase cells were selected at random from each condition. Dr. Tanya Paull generously provided the ER-AsiSI U-2-OS cells (The University of Texas at Austin, USA)<sup>12</sup>. Previously, DLD-1 cells with an auxin-inducible degron on both TRIP13 alleles (DLD1-TRIP13-AID) were documented<sup>13</sup>. DLD-1 and U-2-OS cells were cultured in Dulbecco's Modified Eagle's Medium (11965092; Thermo Fisher Scientific, Waltham, MA, USA) with 10% fetal bovine serum (TMS-013-BKR; Merck) and 1% antibiotic-antimycotic solution (15240112; Invitrogen, Waltham, MA, USA).

### **1.2.2. Sister Chromatid Exchange**

For 48 hours, cells were grown in a medium containing BrdU at a final concentration of 25 µg/ml. 0.2 µg/mL of colcemid was added during the final four hours. Then, metaphase cells were collected by trypsinization. The cells were then swelled in 0.075M KCl for 15 minutes at 37 °C and fixed twice with a 3:2 mixture of methanol and acetic acid. On glass microscope slides, cells were placed and stained with a 5% Giemsa solution.

### **1.2.3. Plasmids**

Bio-ID2 (from #74224, Addgene) was introduced into pcDNA5-Myc-TRIP13 plasmid that had been previously created<sup>13</sup>. Inserting the 2xStrep tag from the pDSG-IBA103 vector (5-5105-001; IBA, Gottingen, Germany) into the pcDNA5-Myc-TRIP13 vector yielded the pcDNA5-2xStrep-TRIP13 plasmid. Gibson assembly cloning was used to replace each NBS1 domain deletion series (FHA for 1–109 aa, BRCT for 110–327 aa, and C-term for 328–754 aa) with full-length NBS1 using the pcDNA5-Myc-BioID2-NBS1 vector. Addgene's pENTR-GFP-MDC1 plasmid (#26284) was purchased for microirradiation. The designated MRE11 fragment was cloned using Gibson assembly cloning and put into the pcDNA5 3xFLAG vector for in vitro pulldown experiment. For the MRN nuclease activity experiment, full-length TRIP13 was obtained from OriGene Technologies (Rockville, Maryland, United States) and site-directed mutagenesis was used to generate mutant versions (K185A and E253Q). Wild-type TRIP13 and its two variant forms (K185A and E253Q) were introduced into the cloning vector pET-His6-Sumo-TEV-LIC (#29659, Addgene).

#### 1.2.4. siRNA knockdown

TRIP13 mRNA-specific-sense siRNA sequence; GCA AAU CAC UGG GUU CUA C

TRIP13 mRNA-specific-antisense siRNA sequence; G UAG AAC CCA GUG AUU UGC

GL2 (Negative control) siRNA sequence

5'-CGUACGCGGAAUACUUCGA=UU-3', 5'-UCGAAGUAUUCCGCGUACG=UU-3'

#### 1.2.5. Antibodies

A list of antibodies used in this study is provided in Table 1.

Target	Species	Dilution (WB)	Dilution (IF)	Company	Cat#
MRE11	Rabbit	1:2000	-	Abcam	ab3621
GAPDH	Rabbit	1:5000	-	Abcam	ab181603
Myc	Mouse	1:1000	-	Santa Cruz	sc-40
TRIP13	Rabbit	1:1000	-	Bethyl	A303-605A
Strep	Rabbit	1:1000	-	Abcam	ab76949
ATM	Rabbit	1:1000	-	Bethyl	A300-299A
NBS1	Mouse	1:1000	-	GeneTex	GTX70222
RAD50	Mouse	1:1000	-	GeneTex	GTX70228
CtIP	Goat	1:1000	-	Santa Cruz	sc5970
Tubulin	Mouse	1:10000	-	Sigma	T-5168
MDC1	Rabbit	1:1000	1:200	Abcam	ab111171
H3	Rabbit	1:1000	-	Santa Cruz	sc-8654R
γH2AX	Rabbit	1:1000	1:200	GeneTex	GTX127340
pATM (S1981)	Rabbit	1:1000	-	Abcam	ab81292
pKAP1	Mouse	1:1000	-	Bethyl	A300-767A
KAP1	Mouse	1:1000	-	Bethyl	A300-274A
pRPA32 (S4/8)	Rabbit	1:1000	-	Bethyl	A300-245A
pRPA32 (S33)	Rabbit	1:1000	-	Bethyl	A300-246A
RPA32	Rabbit	1:1000	-	Bethyl	A300-244A
pNBS1	Rabbit	1:1000	-	Cell Signaling	3002S

**Table 1. A list of the antibodies used in this study**

IF, immunofluorescence; WB, western blotting.

### **1.2.6. Regulation of MRE11 exonuclease activity and TRIP13 expression**

As previously disclosed, DLD1-TRIP13-AID cells were treated with 500 M IAA (1003530010; Merck Millipore, Burlington, MA, USA) for 14 hours to deplete TRIP13<sup>13</sup>. To inhibit MRE11 exonuclease activity, treatment with 100 M mirin (J67462.MA; Thermo Fisher Scientific, Waltham, MA, USA) was also conducted.

### **1.2.7. DSB induction**

10 Gy IR with SkyScan 1176 was used to produce DSBs in cultured cells (SKYSCAN, Kontich Belgium). For microirradiation, cells in fresh media were pretreated with Hoechst 33342 (62249, Thermo Fisher Scientific) for 5 min at 37°C and then irradiated with a 405 nm laser for 10 iterations in a region of interest (ROI) using an LSM 880 confocal microscope (Carl Zeiss AG, Oberkochen, Germany). After microirradiation, every 5 seconds of time-lapse photos were captured using an LSM 880 confocal microscope. Using the ZEN blue application, ROI intensities were assessed (Carl Zeiss AG).

### **1.2.8. Immunofluorescence imaging**

10 minutes was spent treating cells with 1 mL of ice-cold permeabilization solution (CSK buffer; 10 mM PIPES, 100 mM NaCl, 300 mM sucrose, 3 mM MgCl<sub>2</sub>, and 1 mM EGTA with 0.5% Triton X-100). The cells were then rinsed twice with 1 mL of ice-cold phosphate-buffered saline (PBS) and fixed for 15 minutes at room temperature with 500 L of PBS containing 4% paraformaldehyde. The cells were then treated with 1 mL of -20°C-chilled 100% methanol for 10 minutes, washed twice with 1 mL PBS, then incubated with 500 L blocking solution (PBS containing 10% FBS) for 30 minutes. After removing the blocking solution, a primary antibody was administered for one hour. The cells were rinsed with PBS containing 0.05% Triton X-100 for 5 minutes, incubated with a secondary antibody at room temperature in the dark for 30 minutes, then washed thrice with PBS containing 0.05% Triton X-100 for 5 minutes. The surrounding chamber was removed from the slide after a further washing phase with PBS and distilled water. Each sample was given a drop of mounting reagent (H-1200; Vector Laboratories) and the slide was covered with a cover glass. The slides were totally dry and sealed. The LSM 880 confocal microscope and ZEN software were used to detect and visualize protein foci. Statistical analysis was carried by utilizing Prism5 software (Version 5.01; GraphPad, San Diego, CA, USA).

### 1.2.9. Proteomics experiments with SILAC

Cell lysates were mixed at a 1:1 ratio and processed by in-gel digestion, as previously described 293AD cells (Cell BioLabs, Inc., San Diego, CA, USA) grown in light isotope-labeled lysine and arginine (88429 and 89989, Thermo Fisher Scientific) and heavy isotope-labeled lysine and arginine (88209 and 89990, Thermo Fisher Scientific) were transfected with Myc-BioID2-TRIP13 and Myc-BioID2 Cell lysates were combined at a ratio of 1:1 and digested in-gel as previously described<sup>14</sup>. 20 mg of protein was reduced with 25 mM DTT, alkylated with 25 mM iodoacetamide, and digested at 37°C for 12 hours with trypsin. The answer was acidified with 0.1% trifluoroacetic acid and desalted using C18 tips (87784, Thermo Fisher Scientific). Orbitrap Fusion Lumos was used to examine samples (Thermo Fisher Scientific). Using Proteome Discoverer (Thermo Fisher Scientific) and Scaffold software, proteins were identified (Version 4.11.0; Proteome Software, Portland, OR, USA).

### 1.2.10. Western blot analysis

In RIPA buffer (150 mM NaCl, 1% NP-40 or Triton X-100, 0.5% sodium deoxycholate, 0.1% SDS, 50 mM Tris (pH 8.0), 10 mM NaF, 1 mM Na<sub>3</sub>VO<sub>4</sub>, and protease inhibitors (Roche, Basel, Switzerland)), the cells were lysed. At 95°C, lysates were cooked three times for 5 minutes. Table 2: Antibodies used for western blotting. Using the Odyssey Imaging System, images were quantitatively evaluated (Li-COR Biosciences, Lincoln, NE, USA).

### 1.2.11. *In vitro* pulldown assay

Purified proteins were treated in a buffer (50 mM Tris-HCl, 50 mM NaCl, 1 mM DTT, 2 mM MgCl<sub>2</sub>, and 0.1% Triton X-100) containing 10 M ATPS at 4°C for 1 hour (11162306001, Roche). Purified proteins were treated for 1 hour at 4°C with MagStrep type 3 XT beads or 3xFLAG agarose beads. In BXT buffer or Tris-buffered saline (50 mM Tris-HCl pH 7.5 containing 150 mM NaCl) containing 100 g/ml 3xFLAG peptide, samples were eluted.

### 1.2.12. Colony formation assay

5x10<sup>5</sup> cells were sown onto a 35 mm dish, cultured overnight, and then treated with the specified chemicals and IR. Then, 500 cells were dispersed in a 35 mm plate, cultured for 14 days, rinsed with 5 mL PBS, and stained for 5 minutes at room temperature with 0.5 mL of 1% methylene blue produced in 70% ethanol. After removing methylene blue, stained cells were rinsed three times each with distilled water and PBS. After 24 hours of drying at room temperature, colonies were photographed. Using ImageJ (Version 1.51), the number of colonies was determined<sup>15</sup>. Prism5 software was used to conduct statistical analyses (Version 5.01, GraphPad).

### 1.2.13. DNA end resection assay

Trypsinized, collected, and resuspended at 37°C in PBS (BE17-517Q; Lonza, Basel, Switzerland) containing 0.6% low-gelling point agarose (1613111; Bio-Rad, Hercules, CA, USA) were ER-AsiSI U-2-OS cells. Then, 50 µL of the cell suspension was deposited on parafilm to form an agar ball, which was transferred to a 1.5 mL tube. The agar ball was treated with 1 mL ESP buffer (0.5 M EDTA, 2% N-lauroylsarcosine, 1 mg/mL proteinase K, and 1 mM CaCl<sub>2</sub>, pH 8.0) for 20 hours at 16 degrees Celsius with rotation, followed by 1 mL HS buffer (1.85 M NaCl, 0.15 M KCl, 5 mM MgCl<sub>2</sub>, 2 mM EDTA, 4 After six washes of 1 mL phosphate buffer (8 mM Na<sub>2</sub>HPO<sub>4</sub>, 1.5 mM KH<sub>2</sub>PO<sub>4</sub>, 133 mM KCl, and 0.8 mM MgCl<sub>2</sub>, pH 7.4) at 4°C with rotation for 1 h each, the agar ball was melted by immersing the tube in a 70°C heat block for 10 minutes. The molten sample was diluted 15-fold with distilled water at 70°C, combined with a 10× NEB restriction enzyme buffer, and kept at 4°C.

qPCR was used to assess the level of resection adjacent to specific DSBs. The primer and probe sequences for qPCR are supplied in Table 1. In total, 20 L of genomic DNA was overnight digested at 37°C using 20 units of restriction enzymes (BsrGI and HindIII-HF; New England Biolabs, Ipswich, MA, USA) or mock enzymes. Then, 3 µL of digested or fake digested samples were used as templates in a 25 µL qPCR reaction including 12.5 µL of 2xTaqMan Universal PCR Master Mix (4304437, Thermo Fisher), 0.5 mM of each primer, and 0.2 mM of the probe on a ViiATM 7 Real-Time PCR System (Thermo Fisher). As previously reported, the percentage of ssDNA (ssDNA%) generated by resection was calculated using the following equation<sup>12</sup>:  $ssDNA\% = 1 / (2^{(\Delta Ct - 1)} + 0.5) \times 100$ . Using Prism5 software, the percentage of ssDNA in each sample was evaluated (Version 5.01, GraphPad).

Primer name		Primer sequence
DSB1- 335 bp	Primer FW	5'-GAATCGGATGTATGCGACTGATC-3'
	Primer REV	5'-TTCCAAAGTTATTCCAACCCGAT-3'
	Probe	5'-6FAM-CACAGCTTGCCCATCCTTGCAAACC-TAMRA-3'
DSB1- 1618 bp	Primer FW	5'-TGAGGAGGTGACATTAGAACTCAGA-3'
	Primer REV	5'-AGGACTCACTTACACGGCCTTT-3'
	Probe	5'-6FAM-TTGCAAGGCTGCTTCCTTACCATTCAA-TAMRA-3'
DSB1- 3500 bp	Primer FW	5'-TCCTAGCCAGATAATAATAGCTATACAAACA-3'
	Primer REV	5'-TGAATAGACAGACAACAGATAAATGAGACA-3'
	Probe	5'-6FAM-ACCCTGATCAGCCTTCCATGGGTAAAG-TAMRA-3'
No DSB	Primer FW	5'-ATTGGGTATCTGCGTCTAGTGAGG-3'
	Primer REV	5'-GACTCAATTACATCCCTGCAGCT-3'
	Probe	5'-6FAM-TCTCTGCACAGACCGGCTTCCCTTC-TAMRA-3'

**Table 1. A list of the primers and probes used in this study**



#### **1.2.14. MRN endonuclease activity assay**

As previously stated, wild-type TRIP13 and its mutant forms (K185A and E253Q) were purified<sup>13</sup>. The activity assay utilized a previously reported technique, which included purification of components of the MRN complex and other related proteins<sup>16</sup>.

## 1.3. Results

### 1.3.1. TRIP13 participates in the DNA damage response

Previous research suggested that TRIP13 controls the selection of DSB repair pathways via MAD2L2 (Rev7)<sup>3,9</sup>. However, these studies solely examined TRIP13's effect on the HDR pathway. To determine if TRIP13 plays additional roles in DSB repair pathways, we conducted an I-SceI-based GFP-reporter experiment following TRIP13 knockdown<sup>17</sup>. Consistent with earlier observations, depletion of TRIP13 impacted the HDR and single-strand annealing (SSA) pathways (Fig 1.1A)<sup>3,9</sup>. However, no modification of the NHEJ and alternative NHEJ (alt-NHEJ) pathways was seen (Fig 1.1A). These findings imply that TRIP13 is essential for DSB repair, particularly when DNA end resection is required.

Next, a laser microirradiation experiment was conducted to determine when TRIP13 is recruited to DSBs. Proteins that are recruited to DNA lesions may be damage sensors, chromatin remodelers/signal amplifiers, and lesion repair selection/repair proteins. Their recruitment kinetics vary based on their respective functions<sup>18</sup>. If TRIP13 is only involved in the selection of the DSB pathway, it may not be recruited to lesions at an early stage for damage sensing and signal amplification. TRIP13 hydrolyzes ATP to alter the structures of its interaction partners; hence, we employed ATPS, a non-hydrolyzable ATP analog, to sustain the contacts between TRIP13 and its partners. TRIP13 was unexpectedly recruited to the DNA damage site as soon as a DSB was produced (Fig 1.1B). Therefore, we hypothesized that TRIP13 may be involved in the early detection of DNA damage and signal amplification.

To more precisely regulate TRIP13 expression, we employed the auxin-inducible degron (AID) system, which facilitates the quick and efficient degradation of target proteins<sup>19</sup>. Using the AID system to deplete TRIP13 sensitized cells to DSB induction by ionizing radiation (IR) or hydroxyurea (HU) (Fig 1.1C). These findings revealed that TRIP13 participates in the immediate-early response to DSBs.

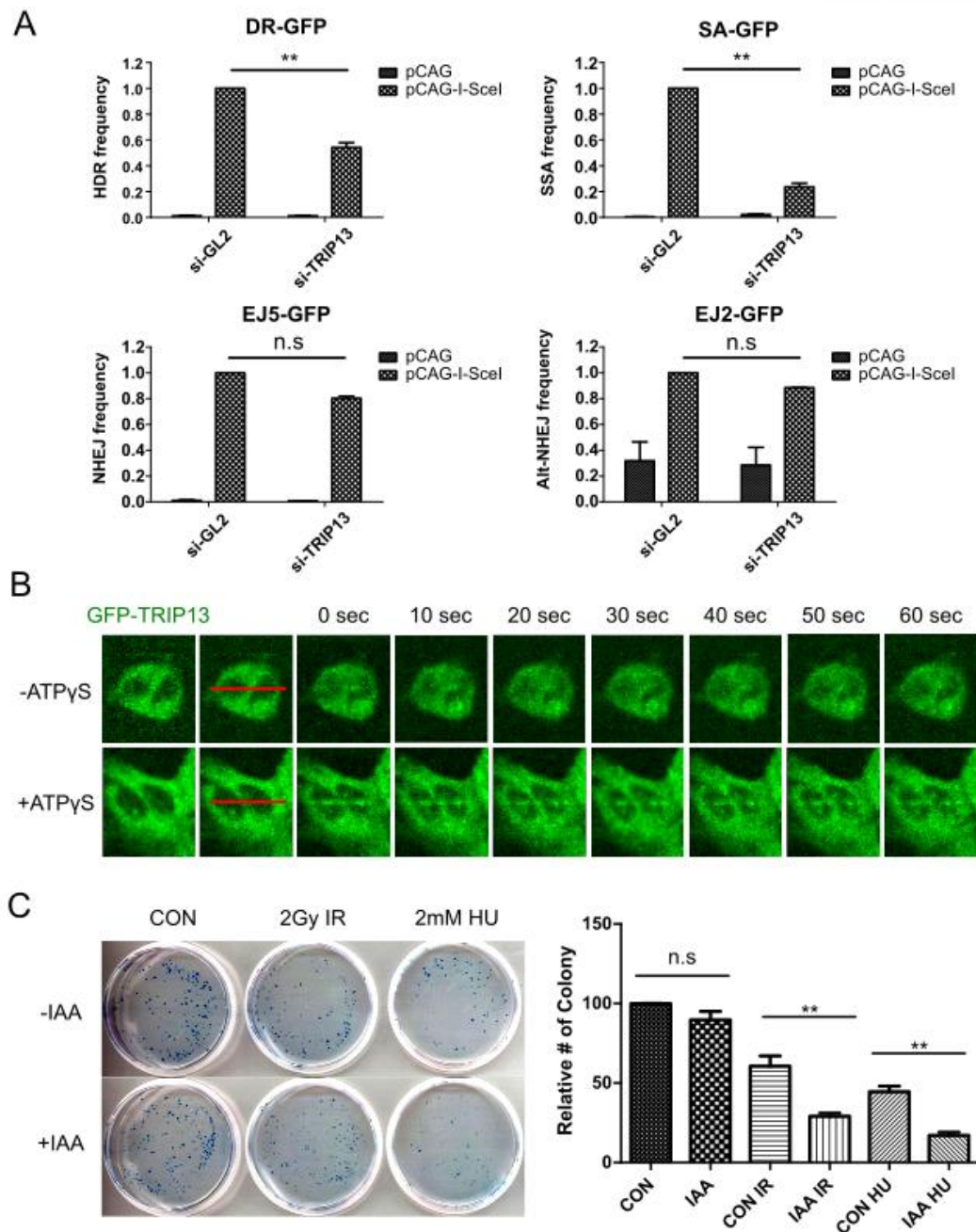


**Figure 1.1. TRIP13 is necessary for DSB maintenance.** (A) Using I-SceI-based GFP-reporter experiments, the contributions of mammalian chromosomal double-strand break repair mechanisms were quantified following TRIP13 knockdown. TRIP13 knockdown inhibited selectively the HDR and SSA processes, but not the NHEJ pathway. HDR, SSA, classical NHEJ, and alternative NHEJ were measured with DR-GFP, SA-GFP, EJ5-GFP, and EJ2-GFP, respectively<sup>17</sup>. (B) UV laser microirradiation rapidly recruited TRIP13 tagged with GFP to DNA damage sites. A colony formation test demonstrated that IAA-induced degradation of TRIP13 altered cellular responses to DNA damage generated by IR or HU treatment. To determine significance, a two-tailed unpaired T-test was used (\*\*p 0.01; n.s., not significant).

### **1.3.2. MRE11 is a novel TRIP13 interaction partner, however this connection is independent of the MRN complex's conformation and nuclease activity.**

Highly dynamic interactions between TRIP13 and its partners make it challenging to discover using traditional immunoprecipitation techniques. Therefore, we conducted quantitative proteomics with proximity tagging to detect nearby proteins, including TRIP13's interaction partners. First, a U-2-OS cell line expressing BioID2-tagged TRIP13 was developed<sup>20</sup>. Afterward, these cells were metabolically labeled for stable isotope labeling using amino acids in cell culture (SILAC)<sup>21,22</sup>. As a negative control, we used solely U-2-OS cells expressing BioID2 as a source of BioID2. Finally, we captured biotin-labeled proteins abundant in BioID2-tagged TRIP13-expressing cells, which may be in close proximity to TRIP13 in vivo. TRIP13 is rapidly recruited to regions of DNA damage, thus we reasoned that identifying its intrinsic interaction partners in the absence of DNA damage would be instructive for understanding its function. Thus, we conducted this experiment without causing DNA damage.

TRIP13 had the highest rank among enriched proteins. We focused on proteins associated with the DNA repair pathway from the 279 identified proteins (the complete list of enriched proteins is presented in Supplemental Table 1). MRE11, a component of the MRN complex, was among the most promising candidates for a TRIP13 interaction partner (Fig 1.2A). Using the known TRIP13-interacting proteins (p31comet, MAD2, and CDC20), the proximal localization of BioID2-TRIP13 was confirmed by western blotting after biotin pulldown (Fig 1.2B). Furthermore, affinity precipitation utilizing 2xStrep-tagged TRIP13, which interacted with both endogenous MRE11 (Fig. 1.2C) and purified 3xFLAG-tagged MRE11, revealed the direct contact between MRE11 and TRIP13 (Fig 1.2D).

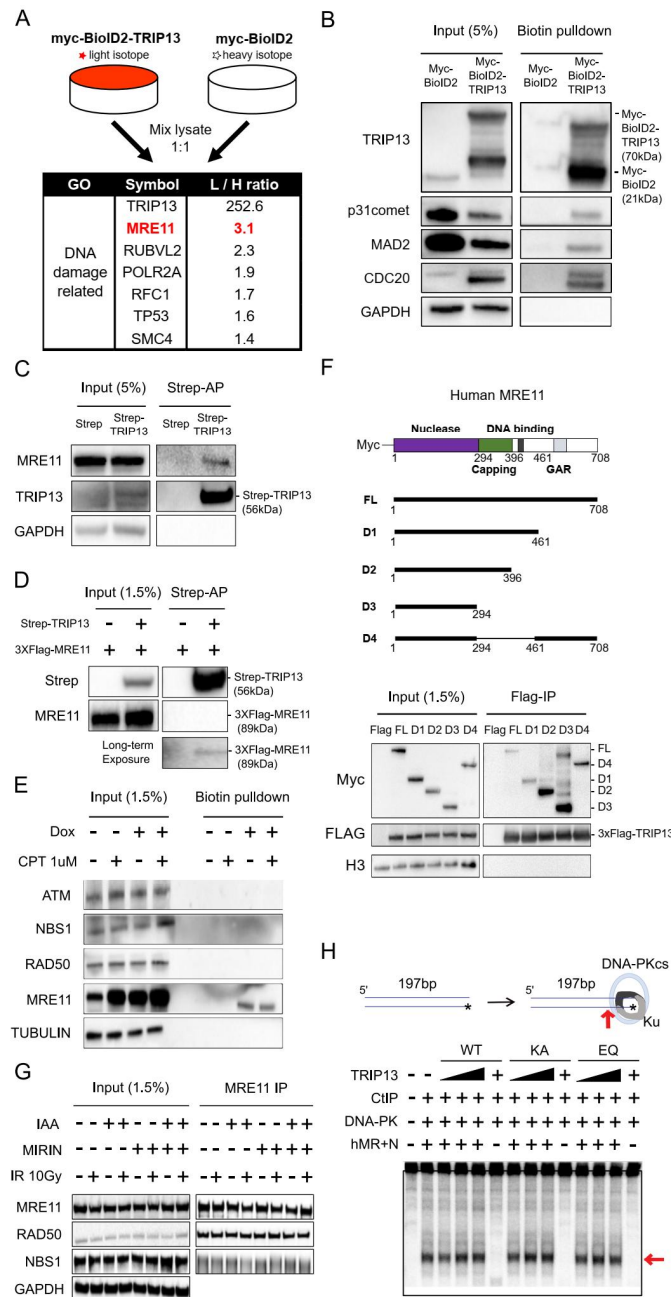


**Figure 1.2. MRE11 is a new TRIP13 interaction partner.** (A) A BioID2-tagged TRIP13 proteomics experiment identified 279 potential interaction partners. (B) BioID2-TRIP13 labeled well-known substrates of TRIP13 (p31comet, MAD2, and CDC20). (C) Strep-AP detected endogenous MRE11 utilizing Strep-tagged TRIP13. (D) Purified 3xFLAG-tagged MRE11 was identified in vitro utilizing purified Strep-tagged TRIP13. Biotin pulldown assays of the MRN complex and cofactors (CtIP and ATM) using BioID2-tagged TRIP13-overexpressing U-2-OS cells exposed to (E) IR or (F) CPT. MRE11 immunoprecipitation verified the connections of MRN complex components with MRE11. The absence of TRIP13 or treatment with mirin had no effect on these interactions. In vitro MRN endonuclease experiments demonstrated that the presence of TRIP13 had no effect on the endonuclease activity of the MRN complex (WT: wild-type, KA: ATP-binding domain mutant, and EQ: ATP hydrolysis mutant). The red arrow represents the main product when DNA-PKcs and Ku are present.

Previously, it was found that NBS1, an additional component of the MRN complex, is a potential interaction partner of TRIP13<sup>10</sup>. Therefore, we examined the interaction between TRIP13 and other components of the MRN complex following irradiation-induced DNA strand breaks (Fig. 1.2E) and camptothecin (CPT) treatment (Fig. 1.2F), which inhibits topoisomerase I during DNA replication. The link between TRIP13 and the MRN complex was seen both with and without DNA damage. Therefore, we hypothesized that TRIP13 may have a role in the control of MRE11 even in the absence of DNA damage.

In addition to MRE11 and RAD50, which are components of the MRN complex, BioID2 fused with TRIP13 was utilized to label ATM and CtIP, which are cofactors of the MRN complex. However, we did not find any NBS1 peptides; hence, BioID2 labeled with TRIP13 may not label NBS1. Therefore, we concluded that TRIP13 interacts with MRE11 in the MRN complex, but not with NBS1.

To determine which domain in MRE11 is responsible for TRIP13 interaction, 3xFLAG-TRIP13 IP was carried out with a Myc-MRE11 domain deletion series that was overexpressed (Fig 1.2F). We separated the MRE11 do-main into the nuclease domain, the Capping domain, and the C-terminal domain containing the Glycine-Arginine domain (GAR) and the DNA binding domain. The deletion of the capping domain or the C-terminal domain did not appear to affect the interaction with TRIP13. Therefore, we hypothesize that the nuclease domain is responsible for the TRIP13 interaction, though additional research is required.

Next, we examined whether TRIP13 affects the MRN complex's stability, which is necessary for its physical interactions. Surprisingly, the connections between Mre11 and other components of the MRN complex remained unchanged whether irradiation and TRIP13 were present or absent (Fig 1.2G). Additionally, an in vitro MRN endonuclease experiment with TRIP13 wild-type, KA mutant (ATP-binding mutant), and EQ mutant (ATP hydrolysis mutant) revealed that TRIP13 did not influence the endonuclease activity of the MRN complex (Fig 1.2H). These findings indicate that TRIP13 contributes to the DNA damage response independently of the endo/exonuclease activity of the MRN complex.

### 1.3.3. TRIP13 depletion inhibits the physical interaction of MDC1 with MRE11 and reduces the recruitment of MDC1 to DNA damage sites

DSBs are detected by the MRN complex, which binds directly to DSB sites<sup>23–25</sup>. The MRN complex recruits and activates ATM kinase, which phosphorylates histone H2AX (H2AX) at double-strand break (DSB) sites, thereby providing a binding site for MDC1<sup>26</sup>. MDC1 at DSB sites attracts more MRN-ATM complex to regions around DSB sites, resulting in H2AX-MDC1 dissemination and amplification of ATM signaling on adjacent chromatin<sup>26</sup>. We predicted that TRIP13 plays a role in recruiting MDC1 to regions of DNA damage.

IR-induced DNA damage increased the chromatin-bound fraction of MDC1, whereas indole-3-acetic acid (IAA)-induced TRIP13 degradation decreased it (Fig 1.3A). MDC1 connects directly to the MRN complex via phosphorylated SDTD motifs<sup>23,27–29</sup>; Consequently, we hypothesized that this interaction is governed by TRIP13. MRE11 immunoprecipitation confirmed the direct connection between MDC1 and the MRE11 complex (Fig 1.3B). The interaction between MDC1 and MRE11 was unaffected by TRIP13 in the absence of DNA damage but was greatly diminished in the absence of TRIP13 in the presence of DNA damage (Fig 1.3B).

To determine how TRIP13 depletion impacts MDC1 chromatin loading, the development of H2AX and MDC1 foci was studied (Fig 1.3C). TRIP13 removal alone dramatically reduced the number of MDC1 foci. To validate the role of TRIP13 in the recruitment of MDC1 to DNA damage sites, GFP-tagged MDC1-expressing cells were laser micro-irradiated. When TRIP13 was demolished, MDC1 recruitment was not only diminished but also delayed (Fig 1.3D). MDC1 directly interacts with the C-terminal region of H2AX<sup>26,30</sup>, MDC1 foci depend on H2AX foci for their existence<sup>31</sup>. Surprisingly, TRIP13 reduction had little effect on H2AX foci (Fig 1.3C). Similarly, treatment with 100 M mirin, which inhibits MRE11 nuclease activity, decreased the amount of MDC1 foci but not H2AX foci. However, the combination of mirin and TRIP13 depletion prevented the development of MDC1 and H2AX foci (Fig 1.3C). Our findings imply that both mirin and TRIP13 regulate H2AX phosphorylation, but TRIP13 is required for MDC1 recruitment to DNA damage sites. It is unclear if TRIP13 regulates ATM signaling pathway independently of mirin because mirin treatment at high dose (above 500 M) has been found to inhibit ATM activity<sup>32</sup>. By modulating the physical contact between the MRN complex and MDC1, TRIP13 collectively enhances recruitment of MDC1 to DNA damage sites.



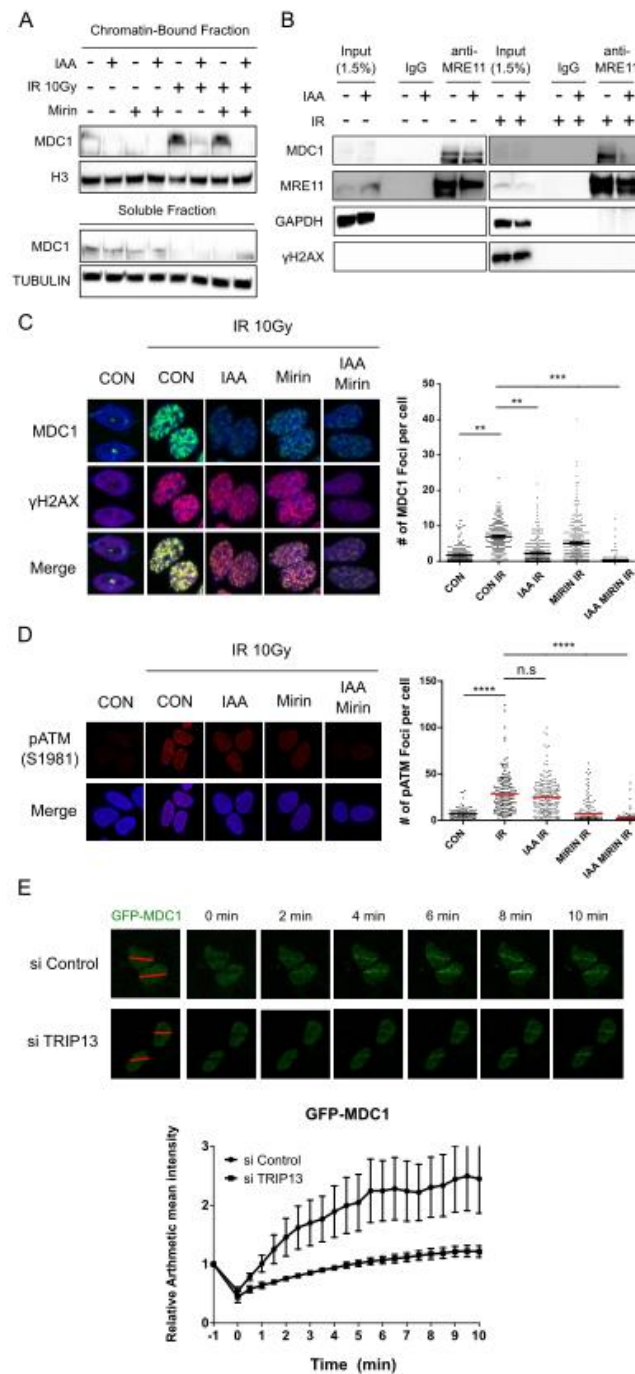


**Figure 1.3. TRIP13 depletion affects MDC1 recruitment to DNA damage sites via reducing the MRN complex's physical contact with MDC1.** (A) TRIP13 depletion affects MDC1 recruitment to DNA damage sites via reducing the MRN complex's physical contact with MDC1. (B) When TRIP13 was degraded by IAA, the chromatin-bound fraction of MDC1 was diminished. (C) Upon TRIP13 degradation and mirin treatment, the formation of phosphor-ATM (S1981) foci was analyzed. (D) When TRIP13 was depleted, the interaction between MDC1 and MRE11 was diminished upon IR exposure. The significance was determined using a two-way ANOVA (n.s, not significant; \*\*\*\*p < 0.001). (E) The formation of MDC1 foci was studied when TRIP13 was degraded, and mirin was applied. To evaluate significance, a two-tailed unpaired T-test was done (\*\*p 0.01; \*\*\*p 0.001). TRIP13 inhibition slowed the recruitment of MDC1 to DNA damage sites. The red lines represent radioactive areas.



#### **1.3.4. TRIP13 promotes DNA resection and homologous recombination via modulating ATM-mediated downstream signaling.**

TRIP13 governs MDC1 recruitment to DNA damage sites via the MRN complex; thus, we studied which downstream signaling pathways are controlled by these interactions. The phosphorylated forms of ATM kinase substrates, including ATM, NBS1, KAP1, and RPA32 (S4/8), were not completely inhibited by mirin treatment or IAA-induced TRIP13 depletion, but they were markedly downregulated by mirin-induced TRIP13 depletion (Fig 1.4A). Interestingly, TRIP13 removal had no effect on ATR kinase-phosphorylated RPA32(S33). Although inhibiting the MRN complex with mirin affects both the ATM and ATR pathways, inhibiting TRIP13 solely impacts the ATM route. In addition, TRIP13 depletion and MRN complex inhibition by mirin treatment had an additive inhibitory effect on ATM downstream proteins, indicating that TRIP13 regulates DSB signaling proteins independently of mirin.

TRIP13 removal decreased RPA32(S4/S8) phosphorylation. Therefore, we conducted an ER-AsiSI-based DNA resection test to assess the effect of TRIP13 knockdown on DNA resection (Fig 4B). ER-AsiSI quantified DNA resection at 335, 1618, and 3500 bp from the DSB<sup>33</sup>. Even in the control group, the DSB did not undergo long-range resection (3500 bp) according to our experimental schedule. TRIP13 depletion or mirin therapy decreased short- and intermediate-range resection by 335 and 1618 base pairs, respectively. Similar to the effects on ATM signaling (Fig. 1.3C and 1.4A), the combination of TRIP13-targeting siRNA and mirin reduced both short- and intermediate-range resection additively.

The frequency of sister chromatid exchange (SCE) is an indicator of homologous recombination<sup>34-36</sup>. We examined the function of TRIP13 in SCE. As anticipated, TRIP13 depletion or mirin therapy decreased the frequency of SCEs, and their effects were cumulative (Fig 4C). Using the GFP-reporter system, we also evaluated the influence of TRIP13 on the HDR and SSA frequencies. Similar to the effect of RAD51 knockdown, both TRIP13 depletion and mirin therapy inhibited the HDR pathway (Fig 1.4D). Moreover, TRIP13 depletion and mirin therapy blocked the SSA pathway in a manner comparable to that of RAD52 knockdown (Fig 4E). TRIP13 is implicated in ATM signaling and the HDR pathway via its direct contact with MRE11, which modulates connections between MDC1 and the MRN complex, as revealed by our data.

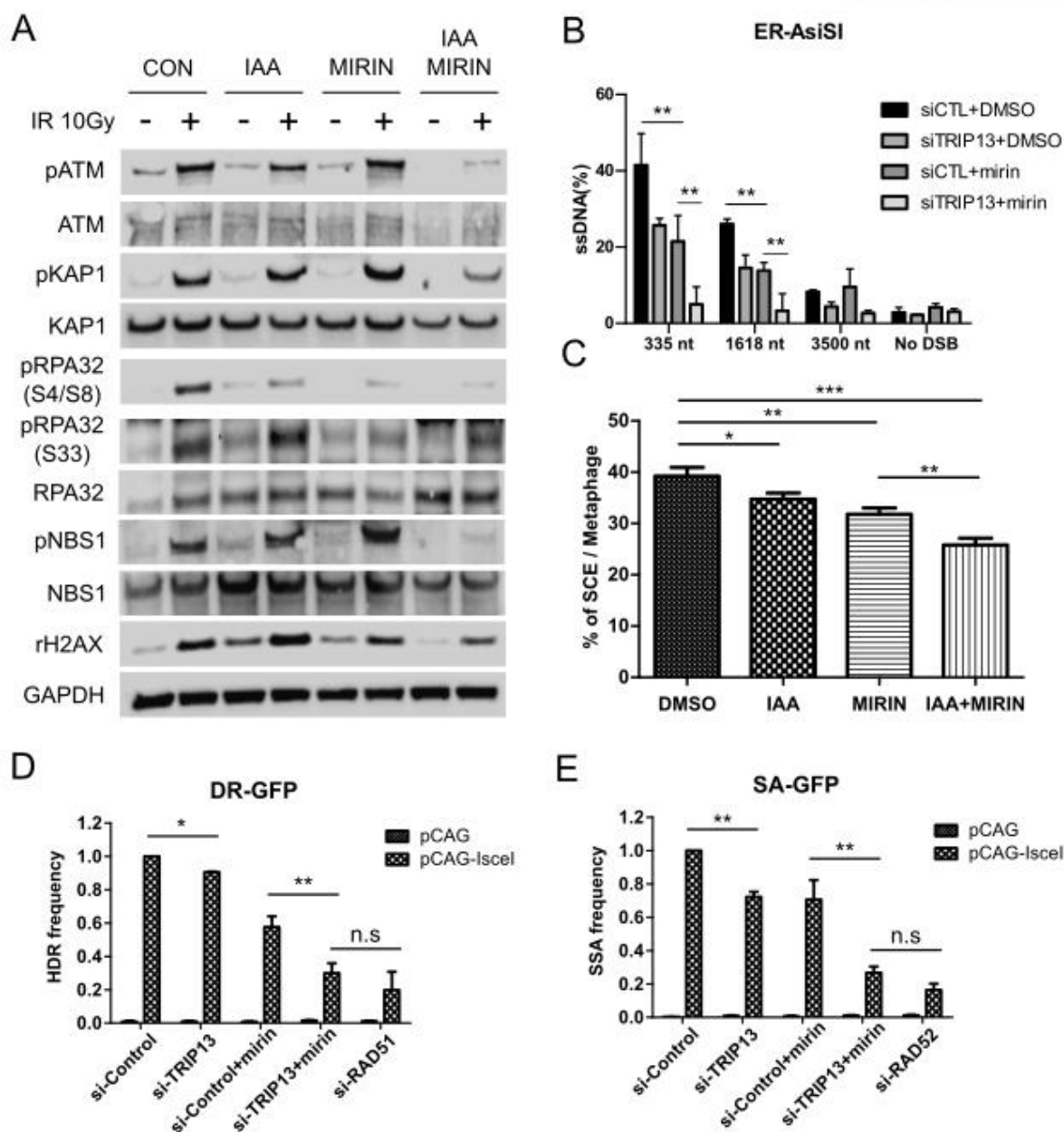


**Figure 1.4. Independent of MRE11 exonuclease activity, TRIP13 promotes HR by modulating ATM downstream signaling and DNA end resection.** (A) Upon TRIP13 degradation with mirin treatment, IR-induced ATM downstream signaling pathways were downregulated. Using the ER-AsiSI system, a quantitative DNA resection experiment revealed that TRIP13 knockdown and mirin administration hindered DNA end resection. (C) Mirin therapy with TRIP13 depletion decreased the production of SCE. (D–E) GFP-reporter experiments revealed that TRIP13 knockdown and mirin administration have cumulative effects on HDR and SSA. The significance was determined using the two-tailed unpaired T-test (\*p 0.05; \*\*p 0.01; \*\*\*p 0.001; n.s., not significant).

## 1.4. Discussion

Recent classification by Kieffer and Lowndes of the DSB repair procedure into three phases<sup>37</sup>. The 'immediate-early step' response is to detect the formation of the DSB area. The 'early phase' reaction involves chromatin modifications and ATM signaling through the recruitment of critical enzymes in order to safeguard the damage and prepare for repair. The 'late step' reaction entails selecting the appropriate repair pathway based on the circumstance. TRIP13's participation in the DNA damage response has only been documented in the "late step" reaction, which controls the selection between HDR and NHEJ<sup>3,9</sup>. TRIP13 is recruited to a DNA damage site within a few seconds, indicating that reduction of TRIP13 does not improve NHEJ. In addition, TRIP13 depletion reduces the amplification of DNA damage signaling and the recruitment of its downstream signaling proteins, which corresponds to an "early step" response. These findings show that TRIP13 participates in both the 'late step' and 'immediate-early step' responses to DNA damage.

We found interacting partners of TRIP13 implicated in the "intermediate-early phase" response to DNA damage using a quantitative proteomics technique with proximity-labeling. MRE11 was selected from various DNA repair-related proteins because the MRN complex initiates DNA strand break sensing and ATM activation<sup>38-40</sup>. We confirmed that TRIP13 interacts directly with MRE11 and RAD50, but not with NBS1, when DNA damage is induced (Fig 1.2E). The inability of proximity-labeling proteomics and traditional immunoprecipitation to detect the interaction between TRIP13 and NBS1 (Fig 1.2E, 1.2F) leads us to hypothesize the existence of an MRN complex containing just MRE11 and RAD50, but not NBS1. In actuality, overexpression of the yeast ATM ortholog TEL1 sustains DSB repair and telomere preservation in the absence of NBS1<sup>41</sup>. In addition, the database of protein complexes is based on a large co-elution profile (hu.MAP v2)<sup>42</sup> reported a complex with only MRE11 and RAD50 (HuMAP2 02474; p-value 1.98e-04) and a complex with all known MRN complex components (MRE11, NBN (NBS1), RAD50, FAM219A, and HEATR1; HuMAP2 01080; p-value 4.96e-04). To confirm the specificity of the interaction between TRIP13 and the MRE11-RAD50 complex, additional research is required.

TRIP13 appears to interact with MRE11 even in the absence of DNA damage, which is intriguing. MRE11 was discovered as a TRIP13 interaction partner through the SILAC approach in the absence of DNA damage, and this interaction was not affected by DNA damage (Fig 1.2A). Consequently, TRIP13 may interact with MRE11 in the absence of DNA damage. Another theory is that TRIP13 interacts with MRE11 in the initial DNA damage response. Within seconds of UV exposure, TRIP13 was recruited to DNA damage sites. Therefore, TRIP13 is able to interact with MRE11 even in the absence of DNA damage and swiftly responds to spontaneous DNA damage. Further studies should investigate these hypotheses.

Upon TRIP13 depletion, recruitment of MDC1 to DNA damage sites and physical interaction of MDC1 with the MRN complex were drastically diminished. Two motifs, Walker A (for ATP binding) and Walker B (for ATP hydrolysis), are essential for this activity<sup>43</sup>. Moreover, TRIP13 dissociates a substrate from a protein complex by causing a conformational shift in the substrate<sup>3,4,44</sup>. Nevertheless, our findings indicate that TRIP13 facilitates the interaction between MRE11 and MDC1, as opposed to causing the release of MRE11 from the MRN complex or MDC1. In the future, it would be intriguing to completely understand how TRIP13 governs the interaction between MDC1 and the MRN complex. TRIP13 modulates ATM signaling amplification and influences the connection between MDC1 and the MRN complex by interacting directly with MRE11.

ATM phosphorylates TQXF motifs within MDC1, thereby generating docking sites for the ubiquitin E3 ligase RNF8<sup>45</sup>. This stimulates the recruitment of another E3 ligase, RNF168, by ubiquitylating histone H1 or L3MBTL2<sup>46,47</sup>. RNF168 sequentially ubiquitylates histone H2A and induces the recruitment of DNA damage response factors, including 53BP1 and its downstream proteins, RIF1<sup>48-50</sup>, PTIP<sup>51</sup>, and the Shieldin complex<sup>52</sup>. MAD2L2 (Rev7) is a component of the Shieldin complex, which shields double-strand breaks (DSBs) and supports the NHEJ pathway<sup>53,54</sup>. Previous research has suggested that TRIP13 improves the HDR pathway upon DSB induction by freeing MAD2L2(Rev7) from the Shieldin complex<sup>3,9</sup>. In these investigations, TRIP13 knockdown had an effect on the HDR pathway and not the NHEJ pathway. Using the I-SceI-based GFP-reporter experiment, we confirmed that reduction of TRIP13 hindered the SSA and HDR pathways, but had no effect on NHEJ and alt-NHEJ. TRIP13 appears to regulate DNA end resection at double-strand breaks (DSBs) to allow HDR and SSA, which are essential for intermediate- and long-range resection. It is unknown why TRIP13 depletion had no effect on alt-NHEJ, which necessitates a short-range resection. Importantly, even in wild-type cells, the frequency of alt-NHEJ in the reporter assay was rather low, therefore we were unable to detect a minor change in alt-NHEJ with our experimental design. Alternately, TRIP13 may interact with a different partner protein that induces alt-NHEJ. Despite the fact that TRIP13 promotes DNA end resection, an extra partner that increases alt-NHEJ with TRIP13 may be necessary for proper alt-NHEJ.

In conclusion, TRIP13 plays a function in ATM activation through its interaction with MRE11, in addition to influencing the selection of the DSB repair route. Our findings indicate that TRIP13 participates upstream of the ATM signaling system, which corresponds to an "immediate-early" response in DNA damage sensing, hence boosting HDR and NHEJ. in accordance with prior results<sup>3,9</sup>, Our findings indicate that TRIP13 is an essential regulator of DSB repair at several stages.

## **2. Enrichment of deleterious mutated genes involved in ciliary function and histone modification in brain cancer patient-derived xenograft models**

### **2.1. Introduction**

Brain tumors are among the most difficult to treat, with a 5-year overall survival rate of less than 35% despite the development of numerous tailored therapy alternatives<sup>55</sup>. In 2016, the World Health Organization (WHO) began combining traditional histology with genetic biomarkers to classify central nervous system (CNS) tumor types<sup>56</sup>. Since then, the diagnostic significance of molecular biomarkers in the classification of CNS tumors has increased. For instance, the fifth edition of the WHO Classification of Tumors of the Central Nervous System (CNS5) combines molecular factors with clinicopathologic phenotypes for the most precise classification of CNS tumors<sup>57</sup>.

Large-scale genomic analyses, such as The Cancer Genome Atlas, provide information regarding molecular markers to classify glioblastoma multiforme (GBM) into at least four subtypes based on genetic, epigenetic, and transcriptional changes<sup>58–60</sup>. More recently, cIMPACT-NOW (the Consortium to Inform Molecular and Practical Approaches to CNS Tumor Taxonomy) has updated practical suggestions on recent categorization advancements for CNS tumors<sup>61–66</sup>. Emerging importance of molecular biomarkers for CNS cancers is hampered by the high intra- and inter-tumor heterogeneity of several progressive brain tumor types, such as GBM<sup>67,68</sup>.

Patient-derived xenograft (PDX) models are regarded as a viable platform for customized cancer research due to their ability to replicate the genomic and epigenetic traits and microenvironmental interactions that occur throughout the growth of a brain tumor. Using whole-exome sequencing, the Mayo Clinic Brain Tumor PDX National Resource team evaluated the genetic changes in 83 PDX samples from 24 patient tumors<sup>60</sup>. According to the researchers, PDX samples were able to capture common and uncommon mutations of TERT, EGFR, PTEN, TP53, BRAF, and IDH similar to glioblastoma tissue samples. Despite the fact that tumor driver mutations and their expression profiles were identical between tumors and xenografts, the complete list of genetic alterations found in each circumstance was not disclosed.

Based on whole-genome sequencing, a prior study found discordance in the comprehensive mutation profile between xenograft and patient tumors, ranging from 12% to 64% of common mutations<sup>69</sup>. According to a separate study, certain tumor-PDX couples did not share as many somatic mutation patterns as anticipated, most likely due to their hypermutability capacity<sup>70</sup>. Although we hypothesized that the variety of somatic tumor mutations could lead to genetic incompatibility, host-specific development of xenograft tissues was also a possibility<sup>71</sup>.

Recent analysis of 15 trios of tumor-BTIC (brain tumor-initiating cell)-xenograft samples

revealed that some mutations were common among the trio samples, while others were discovered only in the xenograft model<sup>69</sup>. Further characterization of mutations detected solely in the xenograft model revealed that they were situated in genes involved in ciliary or flagellar movement, sensory organ development, and synaptic control. These data show that cancer genomic investigations employing PDX models should include special selection in the unexplored xenograft environment.

To gain a better understanding of these xenograft-specific mutation patterns, we investigated genome-wide mutations in many brain tumor-PDX models along with their respective primary tumors. Surprisingly, although their histological properties were identical, only a few detrimental somatic mutations were shared by the PDX samples and the primary tumors. By evaluating the PDX-specific enriched mutations, as was done in the prior research, we were able to determine the genetic basis of the disease<sup>69</sup>, we found mutations in genes associated with cilium mobility, microtubule depolymerization, and histone methylation. Although it is necessary to elucidate the relationship between these functions and brain tumors and whether rare tumor mutations are enriched or tumor-unrelated mutations are selected in the PDX model, our study may require further consideration of the model-specific genetic selection properties of PDX models.

## **2.2. Materials and methods**



### **2.2.1. Tumor samples from patients with brain tumors.**

Between September 2015 and April 2017, eleven individuals with brain tumors provided tissue samples. This study was authorized by the Institutional Review Board of Seoul National University Hospital (permission number H-1507-145-696), and informed consent was obtained from all patients. Figure 1 depicts the clinical diagnoses of the examined patients alongside sample histology images. In addition, clinical data such as age, gender, smoking status, stage, tumor size, preoperative chemotherapy, differentiation, vascular invasion, perineural invasion, lymphatic invasion, pleural invasion, recurrence, and survival were extracted from the medical records of the patients. The duration between histological diagnosis and death or the last follow-up was regarded as overall survival. Survival without relapse was defined as the time between histological diagnosis and the first progression or recurrence, disease-related death, or the last follow-up.

### **2.2.2. Establishment of brain tumor-PDX models.**

To construct PDX models, patient tumor tissues were transplanted subcutaneously into the flanks of NSG mice (Jackson Laboratory, Sacramento, CA, USA). After surgical excision, patient tumor tissue was collected within two hours. Tissue from the tumor was implanted as soon as possible after harvesting. The tumor was stored in an appropriate medium (RPMI1 1640) at 4°C before implantation. In the cabinet, an anesthetic chamber was installed, and an oxygen/isoflurane mixture was created. Then, we placed fresh patient tissue in a culture dish and rinsed it twice with serum-free RPMI1640 medium. Using a sharp blade, the viable component of the tumor was diced into 1 mm<sup>3</sup> pieces. The operating table and equipment were sterilized with 70% ethanol, and the surgical instruments (scissors, forceps, and cotton swabs) were sterilized in an autoclave. Mice were placed in the anesthetic chamber containing a mixture of oxygen and isoflurane. Using a plunger, tumor pieces were engrafted, and the needle was gently withdrawn while the engrafted tumor was held with forceps. The mouse's skin was cleansed with alcohol, then it was placed on a heated pad and observed until it regained consciousness. Once the tumor's volume reached 60 mm<sup>3</sup>, its size was assessed twice per week using a caliper. The volume of the tumor was computed as  $0.5 \times (\text{length}) \times (\text{width})^2$ . Mice were slaughtered when the tumor volume reached 600–800 mm<sup>3</sup>, and tumors were taken for further research, such as consecutive passaging and next-generation sequencing analyses. The excised tissues were used to make formalin-fixed paraffin-embedded blocks, while the remaining tissues were kept as snap-frozen fragments of tumor. The Biomedical Research Institute at Seoul National University Hospital approved all animal care and studies (approval number: IACUC 14-0016-C0A0(1)).

### **2.2.3. Histopathological analysis.**

The thickness of fresh patient and PDX tissue slices was 4  $\mu\text{m}$ . Following the manufacturer's instructions, hematoxylin and eosin staining was performed using a Symphony system (Ventana Medical Systems, Inc., Basel, Switzerland). A ScanScope® XT scanner was used for image analysis (Aperio, Leica Biosystems, Newcastle, UK).

### **2.2.4. Mutational analysis.**

Using a TruSeq DNA Exome kit, a sample exon capture library was constructed and sequenced on an Illumina HiSeq 2000. Adapter sequences were cut with trimmomatic (version 0.39)<sup>72</sup> and bwa was used to align the sequences to the human-mouse combined reference genome (hg38 and mm10) (version 0.7.12)<sup>73</sup>. To exclude readings from the mouse host in xenograft samples, the human (hg38) and mouse (mm10) genomes were combined and reads that mapped preferentially to mouse chromosomes were deleted. For uniformity, the same approach was applied to human-only tumor tissue and blood data. Using strelka2, somatic and germline variations were identified (version 2.9.10)<sup>74</sup> with the '--exome' option and examined passed variations for further study. The Variant Effect Predictor (VEP) of Ensembl (version 101)<sup>75</sup> was used to predict the effect of somatic mutations, and genes with mutations predicted to have a significant impact on proteins were studied extensively. From the COSMIC database, cancer census genes and other genes related with brain tumors were extracted (version 94)<sup>76</sup>.

### **2.2.5. Mutational signature analysis.**

Each sample's somatic mutations were evaluated using the COSMIC MutSig reference database<sup>77</sup> and the SigProfiler program for single base substitution (SBS), double base substitution (DBS), and insertion-deletion (ID) signatures (version 3.2 - March 2021) and SigProfiler software (version 3.2 - March 2021)<sup>78</sup>.

### **2.2.6. Gene Ontology (GO) term enrichment analysis.**

The number of tumor or PDX samples in which harmful mutations were found was used to sort genes with deleterious mutations. Using PANTHER Gene List Analysis tools<sup>79</sup> and the PANTHER GO-slim biological process database, an enrichment analysis of GO terms was conducted. We chose enriched phrases with an enrichment score larger than 3 and a false discovery rate lower than 0.05



## 2.3. Results

### 2.3.1. Deleterious somatic mutations are discordant between original tumors and xenograft tissues.

Ten brain cancer patients' tumor samples were used to create 13 PDX models, and the histological characteristics of the brain tumors and their generated xenograft tissues were confirmed (Fig. 2.1). All PDX models were evaluated in vivo first passage, with the exception of SNPDX-045, which was analyzed in the second passage. SNPDX-010 and SNPDX-011 were additionally analyzed in the second passage. Then, we performed whole-exome sequencing on these tissues and each patient's blood in order to discover somatic mutations accumulated in brain tumors and investigate their conservation in xenograft tissues. To focus on mutations that contribute to the development of brain tumors, we chose deleterious mutations having a substantial influence on protein activities, such as peptide truncation and loss of function generated by non-synonymous mutations, as predicted by the Ensembl VEP<sup>75</sup>.

Surprisingly, the overlap of deleteriously altered genes between tumors and generated xenograft tissues was substantially lower than anticipated (6.0–36.7%) because fewer deleteriously mutant genes were present in either sample (Fig. 2.2). Moreover, even for two cases whose xenograft tissues experienced a second passage (SNPDX-010 and SNPDX-011), the two xenograft tissues did not share significantly modified genes (at most, 18.4% of total mutant genes were shared by all three samples in SNPDX-011). When we evaluated direct mutation sites as opposed to mutant genes, the overlap was much lower (Supplementary Fig. 2.1), being less than 3% in eight out of eleven instances. Even for samples with 21.2% overlap (SNPDX-037), overlap fell to 5.2% when 2,067 mutant genes detected in xenograft tissue were examined. Therefore, we unexpectedly concluded that the precise somatic mutation patterns are not retained between the original tumors and the xenograft tissues.

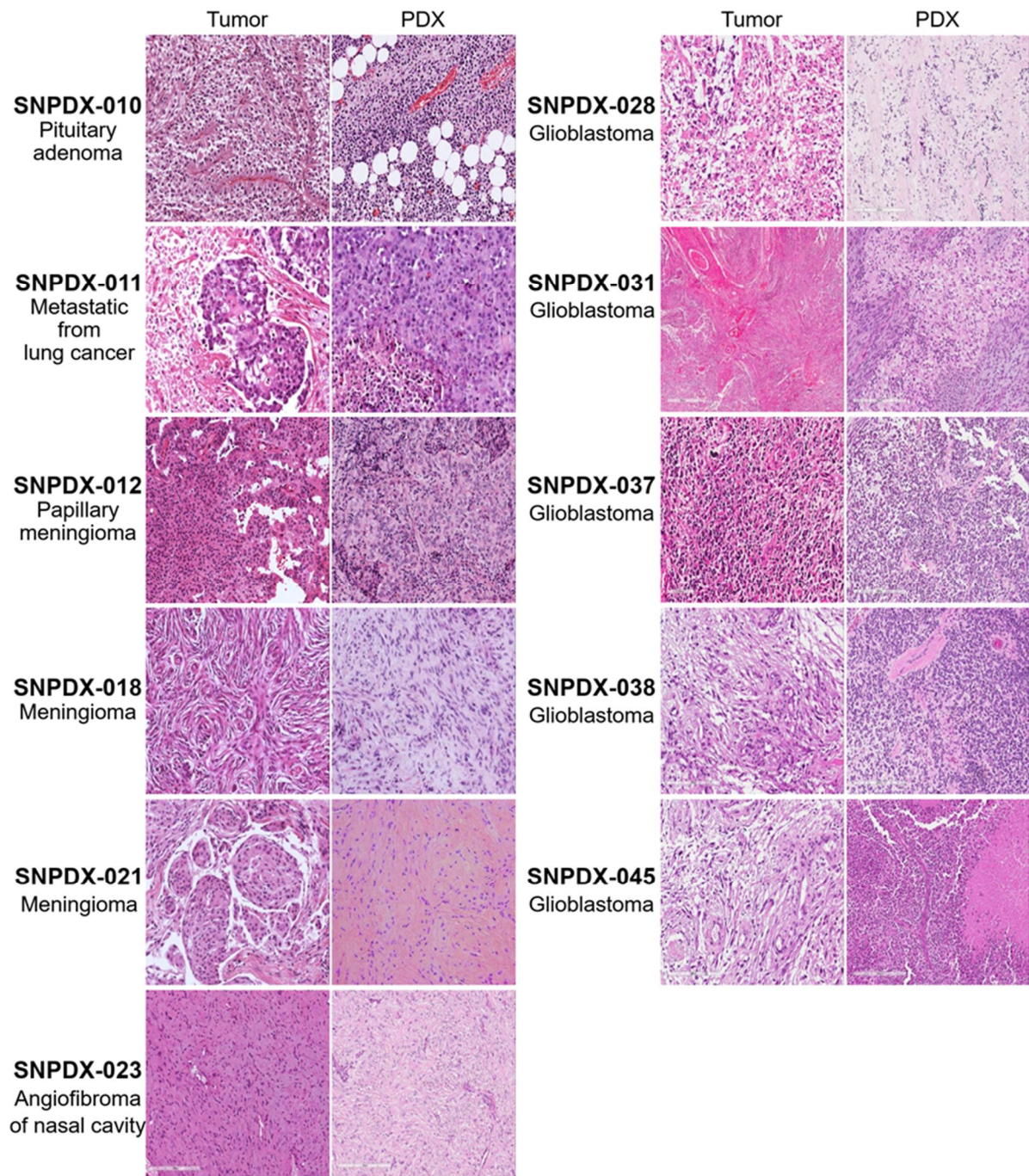


**Figure 2.1. Histological analysis of brain tumor-PDX tissue sources and origins.** We confirmed that the type of brain tumor was preserved in the xenograft state.

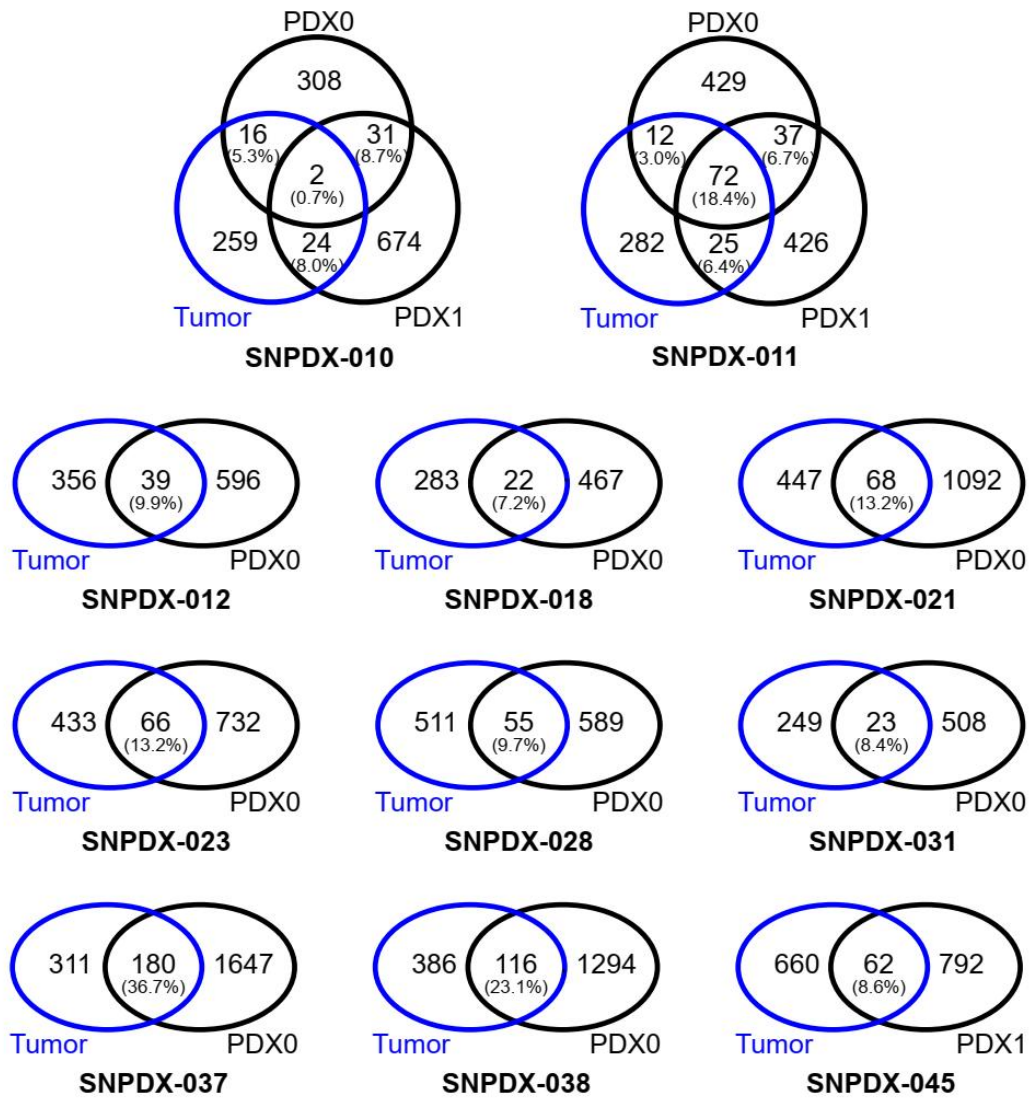
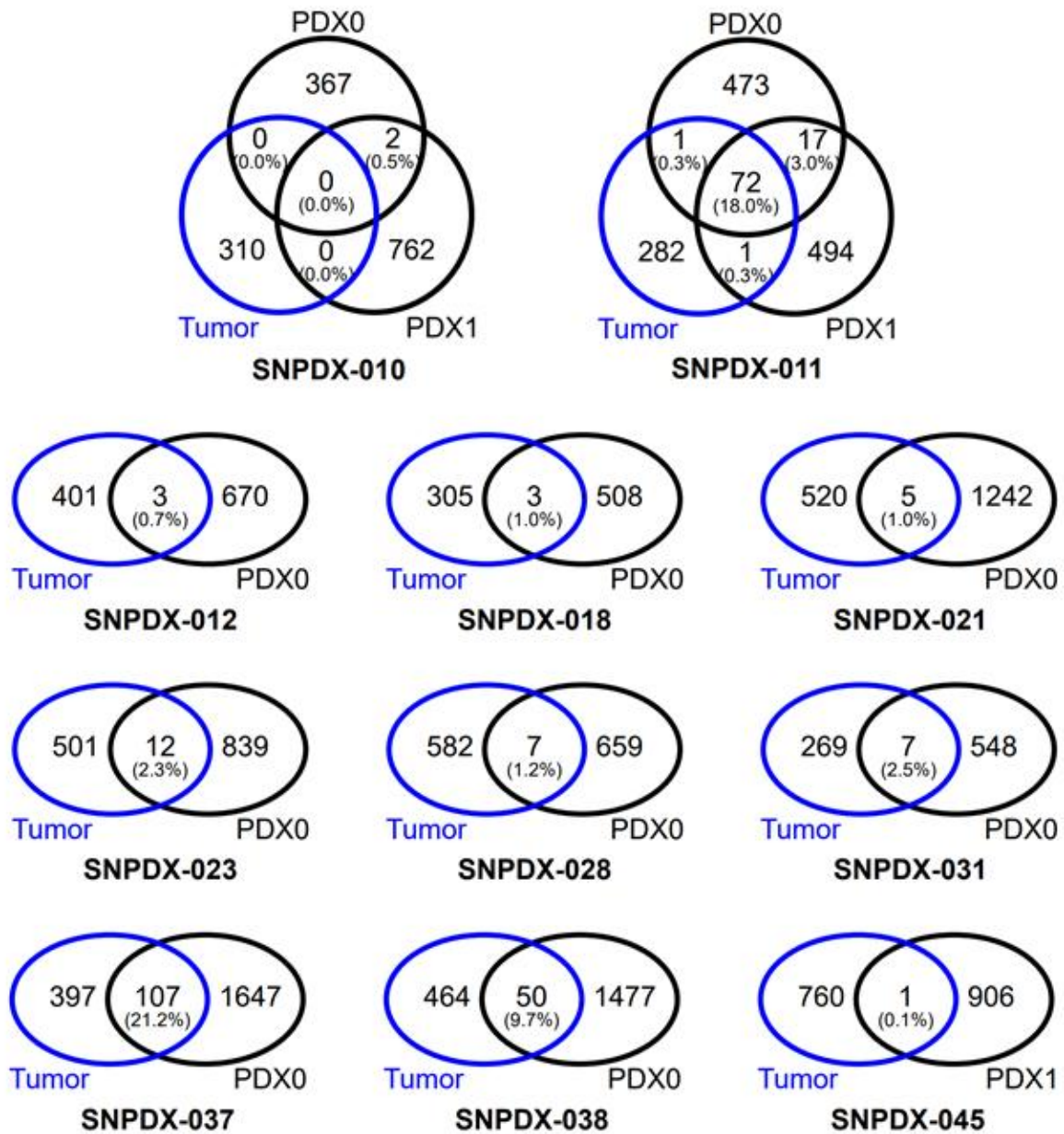


**Figure 2.2. Genes containing deleterious mutations are present in both primary and PDX tumor model.** EnSEMBL VEP assessed the number of genes with deleterious somatic mutations based on mutations with a significant impact. To calculate the percentage of overlapping genes between PDX samples and tumors, the total number of overlapping genes was divided by the total number of genes in the original tumor. The proportion of overlapping genes between PDX0 and PDX1 was calculated by dividing the number of overlapping genes by the total number of genes in the initial PDX sample (PDX0).





**Supplementary Figure 2.1. Overlap deleterious mutations in both original tumor tissues and PDX.** EnSEMBL VEP evaluated the number of genes with deleterious somatic mutations based on mutations with a substantial effect. To determine the proportion of overlapping genes between PDX samples and tumors, the total number of overlapping mutations was divided by the total number of mutations in the original tumor. The percentage of overlapping mutations between PDX0 and PDX1 was determined by dividing the number of overlapping genes by the total number of genes in the initial PDX sample (PDX0).

### **2.3.2. Both primary cancers and xenograft tissues share identical germline mutations.**

Before assessing the specifics of genetic selection in the host, we attempted to confirm that samples shared common global genetic characteristics. If samples are acquired from the same individual, there should be a high degree of germline variation overlap. Therefore, we compared the germline variation of PDX samples to that of tumor and blood samples from each individual. To reduce the effect of the variant calling algorithm and sequencing errors, we solely included homozygous germline variants in this research.

Each sample included an average of 36,240 homozygous variations, and more than 90% of these variants were shared by the blood, tumor, and PDX samples from the same individual (Fig. 2.3). Due to the fact that SNPDX-037 and SNPDX-038 were generated from two different tumor locations in the same patient, their germline variants overlapped substantially. In contrast, the overlapped proportion of homozygous variants among samples from different persons did not surpass 60%, regardless of sample type, with the exception of PDX samples obtained from SNPDX-011, for which the overlap was 62–66%. These findings suggest that these PDX samples retained the genetic background of their matched tumor source and originated from the same tumor source.



**Figure 2.3. Heatmap showing prevalent germline homozygous variations.** When comparing sample variations, only homozygous germline variants were considered. To validate the concordance between tumors and xenograft samples, we utilized the number of germline mutations in a tumor sample as a reference baseline rather than a normal sample. By dividing the number of germline mutations in xenograft samples by the number of germline mutations in tumor samples from each patient, the percentages of overlap were calculated.

### **2.3.3. Mutational signatures are highly preserved between tumors and xenografts, and they reveal the mutational origin.**

Other global genetic characteristics evaluated were mutational signatures, which can be used to infer the origin of somatic mutations in a variety of cancer types<sup>77</sup>. We investigated if mutational changes happened during the creation of PDX. Although the PDX models were well-established from the same tumor source as mentioned above, exposure to a novel mutagen during PDX establishment would result in somatic mutational alterations. To examine the mutational process in the PDX model and original tumor, we compared the mutational signatures of the PDX model and its corresponding original tumor using COSMIC.

Except for SNPDX-037 and SNPDX-038, all samples displayed comparable mutational patterns that are highly related to the SBS18 mutational signature that was previously identified as likely being harmed by reactive oxygen species (Fig. 2.4)<sup>77,80,81</sup>. In addition, DBS and ID mutational signatures were shared between PDX samples and their corresponding malignancies. While somatic mutation patterns of PDX samples and original tumors were widely discordant, PDX samples maintained the mutational signatures of their matched tumor samples. These findings indicate that PDX models can retain both the genetic background and the *in vivo* mutational process of the original tumor.

As stated previously, SNPDX-038 and SNPDX-037 were acquired from the same patient, and their mutational signatures were similar and most similar to the SBS11 signature, which was found to be the temozolomide (TMZ)-related mutation signature (Fig. 2.4)<sup>77,82,83</sup>. Before surgery, the patient who provided SNPDX-037 and SNPDX-038 had received eight cycles of TMZ treatment over the course of eight months. These data indicate that PDX samples preserve the mutational signatures of the original tumors, from which we can estimate the mutation's cause, such as chemotherapy history.



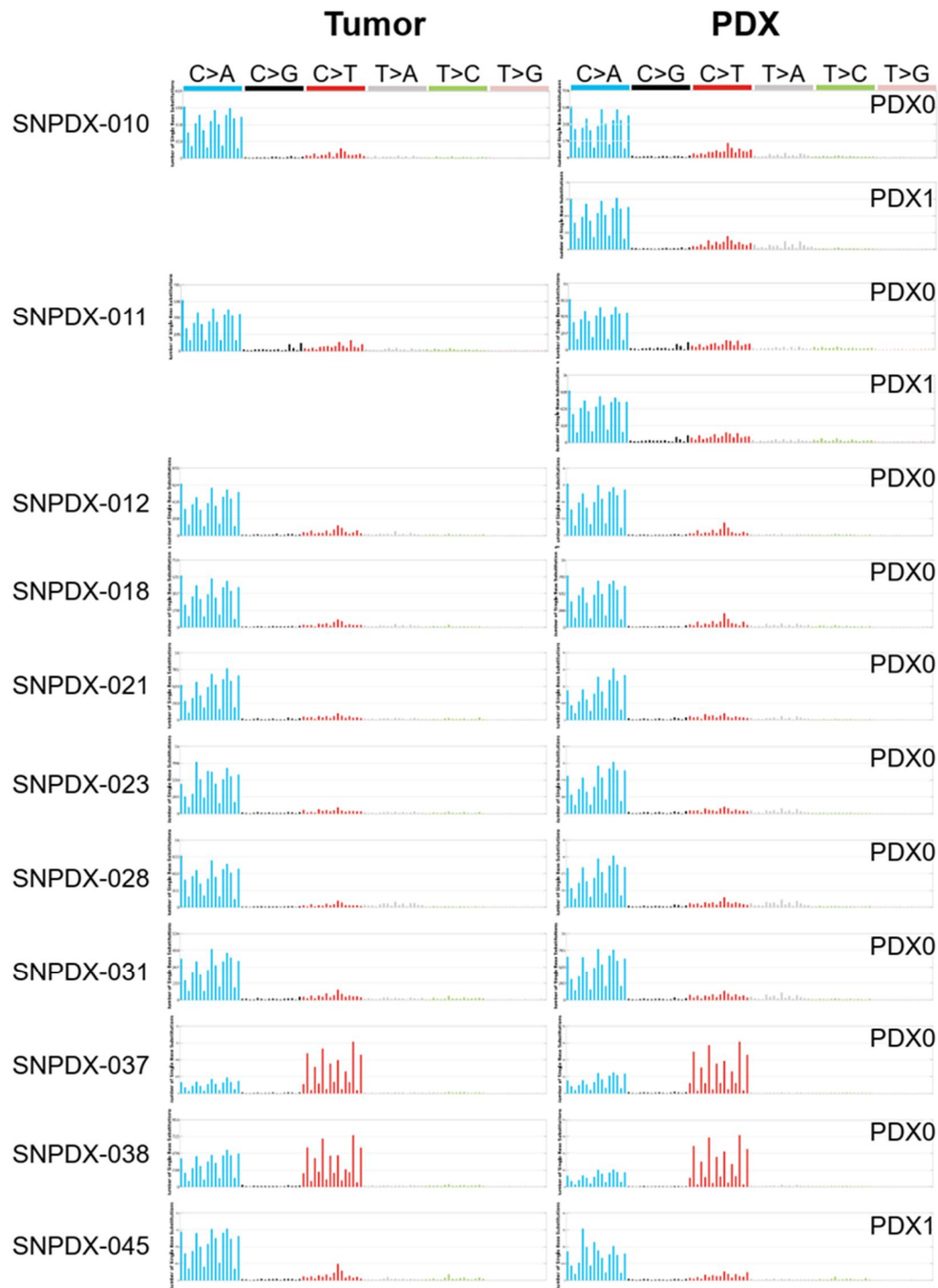


**Figure 2.4. SBS mutational signature analysis.** Mutational signatures were highly conserved between tumor and xenograft tissues. mutational signatures obtained from tumor and PDX samples were subjected to a COSMIC SBS signature analysis (see Methods for details). The SBS mutational signatures of 96 tumor subtypes (left) and PDX samples (right) are shown (right). Additionally, the picture labels the mutational patterns of a xenograft with a second passage (PDX1) in three patients (SNPDX-010, SNPDX-011, and SNPDX-045).



#### 2.3.4. Mutations related with brain tumors are enriched in PDX samples.

Although PDX samples retained the mutational fingerprints and germline variants of the original tumors, their dissimilar somatic mutation profiles were perplexing. We hypothesized that this difference was produced by a combination of tumor heterogeneity and clonal evolution inside the host. Therefore, we investigated genes and their associated biological processes that were concordant or discordant across tumor and PDX samples.

First, we analyzed the somatic mutation patterns of genes related with brain cancer as published in the COSMIC database (Fig. 2.5)<sup>76</sup>. In the original tumor or PDX sample, five genes (ARTX, IDH1, IDH2, BRAF, and MGMT) harbored mutations with moderate or high impact on protein functions. However, even in these oncogenes associated with brain cancers, we detected divergent mutation patterns between tumors and PDX samples, comparable to total somatic mutations. For instance, we identified IDH1 mutations in three tumor samples from two individuals (SNPDX-012 and SNPDX-037/038), whereas six PDX samples showed moderate- or high-impact IDH1 mutations. Although the mutation profiles did not overlap, PDX samples showed more mutations in these genes than tumors, showing that PDX samples are enriched for mutations linked with brain cancers.

In addition, we examined genes with somatic mutations that were enriched in PDX samples or primary tumors. First, we analyzed 723 COSMIC cancer census genes often associated with a variety of cancers (Fig. 2.6a and 2.6b) and determined the top 30 genes enriched in each sample type. Compared to mutant cancer census genes enriched in tumors, a surprising number of PDX-enriched mutated genes were shared in PDX samples. We expanded this to all altered genes and detected 217 mutations in tumor-enriched genes and 1,610 mutations in PDX-enriched genes. We reasoned that tumor-associated mutations are enriched in PDX samples because not only was the number of genetic alterations but also the overlap between samples greater in PDX samples than in tumors.

We identified 409 genes with high-impact mutations (e.g., protein truncation, frameshift mutation) and examined whether these mutations were enriched in tumors or PDX samples by subtracting the number of tumor samples with the modified genes from the number of PDX samples with the same mutated genes (Fig. 2.6e). These mutations were more prevalent in PDX samples than in malignancies. We selected these genes according to the number of mutant samples and analyzed whether PDX samples contained more mutations associated with cancer (Fig. 2.6f). Based on the number of samples in each category, we anticipated that thirteen of the twenty-three samples with specified mutations would be PDX samples (yellow line in Fig. 2.6f). In most instances, PDX samples had more shared mutations than original tumors, and four of these genes (MUC16, NF1, LRP1B, and CSMD3) were classified as COSMIC census genes. We concluded that cancer-associated somatic mutations are enriched in PDX samples despite their absence in the original tumors.

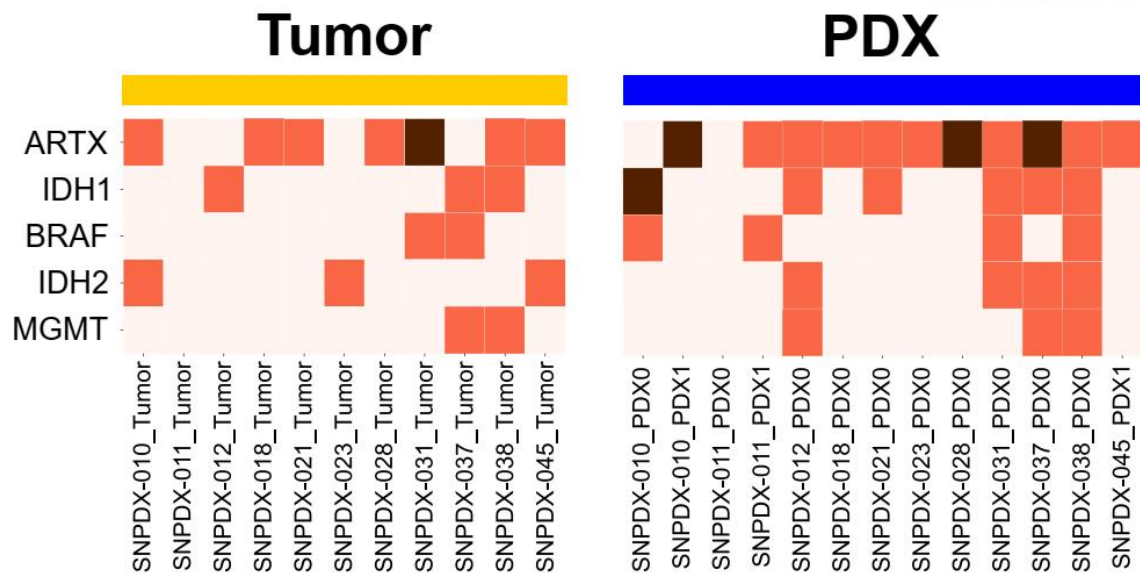


**Figure 2.5. Mutation profile of previously known genes linked to the development of brain tumors.**

The list of genes was acquired from the COSMIC database, and the Ensembl VEP projected that detrimental somatic mutations would have a 'MODERATE' or 'HIGH' effect. Genes with mutations that have a HIGH impact are highlighted in a deeper color.

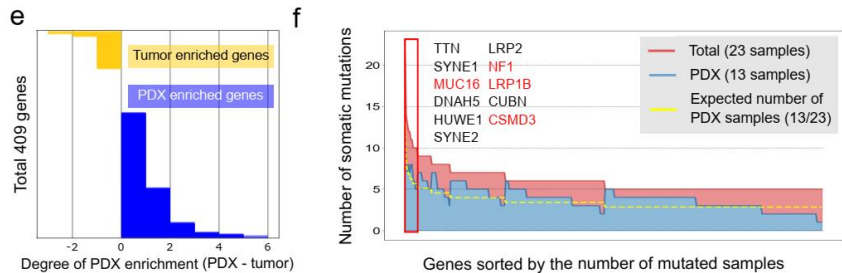


**Figure 2.6. The 30 most often mutated genes found in tumors and PDX samples. We only examined harmful mutations with a significant effect on protein function modification.** (a) COSMIC census genes that are overrepresented in cancers. (b) COSMIC census genes enriched in PDX samples. (c) The top 30 ranked mutant genes out of 217 tumor-enriched mutated genes, (d) The top 30 ranked mutated genes out of 1,610 PDX-enriched mutated genes. (e) We identified 409 genes with high-impact mutations that were enriched in PDX samples (blue) or primary tumors (yellow) and displayed the number of samples with these mutant genes using a bar graph. Cancer genes with deleterious mutations were frequently found in tumors and PDX samples. The yellow line indicates the expected number of PDX samples. This amount is less than the actual number of PDX samples containing mutant genes (blue region), showing that these genes are overrepresented in PDX samples. List of genes altered in more than 10 samples (red box). Genes that have been annotated as COSMIC census genes are colored red.

### **2.3.5. Gene mutations associated with histone methylation and cilium are likely enriched in PDX samples.**

If brain tumor-specific mutations are enriched in PDX samples, we hypothesized that tumor-associated gene mutations not found in the original tumor would also be enriched in the PDX sample. To examine enriched mutant gene sets in tumor and PDX samples, we compiled a list of enriched gene sets for each sample type. Probably as a result of the heterogeneity of tumor samples, there was a greater variety of genes with harmful mutations.

While 761 genes were identified as tumor-enriched, the GO term analysis of the enriched mutant gene set of original tumors revealed no meaningful terms. This was likely due to the low sensitivity of the assay, which was caused by tumor heterogeneity. GO keywords associated to histone methylation, cilium movement, and microtubule depolymerization were significantly overrepresented among the 1,610 genes enriched in PDX samples (Fig. 2.7). These genes corresponded to those found in a recent study involving genes implicated in ciliary or flagellar motility <sup>69</sup>. These PDX-specific alterations involving histone methylation, cilium movement, and microtubule depolymerization were not discovered in the original tumors and may only be advantageous in the PDX environment. However, as mentioned previously, cancer-related genes have more mutations in PDX samples than in the original tumors; hence, it is also possible that rare mutations associated with malignancies are enriched in PDX samples. However, additional research is necessary to determine if this is genuinely connected to the pathophysiology of brain tumors or to preferred mutation in the PDX environment.

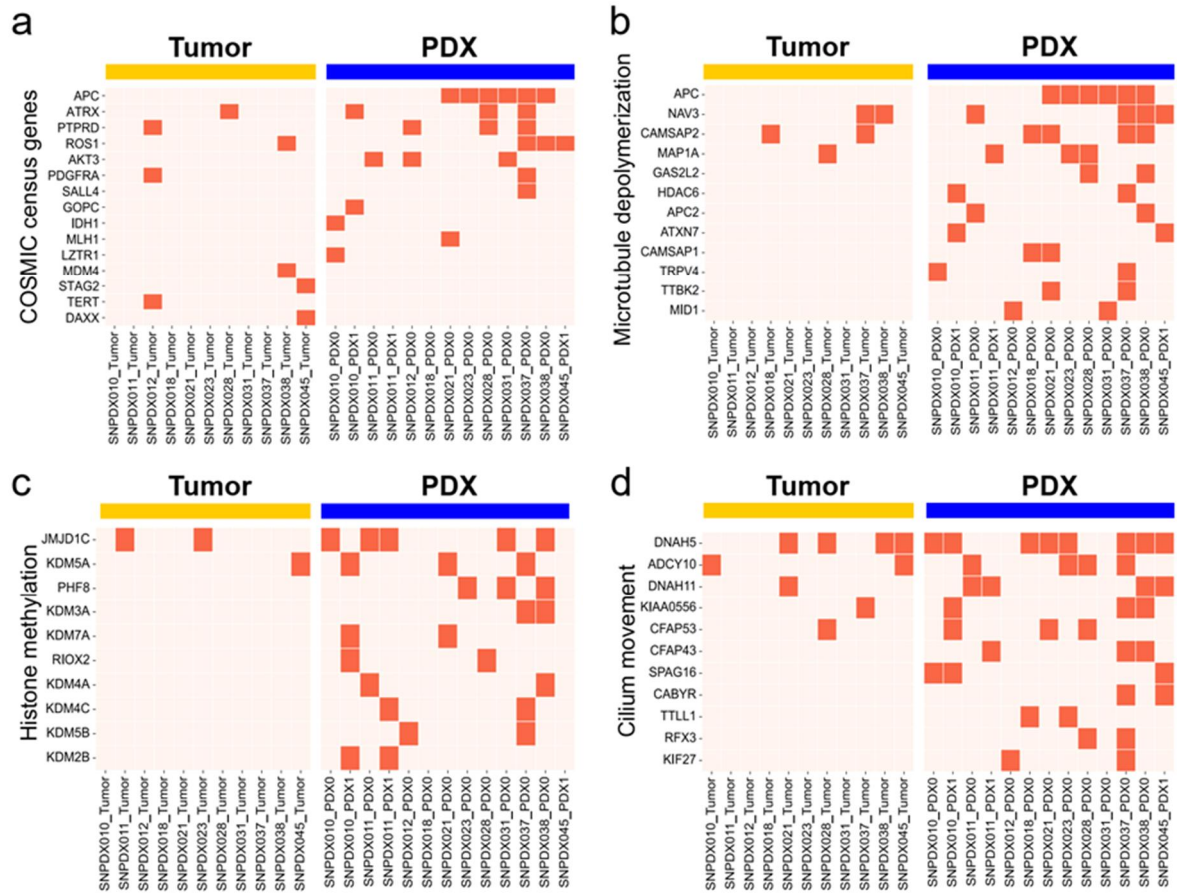


**Figure 2.7. Genes associated with histone methylation and cilia are abundant in PDX samples.** (a) Profile of genes with detrimental mutations in the COSMIC cancer gene census. We only considered genes associated with GBM and CNS malignancies. Among PDX-specific enriched mutant genes, (b) histone methylation (GO:0016571), (c) microtubule depolymerization (GO:0007019), and (d) cilium movement (GO:0003341) genes were highly enriched.

a

Tumor sample	CNS related mutations	Meninges related mutations	COSMIC annotated mutations
SNPDX_010	1	0	151 (6.4%)
SNPDX_011	9	0	191 (6.6%)
SNPDX_012	4	0	189 (6.5%)
SNPDX_018	7	2	165 (6.6%)
SNPDX_021	10	0	206 (5.7%)
SNPDX_023	6	0	205 (5.7%)
SNPDX_028	11	1	250 (5.8%)
SNPDX_031	5	0	123 (6.3%)
SNPDX_037	19	1	398 (9.1%)
SNPDX_038	14	2	348 (8.1%)
SNPDX_045	12	0	338 (5.9%)

b

Tumor sample	PDX	CNS related mutations	Meninges related mutations	COSMIC annotated mutations
SNPDX_010	PDX0	6	0	173 (6.0%)
	PDX1	8	1	326 (5.7%)
SNPDX_011	PDX0	14	0	308 (7.2%)
	PDX1	12	0	337 (7.4%)
SNPDX_012	PDX0	13	2	369 (7.0%)
SNPDX_018	PDX0	10	1	261 (6.7%)
SNPDX_021	PDX0	21	1	529 (6.2%)
SNPDX_023	PDX0	9	2	323 (5.6%)
SNPDX_028	PDX0	10	0	272 (5.5%)
SNPDX_031	PDX0	14	0	253 (6.4%)
SNPDX_037	PDX0	54	2	1476 (8.5%)
SNPDX_038	PDX0	30	2	1139 (8.5%)
SNPDX_045	PDX1	23	3	488 (7.3%)

**Table 2.1. COSMIC database annotated mutations in primary tumor and PDX model.** (a) Central nervous system (CNS), Meninges, all type of cancer related mutations in each original tumor and (b) in PDX model.



a

Tumor sample	TP53 mutation	PDX	TP53 mutation
SNPDX_010	-	PDX0	-
		PDX1	G108V
SNPDX_011	R273G	PDX0	R273G
		PDX1	R273G ,P359S
SNPDX_012	-	PDX0	C238F
SNPDX_018	-	PDX0	-
SNPDX_021	-	PDX0	L206F
SNPDX_023	G59C	PDX0	-
SNPDX_028	Splice_acceptor_variant & Coding_sequence_variant	PDX0	-
SNPDX_031	E28D	PDX0	L29I
SNPDX_037	P316S, R175H	PDX0	E3K, R175H, K386N
SNPDX_038	R175H	PDX0	R175H, R306L, A347T
SNPDX_045	-	PDX1	-

b

Tumor sample	EGFR mutation	PDX	EGFR mutation
SNPDX_010	S1042R	PDX0	-
		PDX1	-
SNPDX_011	Splice_acceptor_variant	PDX0	R832S
		PDX1	-
SNPDX_012	E102K, S655Y	PDX0	G131R, P694H
SNPDX_018	G627*	PDX0	-
SNPDX_021	-	PDX0	S437Y
SNPDX_023	E160*	PDX0	C555*
SNPDX_028	Q188K	PDX0	T354K, R836S
SNPDX_031	P596L	PDX0	P596L
SNPDX_037	H233Y	PDX0	D770N
SNPDX_038	C251*	PDX0	S286N, R999S
SNPDX_045	S286R	PDX1	-

**Table 2.2. TP53 and EGFR status in original tumor and PDX model.** (a) TP53 mutations in each original tumor and PDX model. (b) EGFR mutations in each original tumor and PDX model.

## 2.4. Discussion

Because they can imitate the *in vivo* environment in which cancers grow, PDX models have been widely utilized to study malignancies. Rapid multiplication of tumor cells can enrich cancers in this environment, which can aid in identifying mutations associated with malignancies and studying their properties. However, despite claims that important driver somatic mutations were highly conserved across the original tumors and PDX samples, a systematic investigation of somatic mutations across genomes was not conducted.

Here, the somatic mutation profiles of 13 PDX models derived from ten brain tumor patients and their primary tumors were examined. Even with this small sample size, the discordance of somatic mutations between the original tumors and the PDX samples that were produced from them demonstrated that established PDX models may not replicate the genetic properties of the original tumors. Alternately, inadequate genetic data may have been collected due to the heterogeneity of brain tumors. Therefore, it may be difficult to identify all somatic mutations in both sample types. Recent research indicates that patient-generated explants and glioma sphere lines produced from glioblastoma share genetic similarities<sup>84</sup>. Since the *in vitro* culture selection conditions can alter the heterogeneous tumor population, this method cannot guarantee that the enriched cell population accurately represents the heterogeneous tumor population *in vivo*.

This study may be limited by the small number of total cases and low success rates of PDX models derived from primary brain tumors. In addition, because we utilized a heterotropic PDX model in the mouse flank rather than an orthotropic model in a comparable anatomical location of the brain, our model may not be suitable for simulating the physiological properties of real tumors. Nonetheless, we established pathological histological concordance (Fig. 2.1), matched germline mutations (Fig. 2.3) and somatic mutational signatures (Fig. 2.4) between tumor and PDX tissues; therefore, these resources would be useful for understanding genetic modification in the PDX model.

When we evaluated somatic mutations of genes linked to brain tumor growth, such as ARTX, IDH1, IDH2, BRAF, and MGMT, we discovered that PDX samples contained more mutations than the original tumors (Fig. 5 and Fig. 7a). Moreover, when we evaluated the most frequently altered genes in each group, we found more consistent mutation patterns in PDX samples than in primary tumors (Fig. 6). In addition, the total number of somatic mutations in each sample was compared to the cancer-related mutations listed in the COSMIC database. We discovered that roughly 6% of mutations in each original tumor and PDX sample overlapped with previously identified mutations in the tumor (Supplementary Table 2.1 and Supplementary Figure 2.2). Notwithstanding, the mutation associated with the central nervous system is observed marginally more frequently in the PDX model than in the original tumor, which may support our claim regarding the enrichment of tumor cells in the PDX model.



We hypothesized that PDX samples contained a higher concentration of tumor cells, which would explain why we found more tumor-related somatic mutations in these samples than in the original tumors. Due to the limited sequencing depth and small sample size of this study, however, we were unable to confirm this hypothesis.

We examined the somatic mutations of TP53<sup>85</sup> and EGFR<sup>86</sup>. Two genes undergo frequent mutations in glioma (Supplementary Table 2.2). TP53 is a well-known tumor suppressor that plays a key role in cellular stress signaling and is the most prevalent human cancer suppressor<sup>87</sup>. TP53 mutation is characteristic of the early development of low-grade astrocytic glioma in particular<sup>88</sup>. With the exception of two samples in this study (SNPDX-018 and SNPDX-045), TP53 mutations are observed in the majority of original tumors and PDX samples (Supplementary Table 2.2). The mutations R273G in SNPDX-011 and R175H in SNPDX-037/038 were observed in both the original tumor and the PDX. On the other hand, the EGFR mutation patterns of the original tumor and the PDX were quite distinct (Supplementary Table 2.2). 0.39 percent of all WHO grade III glioma patients and 0.25 percent of all glioblastoma patients carry the P568L mutation<sup>89</sup> that was observed both primary tumor and PDX present in SNPDX-031. Although known tumor-related mutations are enriched in the PDX, putative driver mutation patterns on TP53 and EGFR were not identical between the original tumor and the PDX. It is unclear, however, whether this is due to the limited detectability of rare mutations in this study due to low sequencing depth or clonal selection of these mutations in the heterotrophic PDX model.

Previous research demonstrated the similarity of genome-wide functional characteristics, such as copy number variations and patterns of gene expression, between PDX samples and the original tumors. In addition, we confirmed that the mutational signatures of each PDX sample matched those of their respective primary tumors. Moreover, two samples (SNPDX-037 and SNPDX-038) retained the mutational signatures resulting from TMZ treatment. According to our records (Supplementary Table 1), patients SNPDX-028 and SNPDX-045 had also been treated with TMZ, but we did not observe the SBS11 signature in these samples. These patients had not been treated with TMZ within a year prior to biopsy, so we hypothesized that the SBS11 signature associated with TMZ therapy was diminished. This indicates that our PDX models can be utilized to replicate the mutational process of primary tumors.

PDX samples were enriched with gene mutations associated with histone methylation and ciliary function. Recent research revealed that glioma stem cells (GSCs) derived from a GBM patient suppressed ciliogenesis, resulting<sup>90</sup>. GSCs began to differentiate and escaped the self-renewal process following the restoration of cilia. Therefore, the deleterious mutations associated with ciliogenesis found in our PDX samples may be advantageous for tumor cells by inhibiting differentiation and promoting self-renewal for proliferation. Another study found that glioblastoma-initiating cells (GICs) exhibited stem cell-like chromatin characteristics and a loss of H3K9me3<sup>91</sup>. Histone demethylase knockdown increased the H3K9me3 level, which induced apoptosis in GICs but not in differentiated cells. These results suggest that the deleterious mutations associated with histone methylation in PDX samples may aid in the maintenance of GICs during the establishment of PDX.

Although our study demonstrated that a subpopulation of tumor cells may increase in our PDX models due to in vivo growth-promoting properties, additional research is necessary to determine whether the mutations enriched in PDXs are significant in the original brain tumors due to their associations with tumor-initiating cells or tumor stem cells. Alternately, these mutations may enhance cellular fitness in the xenograft environment, regardless of their roles in tumor progression. Analysis of additional PDX models, paired primary tumor cell models, and single-cell level data will clarify how to utilize and interpret the genetic characteristics of PDX tumor models.

### 3. Characterization and integrative omics analysis of patient-derived colorectal cancer organoids

#### 3.1. Introduction

Colorectal cancer (CRC) which could be called colon cancer and rectal cancer is the third most common and second most common cause of cancer death in the world<sup>92</sup>. Numerous mutations occur on genes such as WNT, RAS/MAPK, PI3K, TGF- $\beta$ , altering the WNT pathway and mTOR signaling, as well as on tumor suppressors such as FBXW7, PTEN, CTNNB1, SMAD4, ARID1A, FAM123B, DCC, RET and TGFBR2<sup>93,94</sup>. Epigenetic alterations, such as DNA methylation and histone modifications, play a role in the initiation and progression of colorectal cancer<sup>95</sup>. Several CRC tumors exhibit microsatellite instability (MSI) as a result of the deficiency of essential enzymes of the DNA mismatch repair (MMR) system (i.e. MLH1, MSH2, MSH6 and PMS2)<sup>96</sup>. Due to the high heterogeneity of CRC, numerous studies exploring novel potential biomarkers with prognostic and predictive value for this disease have been conducted in recent years. In this context, genes associated with cell survival and DNA repair pathways have also been linked to CRC susceptibility. In addition to high penetrance mutations of genes involved in hereditary colon cancer, such as APC, MUTYH, and those encoding proteins of the MMR, TP53, and MDM2 families, polymorphisms could be considered potential CRC risk factors<sup>97</sup>.

In 2017, the Food and Drug Administration (FDA) approved the first immune checkpoint inhibitor (ICI) (nivolumab) for colorectal cancer<sup>98</sup>. Patients with stage IV colorectal cancer (deficient mismatch repair) can now be considered with ICIs even if the tumor develops after standard chemotherapy. Deficient mismatch repair (dMMR)/microsatellite instability (MSI) can be used as a biomarker to identify patients who may benefit from immunotherapy, according to a number of studies<sup>99,100</sup>. However, only 5% of metastatic CRC patients are dMMR/MSI-High, and a portion of these patients do not respond to immunotherapy<sup>101</sup>. To expand the population of CRC patients who respond to immunotherapy, it is necessary to search for more effective biomarkers. While researchers have identified a number of biomarkers<sup>102–105</sup>, such as programmed cell death ligand 1 (PD-L1) expression, tumor infiltrating lymphocytes (TILs), POLE mutation, and tumor mutation burden (TMB), companion diagnostics using these biomarker has not yet been refined.

Long ago, cell lines were used to increase our understanding of the origin of CRC and to investigate new treatments for the disease. However, the translation to humans, such as drug response, is frequently limited due to the fact that cell lines do not accurately represent the original tumor characteristics: clinical tumors lack the heterogeneity observed in cell lines<sup>106</sup>. In contrast to in vivo conditions, cell lines are isolated from the tumor microenvironment (TME) in which cancer originates and develops, and 2D-cultured cells lose their polarity and have equal access to various compounds in

the medium<sup>107</sup>. Although the use of animal models has helped overcome some of these limitations, the failure rate of new cancer drugs in clinical trials continues to be extremely high<sup>108</sup>, probably because animal models do not accurately represent human physiology<sup>109</sup>. In contrast, patient-derived xenografts in animal models have attracted increased interest because they are typically accompanied by their TME and more closely resemble the original tumor in terms of growth, progression, and metastatic potential<sup>110</sup>. In distinct, accumulating evidence demonstrated that patient-derived colon organoids (PDCOs) exhibited the similar genomic and transcriptomic features as their primary tumors can be used for high-throughput drug screening to predict response to therapy<sup>111–115</sup>. Therefore, it can be applied to the companion diagnosis of colorectal cancer patients such as identifying the novel biomarkers or predicting response to certain drug by characterizing the features of CRC patient derived organoids.

Here, I characterized the CRC patient-derived organoids based on integrated multi-omics using genomic, transcriptomic features and clinical information to group CRC patients according to their tumor characteristics. Existing biomarkers related to hypermutation, or drug response of several organoids were identified using the genomic characteristic, and colorectal cancer patients were classified into six groups based on whether they shared the same mutation. In the same way, CRC cell lines matching each group were identified, and the reported drug response of cell lines allowed for the prediction of the cell lines' reactivity with other drugs. CMS classification was able to identify the CMS subtype for 17 out of 21 organoids using gene expression, allowing similar organoids to be distinguished from other organoids within the same group. Through examining the difference in drug response between organoids with similar characteristics and other organoids, it will be possible to aid in patient-specific drug selection. In addition, XGboost model, a machine learning technique, was used to identify genes related to drug response or metastasis by classifying four pairs of organoids with recurrent or metastasis after being treated first-line therapy in clinical data from the rest of the organoids. These genes would be verified in further drug response experiments using the CRC organoids.

## 3.2. Materials and methods

### 3.2.1. Organoid culture

The matched human colorectal normal and tumor tissues were obtained from each patient who underwent surgery at the Asan hospital (IRB protocol number:XXX). Organoid establishment and culture were performed by Hye-jin Jeong from mTEN lab (Prof. Tae-Eun Park) in UNIST. To generate human colorectal normal organoids (CNOs), human colorectal normal tissues were washed in Dulbecco's phosphate-buffered saline (DPBS, Welgene) with 1X P/S antibiotics (Penicillin Streptomycin, Gibco) and pinned on Polydimethylsiloxane (PDMS)-coated plates. From whole tissue, the mucosa containing colonic crypts was dissected. After repining the colon with the lumen facing up, the mucus layer was scraped away with curved forceps. To isolate colonic normal crypts containing colonic stem cells from the tissue, the mucosa was treated for 20 minutes at 4°C with 0.5 mM EDTA chelation buffer (2% D-sorbitol, 1% Sucrose, 1% Bovine serum albumin, and 1X P/S in DPBS). The mucosa was washed with ice-chelation buffer without EDTA and the crypts were removed from the tissue using curved forceps. The isolated colonic crypts were placed in advanced DMEM/F12 basal media supplemented with 5% fetal bovine serum (FBS, Merck) and centrifuged at 250 x g for 5 minutes at 4°C. The colonic crypts were suspended in Matrigel (Corning), which was then gelatinized for 30 min at 37°C and filled by culture media. The human colorectal tumor tissues were then vigorously washed in DPBS with additional antibiotics (Primocin and Plasmocin, InvivoGen) and P/S to generate human colorectal tumor organoids (CTOs). These fragments were suspended in the digestion buffer (1.5 mg/ml collagenase type II and 20 g/ml Hyaluronidase in advanced DMEM/F12 with 1X P/S) for one hour. To terminate the enzymatic reaction, the digestion buffer containing tumor fragments was mixed with 5% FBS and pipetted vigorously with a serological pipette tip coated with chelation buffer. The isolated clusters of tumor stem cells were encapsulated in Matrigel and cultured in media for CTO generation. In Table 3.1, information on media components is provided.

No.	Components	Manufacturer	CNO	CTO
1	Advanced DMEM/F12	Gibco	+	+
2	Primocin (100 µg/ml)	InvivoGen	+	+
3	Plasmocin (5 µg/ml)	InvivoGen	+	+
4	GlutaMAX (2 mM)	Gibco	+	+
5	HEPES (10 mM)	Welgene	+	+
6	Nicotinamide (10 mM)	Sigma	+	+
7	N-acetyl-L-cysteine (1.25 mM)	Sigma	+	+
8	B27 supplement (1X)	Gibco	+	+
9	EGF (50 ng/ml)	Peprtech	+	+
10	A83-01 (500 nM)	Biogems	+	+
11	SB202190 (10 µM)	Biogems	+	+
12	Gastrin (10 nM)	Sigma	+	+
13	Prostaglandin E2 (10 nM)	Peprtech	+	+
14	Y27632 (10 µM)	TOCRIS	+	+
15	L-WRN conditioned media (50%)	Lab-made	+	-
16	FBS (5%)	Merck	-	+
17	Noggin (100 ng/ml)	Peprtech	-	+
18	R-spondin1 conditioned media (10%)	Lab-made	-	+

**Table 3.1. The elements list of organoid culture media.**

### **3.2.2. Whole Genome Sequencing (WGS)**

Genomic DNA was extracted using Quick-RNA Mini-prep Kit (Zymo Research). The Variant Effect Predictor (VEP) of Ensembl (version 101)<sup>75</sup> was applied to predict the impact of somatic mutations, and genes whose mutations were predicted to have a significant effect on proteins were extensively studied. Cancer census genes and other genes associated with CRC tumors were extracted from the COSMIC database (version 94)<sup>76</sup>.

### **3.2.3. Mutational signature analysis.**

The somatic mutations of each sample were analyzed utilizing the COSMIC MutSig reference database<sup>77</sup> and the SigProfiler software for single base substitution (SBS), double base substitution (DBS), and insertion-deletion (ID) signatures (version 3.2 - March 2021)<sup>78</sup>.

### **3.2.4. RNA-seq**

Total RNA from crypts and organoids was isolated using Quick-RNA Mini-prep Kit (Zymo Research). For Pearson correlation analysis and plotting the expression, counts per million mapped reads (CPM) was used.

### **3.2.5. CMS classification**

CMS classification was performed using CMScaller (v0.9.2) R/Bioconductor packages.

### 3.3. Results

#### 3.3.1. Four of colorectal cancer organoids shows high tumor mutational burden

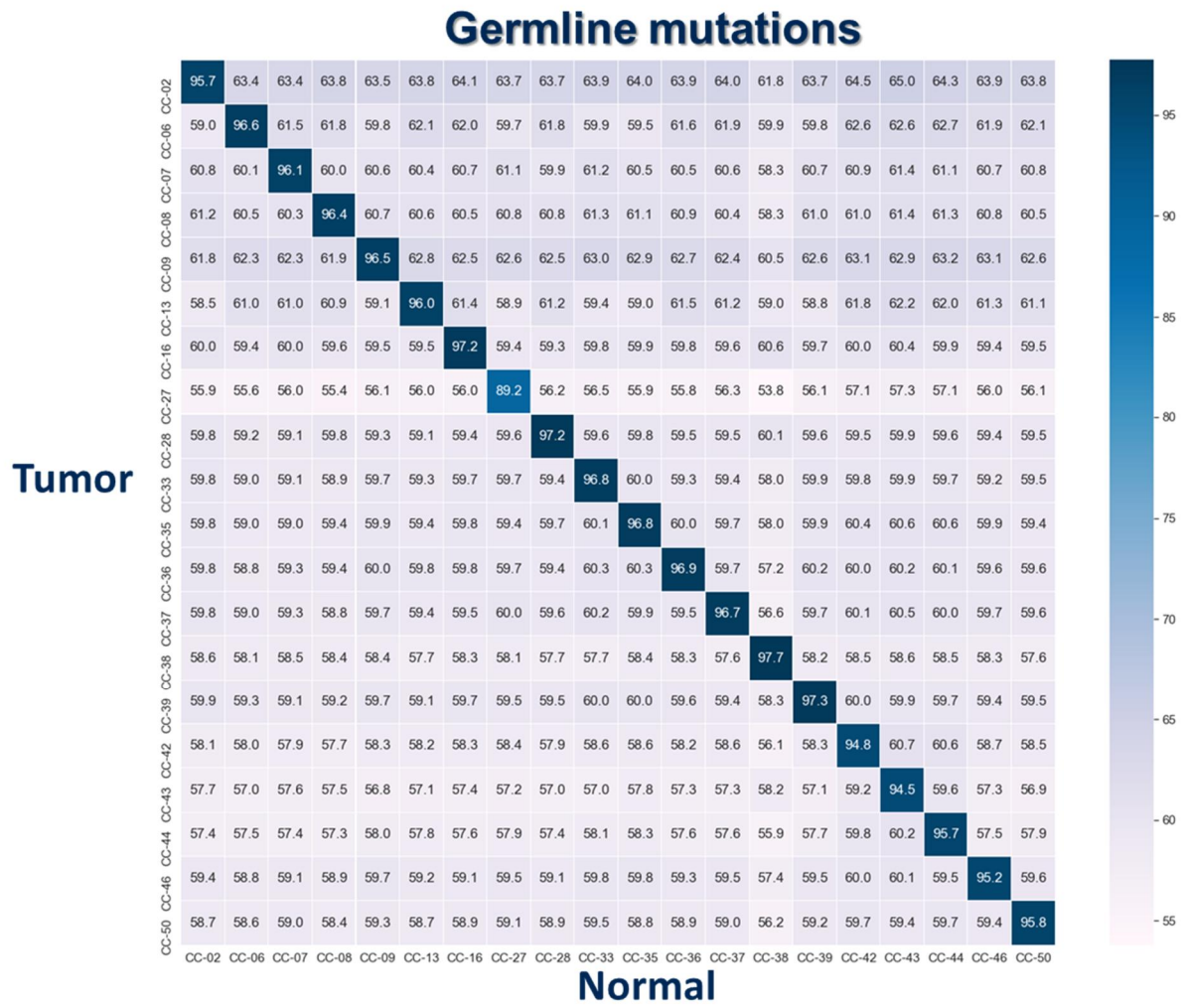
The human colorectal tumor and normal tissues from CRC patients were obtained from Asan hospital. Among them, twenty-three pairs of tumor and normal organoid derived from colorectal cancer patients were established by Hye-jin Jeong in UNIST. Among them, I performed whole-genome sequencing of these Twenty-three CRC organoid pairs and the gene expression of twenty-one pairs of CRC organoids was analyzed using RNAseq. There are four CRC patients with no adjuvant chemotherapy (adj CTx) record in clinical information and five CRC patients who experience the recurrence or metastasis (Table 3.1). To test that the normal and tumor organoids were well established from each patient, the germline mutation of twenty-three pairs of normal and tumor organoids was compared. We included only homozygous germline variations in this study to decrease the impact of variant calling technique and sequencing errors. It was observed that the germline mutation of normal and cancer organoids obtained in the same patient was 95% or more consistent, and the results were approximately 60% consistent with other patients (Supplementary Fig 3.1).

Next, I checked the number of somatic mutations, the deleterious mutations, the corresponding genes and the COSMIC annotated genes as colorectal cancer related genes (Table 3.2). It was confirmed that CC-27, CC-38, CC-41 and CC-50 have 100 times more mutations than other CRC samples. Tumor mutation burden (TMB) refers to the number of nonsynonymous mutations in cancer cells, which can be determined using next-generation sequencing (NGS) or whole-exome sequencing (WES). The greater the TMB, the greater the type and quantity of neoantigens produced by tumor cells, and the greater the likelihood of immune recognition<sup>116</sup>. Recent study exploring the TCGA database showed that CRC cases carrying mutations in one of the 13 most frequently mutated DNA repair genes (ATM, MRCA2, MSH6, MLH1, LIG1, POLE, BRCA1, MSH2, SLX4, FANCM and FANCD2) exhibited high tumor mutational burden<sup>117</sup>. There is growing evidence that tumors with a high mutational burden may be more responsive to immune checkpoint inhibitor<sup>118</sup>. So, I grouped the four hypermutated patients into tumor mutation burden high (TMB-H) group and other 19 patients into tumor mutation burden low (TMB-L) group.



Patient Code	Whole Genome Sequencing	RNAseq	Clinical note
CC-02	○	○	
CC-06	○	○	No adj CTx
CC-07	○	○	
CC-08	○	○	No adj CTx
CC-09	○	○	Liver metastasis
CC-13	○	○	
CC-16	○	○	Lung metastasis
CC-27	○	○	
CC-28	○	○	
CC-33	○	-	Liver metastasis
CC-35	○	○	
CC-36	○	-	
CC-37	○	○	No adj CTx
CC-38	○	○	
CC-39	○	○	
CC-41	○	○	No adj CTx
CC-42	○	○	Recurrence
CC-43	○	○	
CC-44	○	○	Lung metastasis
CC-46	○	○	
CC-47	○	○	
CC-48	○	○	
CC-50	○	○	

Table 3.2. A table of CRC organoid samples used in integrative multi-omics.



**Supplementary Figure 3.1. The overlap proportion of germline mutations between normal organoids and tumor organoids.**

Patient Code	Somatic mutations	Deleterious mutations	# of mutated genes	CRC related genes
CC-02	60,141	252	201	3
CC-06	31,240	146	134	4
CC-07	52,188	236	215	5
CC-08	60,356	286	255	4
CC-09	42,097	215	184	4
CC-13	43,607	193	179	6
CC-16	22,773	151	108	5
<b>CC-27</b>	<b>1,745,917</b>	<b>2,518</b>	<b>2,148</b>	<b>19</b>
CC-28	24,634	111	100	2
CC-35	32,120	173	146	7
CC-37	38,541	202	171	5
<b>CC-38</b>	<b>1,128,956</b>	<b>2,900</b>	<b>2,447</b>	<b>18</b>
CC-39	14,989	117	91	1
<b>CC-41</b>	<b>1,459,157</b>	<b>1,756</b>	<b>1,552</b>	<b>9</b>
CC-42	29,149	159	140	3
CC-43	54,123	271	237	6
CC-44	27,465	176	161	3
CC-46	40,658	164	147	4
CC-47	56,297	263	240	3
CC-48	36,524	181	158	6
<b>CC-50</b>	<b>1,497,666</b>	<b>6,677</b>	<b>4,690</b>	<b>23</b>

**Table 3.3. The number of somatic mutations represent high tumor mutation burden (TMB-H).**

The CRC organoid samples that show high tumor mutation burden were highlighted on red.

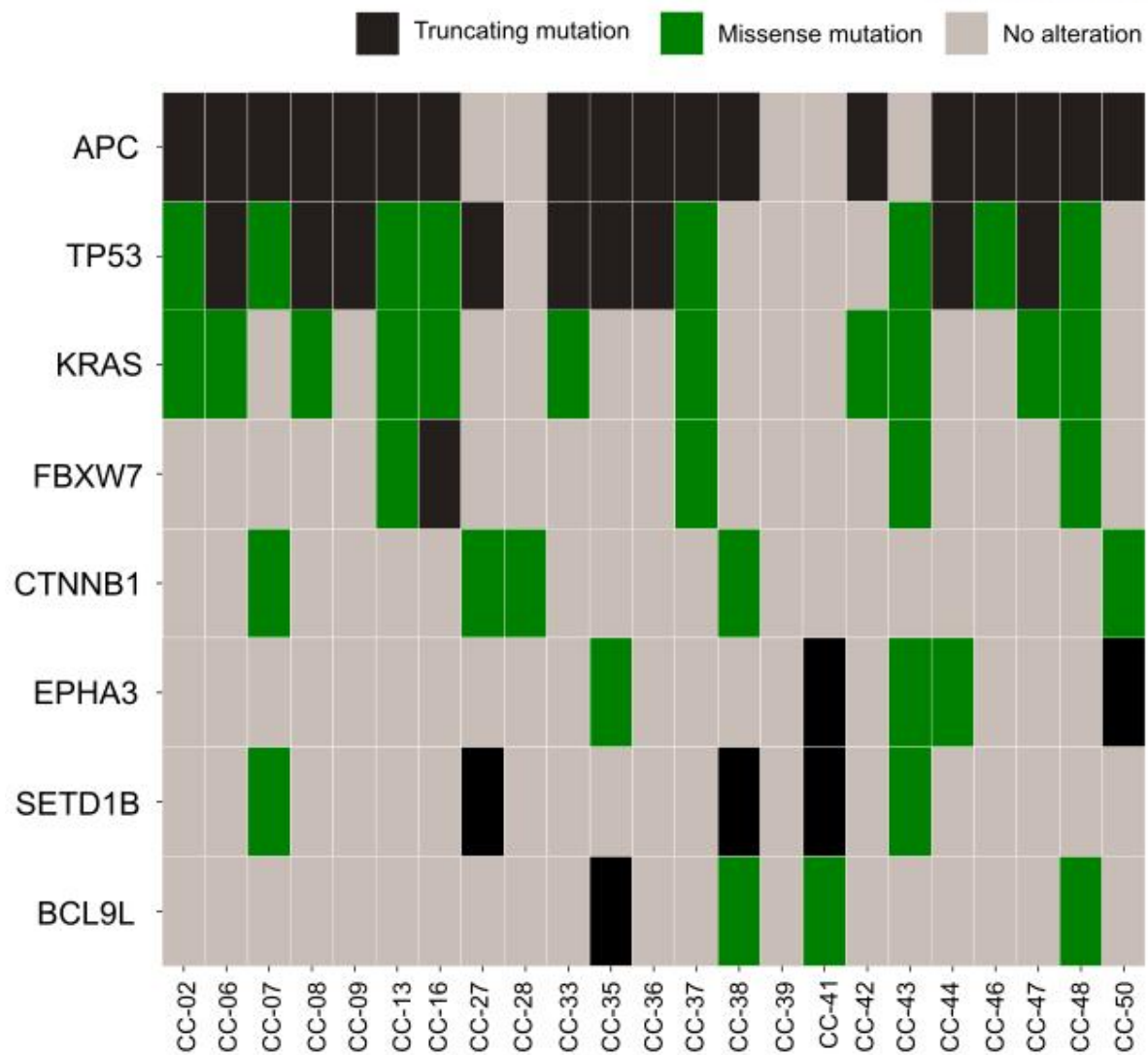


**Figure 3.1. Top-ranked genes with high mutational frequency among our CRC organoid samples.**

### **3.3.2. COSMIC SBS mutational signature analysis reveals POLE exonuclease domain mutation in CC-50.**

To analyze patient-specific mutant causes and mutational patterns in the mutation process of CRC organoids, COSMIC mutational signature analysis using somatic mutations of CRC organoids was performed (Fig 3.2). While similar mutation patterns were observed in most organoids on SBS mutational signatures, but the three tumor organoids (CC-27, CC-38, CC-41) in TMB-H group except CC-50 showed dominant SBS44 signature unlike the other tumor organoids in TMB-L group. Because SBS44 signature was one of the signatures related to defective mismatch repair, the main cause of hypermutated feature of these three tumor organoids was considered as mismatch repair defects. The most exposed signatures in CC-50 tumor organoid were SBS28 and SBS10a signatures. The mutational cause about SBS28 was still unknown but the SBS10a signature has been observed to generate a high number of somatic mutations (>100 mutations per millions of base pairs), and samples with this signature have been called hypermutators. Even, the polymerase epsilon (POLE) exonuclease domain mutations were reported as main mutational cause of SBS10a signature. I found that CC-50 have a POLE P286R mutation that would attributed to a hypermutating phenotype independently of mismatch repair deficiency<sup>119</sup>. It is observed that other 3 CRC organoids (CC-27, CC-38, CC-41) of TMB-H group shows higher exposure on seven types of SBS mutational signatures related to mismatch repair defect than other CRC organoids. In conclusion, CC-50 organoid was considered to be hypermutated due to the POLE P286R mutation as the main driver mutation and the mutational cause of other three organoids (CC-27, CC-38, CC-41) in TMB-H group was seen as the mismatch repair defects.

### **3.3.3. CRC tumor organoids and CRC cell lines were subdivided by shared deleterious mutations.**

While the mutational frequency of genes except TP53, APC, KRAS, FBXW7 was not enough high to group the CRC patient through mutated gene profiles, I hypothesize that the colorectal cancers who have same mutation site would share similar mutational process and phenotype such as drug response. Based on the hypothesis, CRC tumor organoids were divided by five groups according to their mutations shared with each other (Fig 3.3). Interestingly, the TMB-H group except CC-50 that have a POLE exonuclease domain mutation was well separated from other organoids (annotated as D group). Even though the CC-50 organoid shares the APC R1114\* truncation mutation with some of CRC organoids in A group, it would be classified as the A-1 group because the POLE P286R mutation was considered as the main driver mutations in mutational signature analysis. Five of CRC cell lines (HCT116, SNU1040, SNU81, SW620, SW480) were also classified into each organoid group in the same way, which can be used to predict the drug reactivity of organoids based on the drug reactivity of the reported cell lines (Fig 3.3).

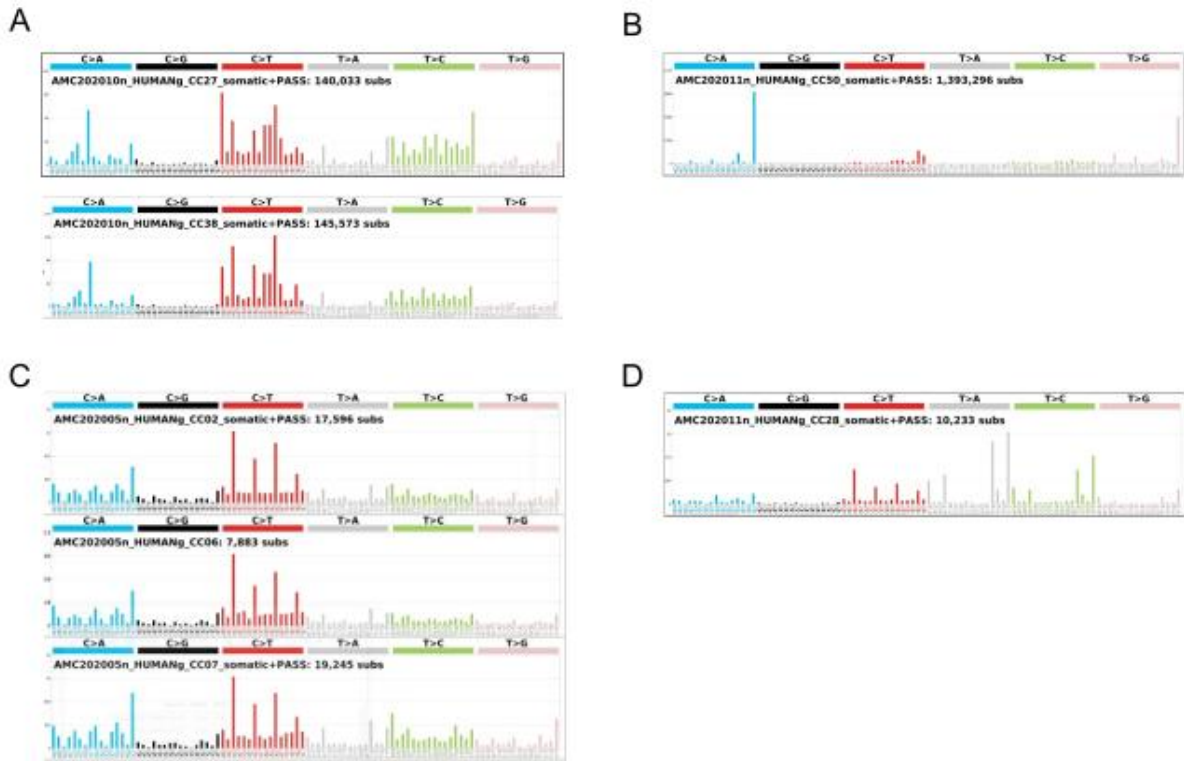


**Figure 3.2. Representative SBS mutational patterns in CRC tumor organoids.** (A) SBS mutational signatures in TMB-H groups except CC-50. (B) SBS mutational signature of CC-50 organoid that have POLE exonuclease domain mutation in TMB-H group. (C) SBS mutational signature of most CRC organoids in TMB-L group. (D) SBS mutational signature of CC-28 organoid differ from that of other organoids in TMB-L groups.

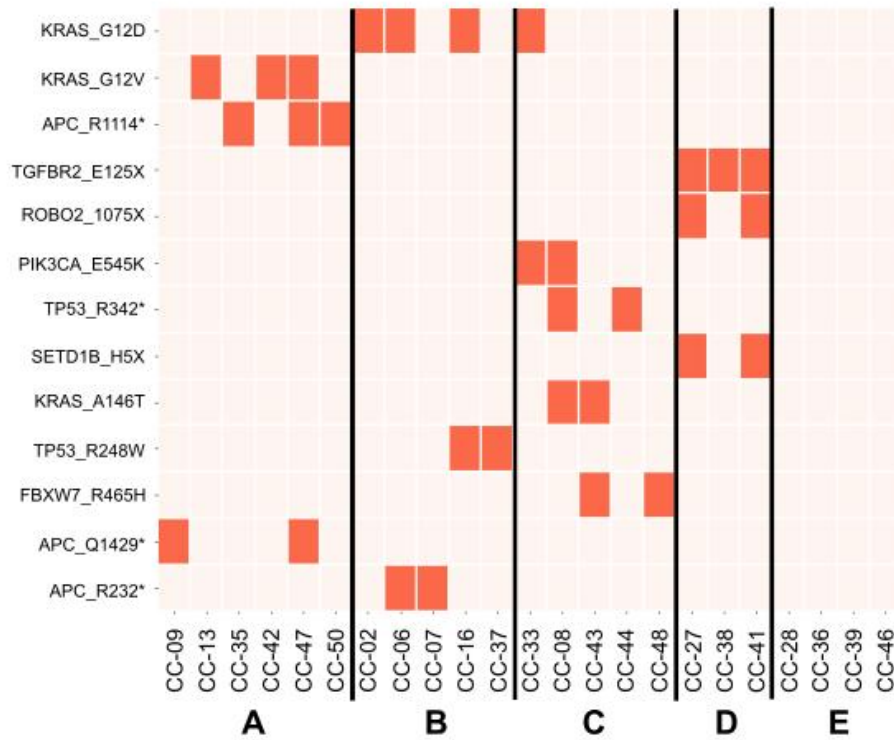


#### **3.3.4. Colorectal cancer organoid classification with gene expression.**

In addition to genomic analysis, transcriptional analysis of 21 pairs of organoids was also performed. The expression level was normalized by counts per million (CPM). To compare the gene expression profiles of CRC tumor and normal organoids, the relationship between each normal and tumor organoid was presented using Pearson correlation coefficient on heatmap (Supplementary Fig 3.2). While the expression levels of normal organoid highly correlated with each other, the profile of gene expression in tumor organoids was heterogeneous. The consensus molecular subtypes (CMS) is a conventional classification system that combines six classifications based on the comprehensive gene expression levels of stage I–IV CRCs<sup>120–125</sup>. Twenty one CRC organoids were grouped through the consensus molecular subtype (CMS) classification using CMScaller<sup>126</sup>. Four organoids of CMS1, seven organoids of CMS2, three organoids of CMS3, three organoids of CMS4 and four organoids were not classified (Fig 3.4B). It can be used to distinguish similar organoids from other organoids within the same group of genetic feature-based classification (Fig 3.4D), and it will be used to select and interpret organoids to be used in the drug response test.



A



B

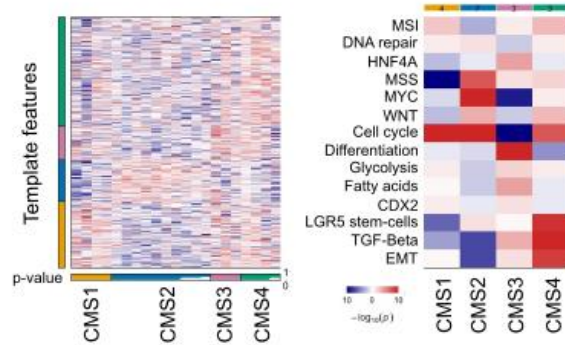
	A	B	C	D	E	A-1
<b>Tumor Mutation Burden</b>	TMB-L	TMB-L	TMB-L	<b>TMB-H</b>	TMB-L	<b>TMB-H</b>
<b>MSI status</b>	MSS	MSS	MSS	<b>MSI</b>	MSS	MSS
<b>Candidate driver genes</b>	APC/ KRAS	TP53/ KRAS/APC	KRAS/ FBXW7/TP53	SETD1B/ TGFBR2	-	POLE P286R
<b>Samples</b>	CC-09	CC-02	CC-08	CC-27	CC-28	CC-50
	CC-13	CC-06	CC-43	CC-38	CC-36	
	CC-35	CC-07	CC-44	CC-41	CC-39	
	CC-42	CC-16	CC-48		CC-46	
	CC-47	CC-33	CC-33			
		CC-37				

**Figure 3.3. A novel CRC organoids classification using shared deleterious mutations.** (A) CRC organoids were subdivided by five groups using shared mutated sites. (B) A table of CRC patients grouped according to their genetic characteristics.

A

CMS1	CMS2	CMS3	CMS4	N/A
CC-27	CC-06	CC-16	CC-37	CC-02
CC-41	CC-07	CC-28	CC-38	CC-08
CC-43	CC-09	CC-39	CC-42	CC-13
CC-50	CC-35			CC-47
	CC-44			
	CC-46			
	CC-48			

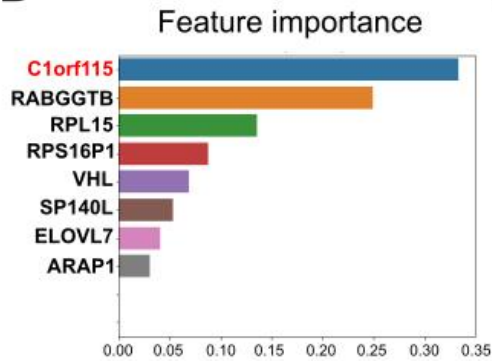
B



C

	A	B	C	D	E	F	G
Tumor Mutation Burden	TMB-L	TMB-L	TMB-L	<b>TMB-H</b>	TMB-L	<b>TMB-H</b>	<b>TMB-H</b>
MSI status	MSS	MSS	MSS	<b>MSI</b>	MSS	MSS	<b>MSI</b>
Candidate driver genes	APC/ KRAS	TP53/ KRAS/APC	KRAS/ FBXW7/TP53	SETD1B/ TGFB2	-	POLE P286R	POLE
Samples	CC-09	CC-02	CC-08	CC-27	CC-28	CC-50	-
	CC-13	CC-06	CC-43	CC-38	CC-36		
	CC-35	CC-07	CC-44	CC-41	CC-39		
	CC-42	CC-16	CC-48		CC-46		
	CC-47	CC-33	CC-33				
		CC-37					

D



F

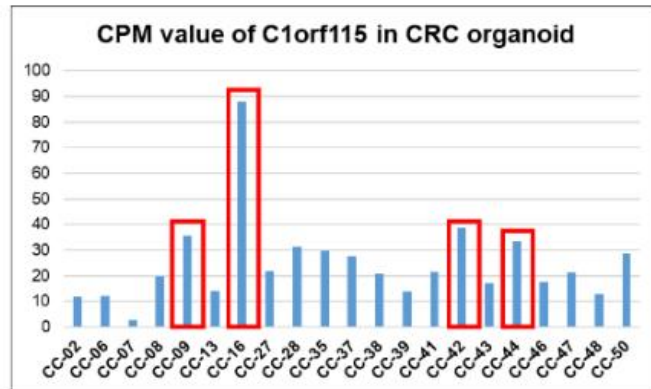
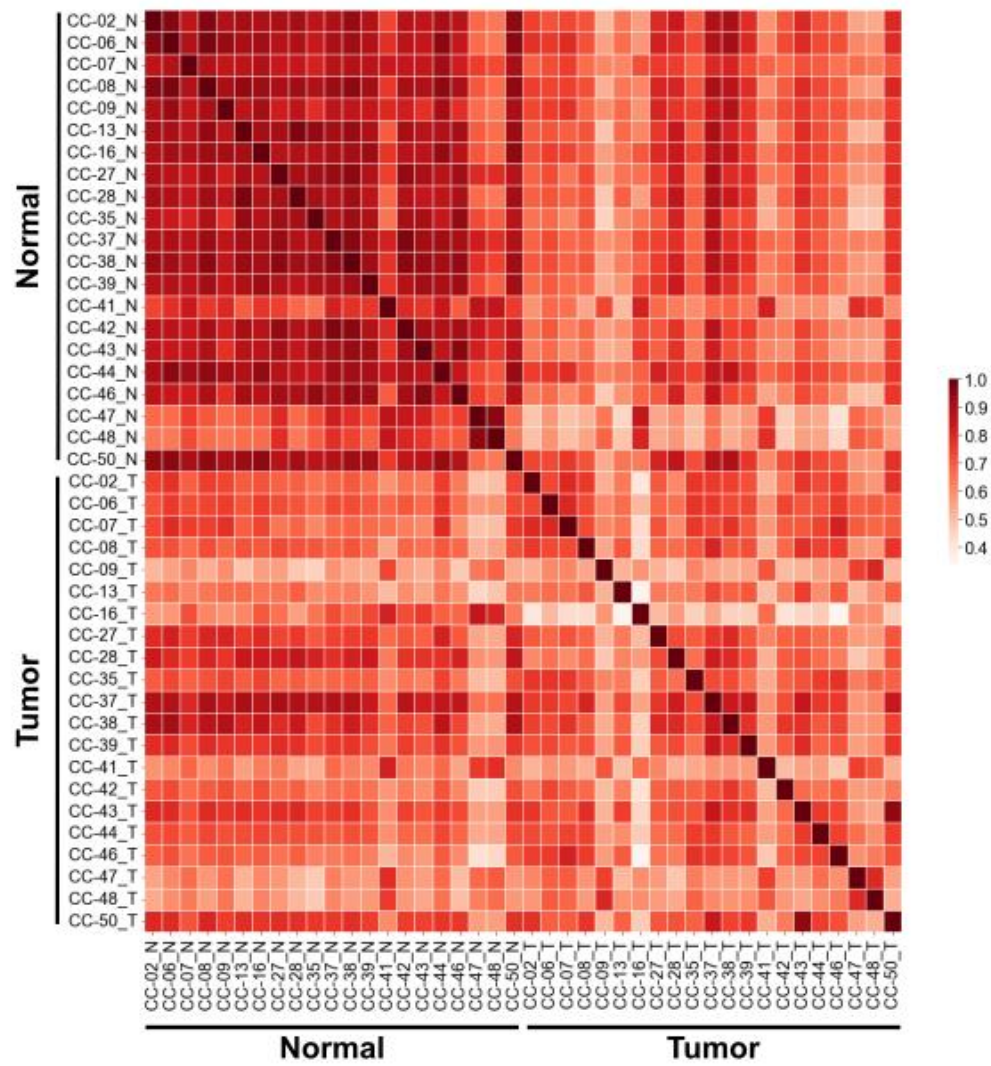


**Figure 3.4. CMS classification and feature extraction using gene expression of CRC organoids.** (A) A table of CRC organoids classified by CMS classification. (B) CMS marker gene and related-pathway expression profiles of CRC organoids (C) Genetic classification was further subdivided in combination with CMS classification. (D) Top eight genes that have high feature importance when differentiating between patients with recurrence or metastasis and the others using XGboost model. (F) Four CRC organoids that established from the patients who had recurrence or metastasis have relatively high expression of C1orf115.

### **3.3.5. Feature selection in the fold change of expression compared to normal reveals C1orf115, MKRN2.**

Through clinical data, it was confirmed that recurrent or metastasis occurred after the treatment of first-line therapy in four patients. To interpret the clinical information and transcriptomic data jointly, the XGboost model was used to calculate the feature importance for classifying the four organoids with recurrent or metastatic disease from the remaining organoids, using gene expression level as a feature. When the expression value of the CRC tumor organoid is set to feature, eight genes have been found to contribute to distinguish the four CRC organoids originated from the patients who experienced the recurrence or metastasis from other CRC organoids. C1orf115, which regulates drug efflux by physically interacting with the major drug exporter ABCB1/MDR1<sup>127</sup>, ranked as the most important gene for a given gene expression level of tumor organoid (Fig 3.4D). It is necessary to determine whether the drug response of organoids differs when C1orf115 is inhibited. Next, changes in the gene expression level of CRC organoids compared to normal organoids can also be the feature of CRC cancer. I set the fold change that was calculated from the expression level of tumor organoid divided by the expression level of normal organoid as a feature, nine genes were ranked with high feature importance. Among them, MKRN2, which prevents migration and invasion of non-small-cell lung cancer (NSCLC)<sup>128</sup> and controls the proliferation and migration of human neuroblastoma<sup>129</sup>, was the most highly ranked gene (Supplementary Figure 3.3).



Supplementary Figure 3.2. Heatmap shows the gene expression profiles of normal and CRC organoids.

### 3.4. Discussion

Colorectal cancer (CRC) is the prototypical cancer caused by aberrant WNT signaling activation in humans<sup>93,130</sup>. Wnt3a is a vital morphogen in organoid cultures because WNT signaling is essential for maintaining organoid stemness; however, because WNT is hyperactive in the majority of CRCs, the normal organoid culture media contains WNT, whereas the tumor organoid culture media does not contain WNT to filter out normal cells. To determine whether there was a difference in gene expression based on media condition, we compared the gene expression in media containing WNT to that in media without WNT, but we observed no significant difference whether WNT was added or not.

Most case of SBS mutational signature analysis, three CRC organoids except CC-50 of TMB-H group have the similar signature and eighteen organoids except CC-28 of TMB-L group shows similar patterns. In the case of CC-28, there was a clear difference from other organoids in SBS mutational signature, but the mutational cause could not be identified yet. BRAF, CTNNB1 mutations. Among the four organoids (CC-28, CC-36, CC-39, CC-46) in E group that did not share mutation with other organoids, CC-39 was found to have mutation in GLI1. While it is reported that Hedgehog-GLI signaling promotes chemoresistance in colorectal cancer cells by regulating ABC transporters<sup>131</sup>, It was anticipated that the CC-39 organoid would respond sensitively to the drug.

Hypermutated CRC was well characterized by well-known biomarkers such as Microsatellite instability (MSI), Tumor mutational burden (TMB) and POLE exonuclease domain mutation., but more studies are still needed to subdivide non-hypermutated CRC into existing biomarkers. I was able to subdivide TMB-L group more than when I used existing biomarkers based on whether to share the mutation site, but it is needed to verify with a future study what this method means.

Feature importance should be careful because it obtains biased information from the given data. When N numbers are limited, such as organoids, the results may not be representative for CRC tumor, but at least information about a given CRC patient can be obtained. Some organoids did not expand well, so genomic results were obtained, but the gene expression level could not be determined. Particularly, the CC-33 patient had metastasis, but no gene expression information was obtained. However, I found that CC-33 has a PIK3CA E545K mutation, and there was a study that PIK3CA exon 9 and exon 20 mutations would be resistance to the first-line therapy<sup>132</sup>. Since CC-08 was found to have the same PIK3CA E545K mutation, CC-08 did not have clinical information because it did not receive the surgery, but it could be predicted that CC-08 would also have a resistance to the first-line therapy.



Based on the clinical information, the characteristics extracted by the expression amount of cancer organoids that have recurrence or metastasis are RABGGTB, RPL15, RPS16P1, VHL, SP140L, ELOVL7, ARAP1 among other genes besides C1orf115, and no reports related to recurrence or metastasis in CRC yet. In the same way, the genes found in the difference in expression between normal organoids and cancer organoids are MKRN2, SNRPD1 (pseudogene), RPS10 (pseudogene), DUSP23, BCL10-AS1, ZRANB2, LINC02773, RWDD3-DT, EML6. Except for MKRN2, there are no reports related to drug response or metastasis. These genes are characteristics found in organoids with limited sample numbers, but the highest ranked genes have been identified in studies pertaining to drug response or metastasis, so it appears that additional research of the remaining genes is required.

## Conclusion

In this dissertation, I identified a novel function on the DNA repair pathway of TRIP13 which is related to cancer by identifying a novel interaction partner through proteome analysis. I also proposed the interpretations and suggestions regarding the genomic analysis of patient-derived xenograft and introduced a novel perspective on the diagnosis and treatment of colorectal cancer patients by using patient-derived organoids through multi-omics analysis.

Accumulation of DNA damage caused by mutagens or DNA damage repair defects is a well-recognized factor in cancer development and progression. To investigate the function on DNA damage repair pathway of TRIP13 that is cancer related gene, BioID2 proximity labeling method combined with SILAC quantitative proteomic approach was applied for identifying a novel interaction partner MRE11. There are several evidences that TRIP13 participate in DNA double strand break repair pathway<sup>3,8,9</sup> in the perspective of the determining repair pathway step. However, I discovered that TRIP13 recruits to DNA damage sites in an early immediate response that MRE11 is also involved. Although the mechanisms by which TRIP13 regulates MRE11 have not been determined, it has been observed that the absence of TRIP13 inhibits the binding between MRE11 and MDC1 and regulates the ATM pathway independently of Mirin. In the result, I revealed that a novel function of TRIP13 in DNA double strand break sensing step.

Next, I attempted to analyze the function of somatic mutations in brain cancers using patient-derived xenograft model. To confirm whether established PDX models could mimic the genetic characteristic of their original tumor, I compared the deleterious mutations of PDX models and their primary tumors. While the deleterious mutations are not well matched between tumor and PDX model, I checked the germline mutations to confirm PDX samples are established from the same patients. It is observed that germline mutations of tumor were well conserved in its PDX model. To examine the possibility that mutagenesis occurs by exposure to novel mutagen during PDX model establishment, the mutational signatures of the PDX model and its corresponding original tumor were compared. The mutational signatures of PDX model and their corresponding tumor were also highly preserved. Therefore, the discordant of somatic mutation between original tumor and PDX model may be caused by high heterogeneity of brain tumors. Then, I investigated the differences of somatic mutation profiles between tumor and xenograft model. It is observed that PDX models shared relatively more somatic deleterious mutations with each other than cancer tissues. The shared mutated genes in PDX samples were associated with histone methylation and cilia. This observation suggested that PDX-specific genes may only be favorable in the PDX environment, or that PDX samples are enriched with rare mutations associated with cancer.



lastly, cancer is a complex disease involving a series of gene-environment interactions in a cumulative process which could occur with impairment in various systems, including DNA repair, apoptotic, and immune functions. Individual cancer patient shows different responses to chemotherapy depending on their genomic and other environmental characteristics. To address the drug response depending on the features of colorectal cancer (CRC) patient, I characterized the CRC organoids by the genetic, transcriptomic, and clinical information using comprehensive multi-omics analysis. First, four of twenty-three CRC organoids have extremely higher number of somatic mutations than other nineteen CRC organoids. The four hypermutated CRC organoids were into high tumor mutational burden (TMB-H) group and other organoids were into low tumor mutational burden (TMB-L) group. Mutational signature analysis revealed the mutational cause of CC-50 organoids in TMB-H group is polymerase epsilon (POLE) exonuclease domain mutation. About half of total exposure of other three organoids in TMB-H group related to mismatch repair defects. It was difficult to subdivide 19 organoids of the TMB-L group using existing biomarkers. Therefore, I tried to subdivide the CRC organoids based on the hypothesis that the CRC organoids would experience similar mutagenesis and show phenotypes like drug response if they share same mutations. The classification succeeded in distinguishing three organoids (CC-27, CC-38, CC41) in the TMB-H group from other organoids. Several CRC cell lines were subdivided in same way. The CRC cell lines were used to predict the phenotypes of CRC organoids in same group. With the genomic analysis, gene expressions of CRC organoids were used to consensus molecular subtypes (CMS) classifications. This CMS group would combine to our genetic classification. In addition, four CRC patients were experienced recurrence or metastasis after first-line chemotherapy treatment. I set gene expression of tumor organoids as the feature to classify this tumor organoids from other CRC organoids. Using XGboost model that is one of tree-based machine learning methods, feature importance was calculated and C1orf115 was top-ranked. It is reported that C1orf115 regulates the major drug exporter ABCB1/MDR1 to influence drug efflux. The C1orf115 expression level of four CRC organoids relatively higher than that of other CRC organoids. Drug response of the CRC organoids under knockdown of C1orf115 would be performed in further study. When I set the fold change of expression of tumor organoid compared to its normal organoid as the feature, MKRN2 was top-ranked in feature importance. MKRN2 gene was reported as inhibiting cell migration and invasion in several cancer cell line.

In summary, I investigated the DNA repair pathway in relation to cancer, analyzed brain cancer genomics via genetic analysis in patient-derived xenografts, and presented a novel perspective on colorectal cancer patient classification methods and candidate biomarkers via comprehensive multi-omics analysis.

## 4. References

- (1) Aravind, L.; Koonin, E. V. The HORMA Domain: A Common Structural Denominator in Mitotic Checkpoints, Chromosome Synapsis and DNA Repair. *Trends in Biochemical Sciences* **1998**, 23 (8), 284–286. [https://doi.org/10.1016/S0968-0004\(98\)01257-2](https://doi.org/10.1016/S0968-0004(98)01257-2).
- (2) Rosenberg, S. C.; Corbett, K. D. The Multifaceted Roles of the HORMA Domain in Cellular Signaling. *Journal of Cell Biology* **2015**, 211 (4), 745–755. <https://doi.org/10.1083/jcb.201509076>.
- (3) Clairmont, C. S.; Sarangi, P.; Ponnien Selvan, K.; Galli, L. D.; Csete, I.; Moreau, L.; Adelmant, G.; Chowdhury, D.; Marto, J. A.; D'Andrea, A. D. TRIP13 Regulates DNA Repair Pathway Choice through REV7 Conformational Change. *Nat Cell Biol* **2020**, 22 (1), 87–96. <https://doi.org/10.1038/s41556-019-0442-y>.
- (4) Wojtasz, L.; Daniel, K.; Roig, I.; Bolcun-Filas, E.; Xu, H.; Boonsanay, V.; Eckmann, C. R.; Cooke, H. J.; Jasin, M.; Keeney, S.; McKay, M. J.; Toth, A. Mouse HORMAD1 and HORMAD2, Two Conserved Meiotic Chromosomal Proteins, Are Depleted from Synapsed Chromosome Axes with the Help of TRIP13 AAA-ATPase. *PLoS Genet* **2009**, 5 (10), e1000702. <https://doi.org/10.1371/journal.pgen.1000702>.
- (5) Musacchio, A. The Molecular Biology of Spindle Assembly Checkpoint Signaling Dynamics. *Curr Biol* **2015**, 25 (20), R1002-1018. <https://doi.org/10.1016/j.cub.2015.08.051>.
- (6) Yost, S.; de Wolf, B.; Hanks, S.; Zachariou, A.; Marcozzi, C.; Clarke, M.; de Voer, R. M.; Etemad, B.; Uijttewaalt, E.; Ramsay, E.; Wylie, H.; Elliott, A.; Picton, S.; Smith, A.; Smithson, S.; Seal, S.; Ruark, E.; Houge, G.; Pines, J.; Kops, G. J. P. L.; Rahman, N. Biallelic TRIP13 Mutations Predispose to Wilms Tumor and Chromosome Missegregation. *Nat Genet* **2017**, 49 (7), 1148–1151. <https://doi.org/10.1038/ng.3883>.
- (7) Zhang, G.; Zhu, Q.; Fu, G.; Hou, J.; Hu, X.; Cao, J.; Peng, W.; Wang, X.; Chen, F.; Cui, H. TRIP13 Promotes the Cell Proliferation, Migration and Invasion of Glioblastoma through the FBXW7/c-MYC Axis. *Br J Cancer* **2019**, 121 (12), 1069–1078. <https://doi.org/10.1038/s41416-019-0633-0>.
- (8) Banerjee, R.; Russo, N.; Liu, M.; Basrur, V.; Bellile, E.; Palanisamy, N.; Scanlon, C. S.; van Tubergen, E.; Inglehart, R. C.; Metwally, T.; Mani, R.-S.; Yocum, A.; Nyati, M. K.; Castilho, R. M.; Varambally, S.; Chinnaiyan, A. M.; D'Silva, N. J. TRIP13 Promotes Error-Prone Nonhomologous End Joining and Induces Chemoresistance in Head and Neck Cancer. *Nat Commun* **2014**, 5, 4527. <https://doi.org/10.1038/ncomms5527>.
- (9) Sarangi, P.; Clairmont, C. S.; Galli, L. D.; Moreau, L. A.; D'Andrea, A. D. P31comet Promotes Homologous Recombination by Inactivating REV7 through the TRIP13 ATPase. *Proc Natl Acad Sci U S A* **2020**, 117 (43), 26795–26803. <https://doi.org/10.1073/pnas.2008830117>.
- (10) Ho, H.-C.; Burgess, S. M. Pch2 Acts through Xrs2 and Tel1/ATM to Modulate Interhomolog Bias and Checkpoint Function during Meiosis. *PLOS Genetics* **2011**, 7 (11), e1002351.

- <https://doi.org/10.1371/journal.pgen.1002351>.
- (11) Villar-Fernández, M. A.; Silva, R. C. da; Firlej, M.; Pan, D.; Weir, E.; Sarembe, A.; Raina, V. B.; Bange, T.; Weir, J. R.; Vader, G. Biochemical and Functional Characterization of a Meiosis-Specific Pch2/ORC AAA+ Assembly. *Life Science Alliance* **2020**, *3* (11). <https://doi.org/10.26508/lsa.201900630>.
  - (12) Zhou, Y.; Caron, P.; Legube, G.; Paull, T. T. Quantitation of DNA Double-Strand Break Resection Intermediates in Human Cells. *Nucleic Acids Res* **2014**, *42* (3), e19. <https://doi.org/10.1093/nar/gkt1309>.
  - (13) Kim, D. H.; Han, J. S.; Ly, P.; Ye, Q.; McMahon, M. A.; Myung, K.; Corbett, K. D.; Cleveland, D. W. TRIP13 and APC15 Drive Mitotic Exit by Turnover of Interphase- and Unattached Kinetochore-Produced MCC. *Nat Commun* **2018**, *9* (1), 4354. <https://doi.org/10.1038/s41467-018-06774-1>.
  - (14) Lee, S.-G.; Kim, N.; Kim, S.-M.; Park, I. B.; Kim, H.; Kim, S.; Kim, B.-G.; Hwang, J. M.; Baek, I.-J.; Gartner, A.; Park, J. H.; Myung, K. Ewing Sarcoma Protein Promotes Dissociation of Poly(ADP-Ribose) Polymerase 1 from Chromatin. *EMBO Rep* **2020**, *21* (11), e48676. <https://doi.org/10.15252/embr.201948676>.
  - (15) Schneider, C. A.; Rasband, W. S.; Eliceiri, K. W. NIH Image to ImageJ: 25 Years of Image Analysis. *Nat Methods* **2012**, *9* (7), 671–675. <https://doi.org/10.1038/nmeth.2089>.
  - (16) Paull, T. T.; Gellert, M. The 3' to 5' Exonuclease Activity of Mre11 Facilitates Repair of DNA Double-Strand Breaks. *Molecular Cell* **1998**, *1* (7), 969–979. [https://doi.org/10.1016/S1097-2765\(00\)80097-0](https://doi.org/10.1016/S1097-2765(00)80097-0).
  - (17) Howard, S. M.; Yanez, D. A.; Stark, J. M. DNA Damage Response Factors from Diverse Pathways, Including DNA Crosslink Repair, Mediate Alternative End Joining. *PLoS Genet* **2015**, *11* (1), e1004943. <https://doi.org/10.1371/journal.pgen.1004943>.
  - (18) Kochan, J. A.; Desclos, E. C. B.; Bosch, R.; Meister, L.; Vriend, L. E. M.; van Attikum, H.; Krawczyk, P. M. Meta-Analysis of DNA Double-Strand Break Response Kinetics. *Nucleic Acids Res* **2017**, *45* (22), 12625–12637. <https://doi.org/10.1093/nar/gkx1128>.
  - (19) Natsume, T.; Kiyomitsu, T.; Saga, Y.; Kanemaki, M. T. Rapid Protein Depletion in Human Cells by Auxin-Inducible Degron Tagging with Short Homology Donors. *Cell Rep* **2016**, *15* (1), 210–218. <https://doi.org/10.1016/j.celrep.2016.03.001>.
  - (20) Kim, D. I.; Jensen, S. C.; Noble, K. A.; Kc, B.; Roux, K. H.; Motamedchaboki, K.; Roux, K. J. An Improved Smaller Biotin Ligase for BioID Proximity Labeling. *Mol Biol Cell* **2016**, *27* (8), 1188–1196. <https://doi.org/10.1091/mbc.E15-12-0844>.
  - (21) Ong, S.-E.; Blagoev, B.; Kratchmarova, I.; Kristensen, D. B.; Steen, H.; Pandey, A.; Mann, M. Stable Isotope Labeling by Amino Acids in Cell Culture, SILAC, as a Simple and Accurate Approach to Expression Proteomics. *Mol Cell Proteomics* **2002**, *1* (5), 376–386. <https://doi.org/10.1074/mcp.m200025-mcp200>.
  - (22) Ong, S.-E.; Mann, M. A Practical Recipe for Stable Isotope Labeling by Amino Acids in Cell Culture (SILAC). *Nat Protoc* **2006**, *1* (6), 2650–2660. <https://doi.org/10.1038/nprot.2006.427>.

- (23) Lee, J.-H.; Paull, T. T. Activation and Regulation of ATM Kinase Activity in Response to DNA Double-Strand Breaks. *Oncogene* **2007**, *26* (56), 7741–7748. <https://doi.org/10.1038/sj.onc.1210872>.
- (24) Wang, Y.; Cortez, D.; Yazdi, P.; Neff, N.; Elledge, S. J.; Qin, J. BASC, a Super Complex of BRCA1-Associated Proteins Involved in the Recognition and Repair of Aberrant DNA Structures. *Genes Dev* **2000**, *14* (8), 927–939.
- (25) Haber, J. E. The Many Interfaces of Mre11. *Cell* **1998**, *95* (5), 583–586. [https://doi.org/10.1016/s0092-8674\(00\)81626-8](https://doi.org/10.1016/s0092-8674(00)81626-8).
- (26) Stucki, M.; Clapperton, J. A.; Mohammad, D.; Yaffe, M. B.; Smerdon, S. J.; Jackson, S. P. MDC1 Directly Binds Phosphorylated Histone H2AX to Regulate Cellular Responses to DNA Double-Strand Breaks. *Cell* **2005**, *123* (7), 1213–1226. <https://doi.org/10.1016/j.cell.2005.09.038>.
- (27) Chapman, J. R.; Jackson, S. P. Phospho-Dependent Interactions between NBS1 and MDC1 Mediate Chromatin Retention of the MRN Complex at Sites of DNA Damage. *EMBO Rep* **2008**, *9* (8), 795–801. <https://doi.org/10.1038/embor.2008.103>.
- (28) Spycher, C.; Miller, E. S.; Townsend, K.; Pavic, L.; Morrice, N. A.; Janscak, P.; Stewart, G. S.; Stucki, M. Constitutive Phosphorylation of MDC1 Physically Links the MRE11-RAD50-NBS1 Complex to Damaged Chromatin. *J Cell Biol* **2008**, *181* (2), 227–240. <https://doi.org/10.1083/jcb.200709008>.
- (29) Wu, L.; Luo, K.; Lou, Z.; Chen, J. MDC1 Regulates Intra-S-Phase Checkpoint by Targeting NBS1 to DNA Double-Strand Breaks. *Proc Natl Acad Sci U S A* **2008**, *105* (32), 11200–11205. <https://doi.org/10.1073/pnas.0802885105>.
- (30) Lee, M. S.; Edwards, R. A.; Thede, G. L.; Glover, J. N. M. Structure of the BRCT Repeat Domain of MDC1 and Its Specificity for the Free COOH-Terminal End of the Gamma-H2AX Histone Tail. *J Biol Chem* **2005**, *280* (37), 32053–32056. <https://doi.org/10.1074/jbc.C500273200>.
- (31) Stewart, G. S.; Wang, B.; Bignell, C. R.; Taylor, A. M. R.; Elledge, S. J. MDC1 Is a Mediator of the Mammalian DNA Damage Checkpoint. *Nature* **2003**, *421* (6926), 961–966. <https://doi.org/10.1038/nature01446>.
- (32) Lee, J.-H.; Mand, M. R.; Deshpande, R. A.; Kinoshita, E.; Yang, S.-H.; Wyman, C.; Paull, T. T. Ataxia Telangiectasia-Mutated (ATM) Kinase Activity Is Regulated by ATP-Driven Conformational Changes in the Mre11/Rad50/Nbs1 (MRN) Complex. *J Biol Chem* **2013**, *288* (18), 12840–12851. <https://doi.org/10.1074/jbc.M113.460378>.
- (33) Zhou, Y.; Paull, T. T. Direct Measurement of Single-Stranded DNA Intermediates in Mammalian Cells by Quantitative Polymerase Chain Reaction. *Anal Biochem* **2015**, *479*, 48–50. <https://doi.org/10.1016/j.ab.2015.03.025>.
- (34) Crossen, P. E.; Drets, M. E.; Arrighi, F. E.; Johnston, D. A. Analysis of the Frequency and Distribution of Sister Chromatid Exchanges in Cultured Human Lymphocytes. *Hum Genet* **1977**, *35* (3), 345–352. <https://doi.org/10.1007/BF00446625>.
- (35) Galloway, S. M.; Evans, H. J. Sister Chromatid Exchange in Human Chromosomes from

- Normal Individuals and Patients with Ataxia Telangiectasia. *Cytogenet Cell Genet* **1975**, *15* (1), 17–29. <https://doi.org/10.1159/000130495>.
- (36) Sonoda, E.; Sasaki, M. S.; Morrison, C.; Yamaguchi-Iwai, Y.; Takata, M.; Takeda, S. Sister Chromatid Exchanges Are Mediated by Homologous Recombination in Vertebrate Cells. *Mol Cell Biol* **1999**, *19* (7), 5166–5169.
- (37) Kieffer, S. R.; Lowndes, N. F. Immediate-Early, Early, and Late Responses to DNA Double Stranded Breaks. *Frontiers in Genetics* **2022**, *13*.
- (38) Lee, J.-H.; Paull, T. T. Direct Activation of the ATM Protein Kinase by the Mre11/Rad50/Nbs1 Complex. *Science* **2004**, *304* (5667), 93–96. <https://doi.org/10.1126/science.1091496>.
- (39) Paull, T. T.; Lee, J.-H. The Mre11/Rad50/Nbs1 Complex and Its Role as a DNA Double-Strand Break Sensor for ATM. *Cell Cycle* **2005**, *4* (6), 737–740. <https://doi.org/10.4161/cc.4.6.1715>.
- (40) Lee, J.-H.; Paull, T. T. ATM Activation by DNA Double-Strand Breaks through the Mre11-Rad50-Nbs1 Complex. *Science* **2005**, *308* (5721), 551–554. <https://doi.org/10.1126/science.1108297>.
- (41) Limbo, O.; Yamada, Y.; Russell, P. Mre11-Rad50-Dependent Activity of ATM/Tel1 at DNA Breaks and Telomeres in the Absence of Nbs1. *Mol Biol Cell* **2018**, *29* (11), 1389–1399. <https://doi.org/10.1091/mbc.E17-07-0470>.
- (42) Drew, K.; Wallingford, J. B.; Marcotte, E. M. Hu.MAP 2.0: Integration of over 15,000 Proteomic Experiments Builds a Global Compendium of Human Multiprotein Assemblies. *Mol Syst Biol* **2021**, *17* (5), e10016. <https://doi.org/10.15252/msb.202010016>.
- (43) Yasugi, T.; Vidal, M.; Sakai, H.; Howley, P. M.; Benson, J. D. Two Classes of Human Papillomavirus Type 16 E1 Mutants Suggest Pleiotropic Conformational Constraints Affecting E1 Multimerization, E2 Interaction, and Interaction with Cellular Proteins. *J Virol* **1997**, *71* (8), 5942–5951. <https://doi.org/10.1128/JVI.71.8.5942-5951.1997>.
- (44) Eytan, E.; Wang, K.; Miniowitz-Shemtov, S.; Sitry-Shevah, D.; Kaisari, S.; Yen, T. J.; Liu, S.-T.; Herskho, A. Disassembly of Mitotic Checkpoint Complexes by the Joint Action of the AAA-ATPase TRIP13 and P31(Comet). *Proc Natl Acad Sci U S A* **2014**, *111* (33), 12019–12024. <https://doi.org/10.1073/pnas.1412901111>.
- (45) Kolas, N. K.; Chapman, J. R.; Nakada, S.; Ylanko, J.; Chahwan, R.; Sweeney, F. D.; Panier, S.; Mendez, M.; Wildenhain, J.; Thomson, T. M.; Pelletier, L.; Jackson, S. P.; Durocher, D. Orchestration of the DNA-Damage Response by the RNF8 Ubiquitin Ligase. *Science* **2007**, *318* (5856), 1637–1640. <https://doi.org/10.1126/science.1150034>.
- (46) Nowsheen, S.; Aziz, K.; Aziz, A.; Deng, M.; Qin, B.; Luo, K.; Jeganathan, K. B.; Zhang, H.; Liu, T.; Yu, J.; Deng, Y.; Yuan, J.; Ding, W.; van Deursen, J. M.; Lou, Z. L3MBTL2 Orchestrates Ubiquitin Signalling by Dictating the Sequential Recruitment of RNF8 and RNF168 after DNA Damage. *Nat Cell Biol* **2018**, *20* (4), 455–464. <https://doi.org/10.1038/s41556-018-0071-x>.
- (47) Thorslund, T.; Ripplinger, A.; Hoffmann, S.; Wild, T.; Uckelmann, M.; Villumsen, B.; Narita, T.; Sixma, T. K.; Choudhary, C.; Bekker-Jensen, S.; Mailand, N. Histone H1 Couples Initiation and

- Amplification of Ubiquitin Signalling after DNA Damage. *Nature* **2015**, 527 (7578), 389–393. <https://doi.org/10.1038/nature15401>.
- (48) Chapman, J. R.; Barral, P.; Vannier, J.-B.; Borel, V.; Steger, M.; Tomas-Loba, A.; Sartori, A. A.; Adams, I. R.; Batista, F. D.; Boulton, S. J. RIF1 Is Essential for 53BP1-Dependent Nonhomologous End Joining and Suppression of DNA Double-Strand Break Resection. *Mol Cell* **2013**, 49 (5), 858–871. <https://doi.org/10.1016/j.molcel.2013.01.002>.
- (49) Escribano-Díaz, C.; Orthwein, A.; Fradet-Turcotte, A.; Xing, M.; Young, J. T. F.; Tkáč, J.; Cook, M. A.; Rosebrock, A. P.; Munro, M.; Canny, M. D.; Xu, D.; Durocher, D. A Cell Cycle-Dependent Regulatory Circuit Composed of 53BP1-RIF1 and BRCA1-CtIP Controls DNA Repair Pathway Choice. *Mol Cell* **2013**, 49 (5), 872–883. <https://doi.org/10.1016/j.molcel.2013.01.001>.
- (50) Zimmermann, M.; Lottersberger, F.; Buonomo, S. B.; Sfeir, A.; de Lange, T. 53BP1 Regulates DSB Repair Using Rif1 to Control 5' End Resection. *Science* **2013**, 339 (6120), 700–704. <https://doi.org/10.1126/science.1231573>.
- (51) Munoz, I. M.; Jowsey, P. A.; Toth, R.; Rouse, J. Phospho-Epitope Binding by the BRCT Domains of HPTIP Controls Multiple Aspects of the Cellular Response to DNA Damage. *Nucleic Acids Res* **2007**, 35 (16), 5312–5322. <https://doi.org/10.1093/nar/gkm493>.
- (52) Noordermeer, S. M.; Adam, S.; Setiawati, D.; Barazas, M.; Pettitt, S. J.; Ling, A. K.; Olivieri, M.; Álvarez-Quilón, A.; Moatti, N.; Zimmermann, M.; Annunziato, S.; Krastev, D. B.; Song, F.; Brandsma, I.; Frankum, J.; Brough, R.; Sherker, A.; Landry, S.; Szilard, R. K.; Munro, M. M.; McEwan, A.; Goullet de Rugy, T.; Lin, Z.-Y.; Hart, T.; Moffat, J.; Gingras, A.-C.; Martin, A.; van Attikum, H.; Jonkers, J.; Lord, C. J.; Rottenberg, S.; Durocher, D. The Shieldin Complex Mediates 53BP1-Dependent DNA Repair. *Nature* **2018**, 560 (7716), 117–121. <https://doi.org/10.1038/s41586-018-0340-7>.
- (53) Xu, G.; Chapman, J. R.; Brandsma, I.; Yuan, J.; Mistrik, M.; Bouwman, P.; Bartkova, J.; Gogola, E.; Warmerdam, D.; Barazas, M.; Jaspers, J. E.; Watanabe, K.; Pieterse, M.; Kersbergen, A.; Sol, W.; Celie, P. H. N.; Schouten, P. C.; van den Broek, B.; Salman, A.; Nieuwland, M.; de Rink, I.; de Ronde, J.; Jalink, K.; Boulton, S. J.; Chen, J.; van Gent, D. C.; Bartek, J.; Jonkers, J.; Borst, P.; Rottenberg, S. REV7 Counteracts DNA Double-Strand Break Resection and Affects PARP Inhibition. *Nature* **2015**, 521 (7553), 541–544. <https://doi.org/10.1038/nature14328>.
- (54) Boersma, V.; Moatti, N.; Segura-Bayona, S.; Peuscher, M. H.; van der Torre, J.; Wevers, B. A.; Orthwein, A.; Durocher, D.; Jacobs, J. J. L. MAD2L2 Controls DNA Repair at Telomeres and DNA Breaks by Inhibiting 5' End Resection. *Nature* **2015**, 521 (7553), 537–540. <https://doi.org/10.1038/nature14216>.
- (55) Lapointe, S.; Perry, A.; Butowski, N. A. Primary Brain Tumours in Adults. *Lancet* **2018**, 392 (10145), 432–446. [https://doi.org/10.1016/S0140-6736\(18\)30990-5](https://doi.org/10.1016/S0140-6736(18)30990-5).
- (56) Wen, P. Y.; Huse, J. T. 2016 World Health Organization Classification of Central Nervous System Tumors. *Continuum (Minneapolis)* **2017**, 23 (6, Neuro-oncology), 1531–1547. <https://doi.org/10.1212/CON.0000000000000536>.
- (57) Louis, D. N.; Perry, A.; Wesseling, P.; Brat, D. J.; Cree, I. A.; Figarella-Branger, D.; Hawkins, C.;



- Ng, H. K.; Pfister, S. M.; Reifenberger, G.; Soffietti, R.; von Deimling, A.; Ellison, D. W. The 2021 WHO Classification of Tumors of the Central Nervous System: A Summary. *Neuro-Oncology* **2021**, *23* (8), 1231–1251. <https://doi.org/10.1093/neuonc/noab106>.
- (58) Brennan, C. W.; Verhaak, R. G. W.; McKenna, A.; Campos, B.; Nounshmehr, H.; Salama, S. R.; Zheng, S.; Chakravarty, D.; Sanborn, J. Z.; Berman, S. H.; Beroukhi, R.; Bernard, B.; Wu, C.-J.; Genovese, G.; Shmulevich, I.; Barnholtz-Sloan, J.; Zou, L.; Vegesna, R.; Shukla, S. A.; Ciriello, G.; Yung, W. K.; Zhang, W.; Sougnez, C.; Mikkelsen, T.; Aldape, K.; Bigner, D. D.; Van Meir, E. G.; Prados, M.; Sloan, A.; Black, K. L.; Eschbacher, J.; Finocchiaro, G.; Friedman, W.; Andrews, D. W.; Guha, A.; Iacocca, M.; O'Neill, B. P.; Foltz, G.; Myers, J.; Weisenberger, D. J.; Penny, R.; Kucherlapati, R.; Perou, C. M.; Hayes, D. N.; Gibbs, R.; Marra, M.; Mills, G. B.; Lander, E.; Spellman, P.; Wilson, R.; Sander, C.; Weinstein, J.; Meyerson, M.; Gabriel, S.; Laird, P. W.; Haussler, D.; Getz, G.; Chin, L.; TCGA Research Network. The Somatic Genomic Landscape of Glioblastoma. *Cell* **2013**, *155* (2), 462–477. <https://doi.org/10.1016/j.cell.2013.09.034>.
- (59) Phillips, H. S.; Kharbanda, S.; Chen, R.; Forrest, W. F.; Soriano, R. H.; Wu, T. D.; Misra, A.; Nigro, J. M.; Colman, H.; Soroceanu, L.; Williams, P. M.; Modrusan, Z.; Feuerstein, B. G.; Aldape, K. Molecular Subclasses of High-Grade Glioma Predict Prognosis, Delineate a Pattern of Disease Progression, and Resemble Stages in Neurogenesis. *Cancer Cell* **2006**, *9* (3), 157–173. <https://doi.org/10.1016/j.ccr.2006.02.019>.
- (60) Verhaak, R. G. W.; Hoadley, K. A.; Purdom, E.; Wang, V.; Qi, Y.; Wilkerson, M. D.; Miller, C. R.; Ding, L.; Golub, T.; Mesirov, J. P.; Alexe, G.; Lawrence, M.; O'Kelly, M.; Tamayo, P.; Weir, B. A.; Gabriel, S.; Winckler, W.; Gupta, S.; Jakkula, L.; Feiler, H. S.; Hodgson, J. G.; James, C. D.; Sarkaria, J. N.; Brennan, C.; Kahn, A.; Spellman, P. T.; Wilson, R. K.; Speed, T. P.; Gray, J. W.; Meyerson, M.; Getz, G.; Perou, C. M.; Hayes, D. N.; Cancer Genome Atlas Research Network. Integrated Genomic Analysis Identifies Clinically Relevant Subtypes of Glioblastoma Characterized by Abnormalities in PDGFRA, IDH1, EGFR, and NF1. *Cancer Cell* **2010**, *17* (1), 98–110. <https://doi.org/10.1016/j.ccr.2009.12.020>.
- (61) Brat, D. J.; Aldape, K.; Colman, H.; Holland, E. C.; Louis, D. N.; Jenkins, R. B.; Kleinschmidt-DeMasters, B. K.; Perry, A.; Reifenberger, G.; Stupp, R.; von Deimling, A.; Weller, M. CIMPACT-NOW Update 3: Recommended Diagnostic Criteria for "Diffuse Astrocytic Glioma, IDH-Wildtype, with Molecular Features of Glioblastoma, WHO Grade IV." *Acta Neuropathol* **2018**, *136* (5), 805–810. <https://doi.org/10.1007/s00401-018-1913-0>.
- (62) Ellison, D. W.; Hawkins, C.; Jones, D. T. W.; Onar-Thomas, A.; Pfister, S. M.; Reifenberger, G.; Louis, D. N. CIMPACT-NOW Update 4: Diffuse Gliomas Characterized by MYB, MYBL1, or FGFR1 Alterations or BRAFV600E Mutation. *Acta Neuropathol* **2019**, *137* (4), 683–687. <https://doi.org/10.1007/s00401-019-01987-0>.
- (63) Louis, D. N.; Wesseling, P.; Aldape, K.; Brat, D. J.; Capper, D.; Cree, I. A.; Eberhart, C.; Figarella-Branger, D.; Fouladi, M.; Fuller, G. N.; Giannini, C.; Haberler, C.; Hawkins, C.; Komori, T.; Kros, J. M.; Ng, H. K.; Orr, B. A.; Park, S.-H.; Paulus, W.; Perry, A.; Pietsch, T.; Reifenberger, G.; Rosenblum, M.; Rous, B.; Sahm, F.; Sarkar, C.; Solomon, D. A.; Tabori, U.; van den Bent, M. J.



- von Deimling, A.; Weller, M.; White, V. A.; Ellison, D. W. CIMPACT-NOW Update 6: New Entity and Diagnostic Principle Recommendations of the CIMPACT-Utrecht Meeting on Future CNS Tumor Classification and Grading. *Brain Pathol* **2020**, *30* (4), 844–856. <https://doi.org/10.1111/bpa.12832>.
- (64) Louis, D. N.; Wesseling, P.; Paulus, W.; Giannini, C.; Batchelor, T. T.; Cairncross, J. G.; Capper, D.; Figarella-Branger, D.; Lopes, M. B.; Wick, W.; van den Bent, M. CIMPACT-NOW Update 1: Not Otherwise Specified (NOS) and Not Elsewhere Classified (NEC). *Acta Neuropathol* **2018**, *135* (3), 481–484. <https://doi.org/10.1007/s00401-018-1808-0>.
- (65) Louis, D. N.; Aldape, K.; Brat, D. J.; Capper, D.; Ellison, D. W.; Hawkins, C.; Paulus, W.; Perry, A.; Reifenberger, G.; Figarella-Branger, D.; Wesseling, P.; Batchelor, T. T.; Gregory Cairncross, J.; Pfister, S. M.; Rutkowski, S.; Weller, M.; Wick, W.; von Deimling, A. CIMPACT-NOW (the Consortium to Inform Molecular and Practical Approaches to CNS Tumor Taxonomy): A New Initiative in Advancing Nervous System Tumor Classification. *Brain Pathol* **2017**, *27* (6), 851–852. <https://doi.org/10.1111/bpa.12457>.
- (66) Louis, D. N.; Aldape, K.; Brat, D. J.; Capper, D.; Ellison, D. W.; Hawkins, C.; Paulus, W.; Perry, A.; Reifenberger, G.; Figarella-Branger, D.; Wesseling, P.; Batchelor, T. T.; Gregory Cairncross, J.; Pfister, S. M.; Rutkowski, S.; Weller, M.; Wick, W.; von Deimling, A. CIMPACT-NOW (the Consortium to Inform Molecular and Practical Approaches to CNS Tumor Taxonomy): A New Initiative in Advancing Nervous System Tumor Classification. *Brain Pathol* **2016**, *27* (6), 851–852. <https://doi.org/10.1111/bpa.12457>.
- (67) Friedmann-Morvinski, D. Glioblastoma Heterogeneity and Cancer Cell Plasticity. *Crit Rev Oncog* **2014**, *19* (5), 327–336. <https://doi.org/10.1615/critrevoncog.2014011777>.
- (68) Parker, N. R.; Khong, P.; Parkinson, J. F.; Howell, V. M.; Wheeler, H. R. Molecular Heterogeneity in Glioblastoma: Potential Clinical Implications. *Front Oncol* **2015**, *5*, 55. <https://doi.org/10.3389/fonc.2015.00055>.
- (69) Shen, Y.; Grisdale, C. J.; Islam, S. A.; Bose, P.; Lever, J.; Zhao, E. Y.; Grinshtein, N.; Ma, Y.; Mungall, A. J.; Moore, R. A.; Lun, X.; Senger, D. L.; Robbins, S. M.; Wang, A. Y.; MacIsaac, J. L.; Kobor, M. S.; Luchman, H. A.; Weiss, S.; Chan, J. A.; Blough, M. D.; Kaplan, D. R.; Cairncross, J. G.; Marra, M. A.; Jones, S. J. M. Comprehensive Genomic Profiling of Glioblastoma Tumors, BTICs, and Xenografts Reveals Stability and Adaptation to Growth Environments. *Proc. Natl. Acad. Sci. U.S.A.* **2019**, *116* (38), 19098–19108. <https://doi.org/10.1073/pnas.1813495116>.
- (70) Vaubel, R. A.; Tian, S.; Remonde, D.; Schroeder, M. A.; Mladek, A. C.; Kitange, G. J.; Caron, A.; Kollmeyer, T. M.; Grove, R.; Peng, S.; Carlson, B. L.; Ma, D. J.; Sarkar, G.; Evers, L.; Decker, P. A.; Yan, H.; Dhruv, H. D.; Berens, M. E.; Wang, Q.; Marin, B. M.; Klee, E. W.; Califano, A.; LaChance, D. H.; Eckel-Passow, J. E.; Verhaak, R. G.; Sulman, E. P.; Burns, T. C.; Meyer, F. B.; O'Neill, B. P.; Tran, N. L.; Giannini, C.; Jenkins, R. B.; Parney, I. F.; Sarkaria, J. N. Genomic and Phenotypic Characterization of a Broad Panel of Patient-Derived Xenografts Reflects the Diversity of Glioblastoma. *Clin Cancer Res* **2020**, *26* (5), 1094–1104. <https://doi.org/10.1158/1078-0432.CCR-19-0909>.

- (71) Ben-David, U.; Ha, G.; Tseng, Y.-Y.; Greenwald, N. F.; Oh, C.; Shih, J.; McFarland, J. M.; Wong, B.; Boehm, J. S.; Beroukhi, R.; Golub, T. R. Patient-Derived Xenografts Undergo Mouse-Specific Tumor Evolution. *Nat Genet* **2017**, *49* (11), 1567–1575. <https://doi.org/10.1038/ng.3967>.
- (72) Bolger, A. M.; Lohse, M.; Usadel, B. Trimmomatic: A Flexible Trimmer for Illumina Sequence Data. *Bioinformatics* **2014**, *30* (15), 2114–2120. <https://doi.org/10.1093/bioinformatics/btu170>.
- (73) Li, H. Aligning Sequence Reads, Clone Sequences and Assembly Contigs with BWA-MEM. *arXiv:1303.3997 [q-bio]* **2013**.
- (74) Kim, S.; Scheffler, K.; Halpern, A. L.; Bekritsky, M. A.; Noh, E.; Källberg, M.; Chen, X.; Kim, Y.; Beyter, D.; Krusche, P.; Saunders, C. T. Strelka2: Fast and Accurate Calling of Germline and Somatic Variants. *Nat Methods* **2018**, *15* (8), 591–594. <https://doi.org/10.1038/s41592-018-0051-x>.
- (75) McLaren, W.; Gil, L.; Hunt, S. E.; Riat, H. S.; Ritchie, G. R. S.; Thormann, A.; Flicek, P.; Cunningham, F. The Ensembl Variant Effect Predictor. *Genome Biol* **2016**, *17* (1), 122. <https://doi.org/10.1186/s13059-016-0974-4>.
- (76) Tate, J. G.; Bamford, S.; Jubb, H. C.; Sondka, Z.; Beare, D. M.; Bindal, N.; Boutselakis, H.; Cole, C. G.; Creatore, C.; Dawson, E.; Fish, P.; Harsha, B.; Hathaway, C.; Jupe, S. C.; Kok, C. Y.; Noble, K.; Ponting, L.; Ramshaw, C. C.; Rye, C. E.; Speedy, H. E.; Stefancsik, R.; Thompson, S. L.; Wang, S.; Ward, S.; Campbell, P. J.; Forbes, S. A. COSMIC: The Catalogue Of Somatic Mutations In Cancer. *Nucleic Acids Research* **2019**, *47* (D1), D941–D947. <https://doi.org/10.1093/nar/gky1015>.
- (77) PCAWG Mutational Signatures Working Group; PCAWG Consortium; Alexandrov, L. B.; Kim, J.; Haradhvala, N. J.; Huang, M. N.; Tian Ng, A. W.; Wu, Y.; Boot, A.; Covington, K. R.; Gordenin, D. A.; Bergstrom, E. N.; Islam, S. M. A.; Lopez-Bigas, N.; Klimczak, L. J.; McPherson, J. R.; Morganella, S.; Sabarinathan, R.; Wheeler, D. A.; Mustonen, V.; Getz, G.; Rozen, S. G.; Stratton, M. R. The Repertoire of Mutational Signatures in Human Cancer. *Nature* **2020**, *578* (7793), 94–101. <https://doi.org/10.1038/s41586-020-1943-3>.
- (78) Bergstrom, E. N.; Huang, M. N.; Mahto, U.; Barnes, M.; Stratton, M. R.; Rozen, S. G.; Alexandrov, L. B. SigProfilerMatrixGenerator: A Tool for Visualizing and Exploring Patterns of Small Mutational Events. *BMC Genomics* **2019**, *20* (1), 685. <https://doi.org/10.1186/s12864-019-6041-2>.
- (79) Mi, H.; Muruganujan, A.; Huang, X.; Ebert, D.; Mills, C.; Guo, X.; Thomas, P. D. Protocol Update for Large-Scale Genome and Gene Function Analysis with the PANTHER Classification System (v.14.0). *Nat Protoc* **2019**, *14* (3), 703–721. <https://doi.org/10.1038/s41596-019-0128-8>.
- (80) Moore, L.; Cagan, A.; Coorens, T. H. H.; Neville, M. D. C.; Sanghvi, R.; Sanders, M. A.; Oliver, T. R. W.; Leongamornlert, D.; Ellis, P.; Noorani, A.; Mitchell, T. J.; Butler, T. M.; Hooks, Y.; Warren, A. Y.; Jorgensen, M.; Dawson, K. J.; Menzies, A.; O'Neill, L.; Latimer, C.; Teng, M.; van Boxtel,

- R.; Iacobuzio-Donahue, C. A.; Martincorena, I.; Heer, R.; Campbell, P. J.; Fitzgerald, R. C.; Stratton, M. R.; Rahbari, R. The Mutational Landscape of Human Somatic and Germline Cells. *Nature* **2021**, 597 (7876), 381–386. <https://doi.org/10.1038/s41586-021-03822-7>.
- (81) Rouhani, F. J.; Nik-Zainal, S.; Wuster, A.; Li, Y.; Conte, N.; Koike-Yusa, H.; Kumasaka, N.; Vallier, L.; Yusa, K.; Bradley, A. Mutational History of a Human Cell Lineage from Somatic to Induced Pluripotent Stem Cells. *PLoS Genet* **2016**, 12 (4), e1005932. <https://doi.org/10.1371/journal.pgen.1005932>.
- (82) Pich, O.; Muiños, F.; Lolkema, M. P.; Steeghs, N.; Gonzalez-Perez, A.; Lopez-Bigas, N. The Mutational Footprints of Cancer Therapies. *Nat Genet* **2019**, 51 (12), 1732–1740. <https://doi.org/10.1038/s41588-019-0525-5>.
- (83) Wang, J.; Cazzato, E.; Ladewig, E.; Frattini, V.; Rosenbloom, D. I. S.; Zairis, S.; Abate, F.; Liu, Z.; Elliott, O.; Shin, Y.-J.; Lee, J.-K.; Lee, I.-H.; Park, W.-Y.; Eoli, M.; Blumberg, A. J.; Lasorella, A.; Nam, D.-H.; Finocchiaro, G.; Iavarone, A.; Rabadan, R. Clonal Evolution of Glioblastoma under Therapy. *Nat Genet* **2016**, 48 (7), 768–776. <https://doi.org/10.1038/ng.3590>.
- (84) LeBlanc, V. G.; Trinh, D. L.; Aslanpour, S.; Hughes, M.; Livingstone, D.; Jin, D.; Ahn, B. Y.; Blough, M. D.; Cairncross, J. G.; Chan, J. A.; Kelly, J. J. P.; Marra, M. A. Single-Cell Landscapes of Primary Glioblastomas and Matched Explants and Cell Lines Show Variable Retention of Inter- and Intratumor Heterogeneity. *Cancer Cell* **2022**, 40 (4), 379–392.e9. <https://doi.org/10.1016/j.ccell.2022.02.016>.
- (85) Nigro, J. M.; Baker, S. J.; Preisinger, A. C.; Jessup, J. M.; Hostetter, R.; Cleary, K.; Bigner, S. H.; Davidson, N.; Baylin, S.; Devilee, P. Mutations in the P53 Gene Occur in Diverse Human Tumour Types. *Nature* **1989**, 342 (6250), 705–708. <https://doi.org/10.1038/342705a0>.
- (86) Wong, A. J.; Bigner, S. H.; Bigner, D. D.; Kinzler, K. W.; Hamilton, S. R.; Vogelstein, B. Increased Expression of the Epidermal Growth Factor Receptor Gene in Malignant Gliomas Is Invariably Associated with Gene Amplification. *Proc Natl Acad Sci U S A* **1987**, 84 (19), 6899–6903. <https://doi.org/10.1073/pnas.84.19.6899>.
- (87) Hernández Borrero, L. J.; El-Deiry, W. S. Tumor Suppressor P53: Biology, Signaling Pathways, and Therapeutic Targeting. *Biochimica et Biophysica Acta (BBA) - Reviews on Cancer* **2021**, 1876 (1), 188556. <https://doi.org/10.1016/j.bbcan.2021.188556>.
- (88) Furnari, F. B.; Fenton, T.; Bachoo, R. M.; Mukasa, A.; Stommel, J. M.; Stegh, A.; Hahn, W. C.; Ligon, K. L.; Louis, D. N.; Brennan, C.; Chin, L.; DePinho, R. A.; Cavenee, W. K. Malignant Astrocytic Glioma: Genetics, Biology, and Paths to Treatment. *Genes Dev* **2007**, 21 (21), 2683–2710. <https://doi.org/10.1101/gad.1596707>.
- (89) AACR Project GENIE Consortium. AACR Project GENIE: Powering Precision Medicine through an International Consortium. *Cancer Discov* **2017**, 7 (8), 818–831. <https://doi.org/10.1158/2159-8290.CD-17-0151>.
- (90) Goranci-Buzhala, G.; Mariappan, A.; Ricci-Vitiani, L.; Josipovic, N.; Pacioni, S.; Gottardo, M.; Ptok, J.; Schaal, H.; Callaini, G.; Rajalingam, K.; Dynlacht, B.; Hadian, K.; Papantonis, A.; Pallini, R.; Gopalakrishnan, J. Cilium Induction Triggers Differentiation of Glioma Stem Cells. *Cell*

- Rep* **2021**, 36 (10), 109656. <https://doi.org/10.1016/j.celrep.2021.109656>.
- (91) Mallm, J.-P.; Windisch, P.; Biran, A.; Gal, Z.; Schumacher, S.; Glass, R.; Herold-Mende, C.; Meshorer, E.; Barbus, M.; Rippe, K. Glioblastoma Initiating Cells Are Sensitive to Histone Demethylase Inhibition Due to Epigenetic Dereglulation. *Int J Cancer* **2020**, 146 (5), 1281–1292. <https://doi.org/10.1002/ijc.32649>.
- (92) Global Burden of Disease Cancer Collaboration; Fitzmaurice, C.; Allen, C.; Barber, R. M.; Barregard, L.; Bhutta, Z. A.; Brenner, H.; Dicker, D. J.; Chimed-Orchir, O.; Dandona, R.; Dandona, L.; Fleming, T.; Forouzanfar, M. H.; Hancock, J.; Hay, R. J.; Hunter-Merrill, R.; Huynh, C.; Hosgood, H. D.; Johnson, C. O.; Jonas, J. B.; Khubchandani, J.; Kumar, G. A.; Kutz, M.; Lan, Q.; Larson, H. J.; Liang, X.; Lim, S. S.; Lopez, A. D.; MacIntyre, M. F.; Marczak, L.; Marquez, N.; Mokdad, A. H.; Pinho, C.; Pourmalek, F.; Salomon, J. A.; Sanabria, J. R.; Sandar, L.; Sartorius, B.; Schwartz, S. M.; Shackelford, K. A.; Shibuya, K.; Stanaway, J.; Steiner, C.; Sun, J.; Takahashi, K.; Vollset, S. E.; Vos, T.; Wagner, J. A.; Wang, H.; Westerman, R.; Zeeb, H.; Zockler, L.; Abd-Allah, F.; Ahmed, M. B.; Alabed, S.; Alam, N. K.; Aldhahri, S. F.; Alem, G.; Alemayohu, M. A.; Ali, R.; Al-Raddadi, R.; Amare, A.; Amoako, Y.; Artaman, A.; Asayesh, H.; Atnafu, N.; Awasthi, A.; Saleem, H. B.; Barac, A.; Bedi, N.; Bensenor, I.; Berhane, A.; Bernabé, E.; Betsu, B.; Binagwaho, A.; Boneya, D.; Campos-Nonato, I.; Castañeda-Orjuela, C.; Catalá-López, F.; Chiang, P.; Chibueze, C.; Chitheer, A.; Choi, J.-Y.; Cowie, B.; Damtew, S.; das Neves, J.; Dey, S.; Dharmaratne, S.; Dhillon, P.; Ding, E.; Driscoll, T.; Ekwueme, D.; Endries, A. Y.; Farvid, M.; Farzadfar, F.; Fernandes, J.; Fischer, F.; G/Hiwot, T. T.; Gebru, A.; Gopalani, S.; Hailu, A.; Horino, M.; Horita, N.; Hussein, A.; Huybrechts, I.; Inoue, M.; Islami, F.; Jakovljevic, M.; James, S.; Javanbakht, M.; Jee, S. H.; Kasaeian, A.; Kedir, M. S.; Khader, Y. S.; Khang, Y.-H.; Kim, D.; Leigh, J.; Linn, S.; Lunevicius, R.; El Razek, H. M. A.; Malekzadeh, R.; Malta, D. C.; Marcenes, W.; Markos, D.; Melaku, Y. A.; Meles, K. G.; Mendoza, W.; Mengiste, D. T.; Meretoja, T. J.; Miller, T. R.; Mohammad, K. A.; Mohammadi, A.; Mohammed, S.; Moradi-Lakeh, M.; Nagel, G.; Nand, D.; Le Nguyen, Q.; Nolte, S.; Ogbo, F. A.; Oladimeji, K. E.; Oren, E.; Pa, M.; Park, E.-K.; Pereira, D. M.; Plass, D.; Qorbani, M.; Radfar, A.; Rafay, A.; Rahman, M.; Rana, S. M.; Søreide, K.; Satpathy, M.; Sawhney, M.; Sepanlou, S. G.; Shaikh, M. A.; She, J.; Shiue, I.; Shore, H. R.; Shrimme, M. G.; So, S.; Soneji, S.; Stathopoulou, V.; Stroumpoulis, K.; Sufiyan, M. B.; Sykes, B. L.; Tabarés-Seisdedos, R.; Tadese, F.; Tedla, B. A.; Tessema, G. A.; Thakur, J. S.; Tran, B. X.; Ukwaja, K. N.; Uzochukwu, B. S. C.; Vlassov, V. V.; Weiderpass, E.; Wubshet Terefe, M.; Yebayo, H. G.; Yimam, H. H.; Yonemoto, N.; Younis, M. Z.; Yu, C.; Zaidi, Z.; Zaki, M. E. S.; Zenebe, Z. M.; Murray, C. J. L.; Naghavi, M. Global, Regional, and National Cancer Incidence, Mortality, Years of Life Lost, Years Lived With Disability, and Disability-Adjusted Life-Years for 32 Cancer Groups, 1990 to 2015: A Systematic Analysis for the Global Burden of Disease Study. *JAMA Oncol* **2017**, 3 (4), 524–548. <https://doi.org/10.1001/jamaoncol.2016.5688>.
- (93) Prossomariti, A.; Piazzini, G.; Alquati, C.; Ricciardiello, L. Are Wnt/ $\beta$ -Catenin and PI3K/AKT/MTORC1 Distinct Pathways in Colorectal Cancer? *Cell Mol Gastroenterol Hepatol* **2020**, 10 (3), 491–506. <https://doi.org/10.1016/j.jcmgh.2020.04.007>.

- (94) Naeem, A.; Tun, A. M.; Guevara, E. Molecular Genetics and the Role of Molecularly Targeted Agents in Metastatic Colorectal Carcinoma. *J Gastrointest Cancer* **2020**, *51* (2), 387–400. <https://doi.org/10.1007/s12029-019-00272-3>.
- (95) Jung, G.; Hernández-Illán, E.; Moreira, L.; Balaguer, F.; Goel, A. Epigenetics of Colorectal Cancer: Biomarker and Therapeutic Potential. *Nat Rev Gastroenterol Hepatol* **2020**, *17* (2), 111–130. <https://doi.org/10.1038/s41575-019-0230-y>.
- (96) Boland, C. R.; Goel, A. Microsatellite Instability in Colorectal Cancer. *Gastroenterology* **2010**, *138* (6), 2073–2087.e3. <https://doi.org/10.1053/j.gastro.2009.12.064>.
- (97) Elshazli, R. M.; Toraih, E. A.; Elgaml, A.; Kandil, E.; Fawzy, M. S. Genetic Polymorphisms of TP53 (Rs1042522) and MDM2 (Rs2279744) and Colorectal Cancer Risk: An Updated Meta-Analysis Based on 59 Case-Control Studies. *Gene* **2020**, *734*, 144391. <https://doi.org/10.1016/j.gene.2020.144391>.
- (98) Overman, M. J.; McDermott, R.; Leach, J. L.; Lonardi, S.; Lenz, H.-J.; Morse, M. A.; Desai, J.; Hill, A.; Axelson, M.; Moss, R. A.; Goldberg, M. V.; Cao, Z. A.; Ledeine, J.-M.; Maglinte, G. A.; Kopetz, S.; André, T. Nivolumab in Patients with Metastatic DNA Mismatch Repair-Deficient or Microsatellite Instability-High Colorectal Cancer (CheckMate 142): An Open-Label, Multicentre, Phase 2 Study. *Lancet Oncol* **2017**, *18* (9), 1182–1191. [https://doi.org/10.1016/S1470-2045\(17\)30422-9](https://doi.org/10.1016/S1470-2045(17)30422-9).
- (99) Le, D. T.; Durham, J. N.; Smith, K. N.; Wang, H.; Bartlett, B. R.; Aulakh, L. K.; Lu, S.; Kemberling, H.; Wilt, C.; Luber, B. S.; Wong, F.; Azad, N. S.; Rucki, A. A.; Laheru, D.; Donehower, R.; Zaheer, A.; Fisher, G. A.; Crocenzi, T. S.; Lee, J. J.; Greten, T. F.; Duffy, A. G.; Ciombor, K. K.; Eyring, A. D.; Lam, B. H.; Joe, A.; Kang, S. P.; Holdhoff, M.; Danilova, L.; Cope, L.; Meyer, C.; Zhou, S.; Goldberg, R. M.; Armstrong, D. K.; Bever, K. M.; Fader, A. N.; Taube, J.; Housseau, F.; Spetzler, D.; Xiao, N.; Pardoll, D. M.; Papadopoulos, N.; Kinzler, K. W.; Eshleman, J. R.; Vogelstein, B.; Anders, R. A.; Diaz, L. A. Mismatch Repair Deficiency Predicts Response of Solid Tumors to PD-1 Blockade. *Science* **2017**, *357* (6349), 409–413. <https://doi.org/10.1126/science.aan6733>.
- (100) Dudley, J. C.; Lin, M.-T.; Le, D. T.; Eshleman, J. R. Microsatellite Instability as a Biomarker for PD-1 Blockade. *Clin Cancer Res* **2016**, *22* (4), 813–820. <https://doi.org/10.1158/1078-0432.CCR-15-1678>.
- (101) Fabrizio, D. A.; George, T. J.; Dunne, R. F.; Frampton, G.; Sun, J.; Gowen, K.; Kennedy, M.; Greenbowe, J.; Schrock, A. B.; Hezel, A. F.; Ross, J. S.; Stephens, P. J.; Ali, S. M.; Miller, V. A.; Fakih, M.; Klemperer, S. J. Beyond Microsatellite Testing: Assessment of Tumor Mutational Burden Identifies Subsets of Colorectal Cancer Who May Respond to Immune Checkpoint Inhibition. *J Gastrointest Oncol* **2018**, *9* (4), 610–617. <https://doi.org/10.21037/jgo.2018.05.06>.
- (102) Kong, J. C.; Guerra, G. R.; Pham, T.; Mitchell, C.; Lynch, A. C.; Warriar, S. K.; Ramsay, R. G.; Heriot, A. G. Prognostic Impact of Tumor-Infiltrating Lymphocytes in Primary and Metastatic Colorectal Cancer: A Systematic Review and Meta-Analysis. *Dis Colon Rectum* **2019**, *62* (4), 498–508. <https://doi.org/10.1097/DCR.0000000000001332>.



- (103) Havel, J. J.; Chowell, D.; Chan, T. A. The Evolving Landscape of Biomarkers for Checkpoint Inhibitor Immunotherapy. *Nat Rev Cancer* **2019**, *19* (3), 133–150. <https://doi.org/10.1038/s41568-019-0116-x>.
- (104) Samstein, R. M.; Lee, C.-H.; Shoushtari, A. N.; Hellmann, M. D.; Shen, R.; Janjigian, Y. Y.; Barron, D. A.; Zehir, A.; Jordan, E. J.; Omuro, A.; Kaley, T. J.; Kendall, S. M.; Motzer, R. J.; Hakimi, A. A.; Voss, M. H.; Russo, P.; Rosenberg, J.; Iyer, G.; Bochner, B. H.; Bajorin, D. F.; Al-Ahmadie, H. A.; Chaft, J. E.; Rudin, C. M.; Riely, G. J.; Baxi, S.; Ho, A. L.; Wong, R. J.; Pfister, D. G.; Wolchok, J. D.; Barker, C. A.; Gutin, P. H.; Brennan, C. W.; Tabar, V.; Mellingerhoff, I. K.; DeAngelis, L. M.; Ariyan, C. E.; Lee, N.; Tap, W. D.; Gounder, M. M.; D'Angelo, S. P.; Saltz, L.; Stadler, Z. K.; Scher, H. I.; Baselga, J.; Razavi, P.; Klebanoff, C. A.; Yaeger, R.; Segal, N. H.; Ku, G. Y.; DeMatteo, R. P.; Ladanyi, M.; Rizvi, N. A.; Berger, M. F.; Riaz, N.; Solit, D. B.; Chan, T. A.; Morris, L. G. T. Tumor Mutational Load Predicts Survival after Immunotherapy across Multiple Cancer Types. *Nat Genet* **2019**, *51* (2), 202–206. <https://doi.org/10.1038/s41588-018-0312-8>.
- (105) Domingo, E.; Freeman-Mills, L.; Rayner, E.; Glaire, M.; Briggs, S.; Vermeulen, L.; Fessler, E.; Medema, J. P.; Boot, A.; Morreau, H.; van Wezel, T.; Liefers, G.-J.; Lothe, R. A.; Danielsen, S. A.; Sveen, A.; Nesbakken, A.; Zlobec, I.; Lugli, A.; Koelzer, V. H.; Berger, M. D.; Castellví-Bel, S.; Muñoz, J.; Epicolon consortium; de Bruyn, M.; Nijman, H. W.; Novelli, M.; Lawson, K.; Oukrif, D.; Frangou, E.; Dutton, P.; Tejpar, S.; Delorenzi, M.; Kerr, R.; Kerr, D.; Tomlinson, I.; Church, D. N. Somatic POLE Proofreading Domain Mutation, Immune Response, and Prognosis in Colorectal Cancer: A Retrospective, Pooled Biomarker Study. *Lancet Gastroenterol Hepatol* **2016**, *1* (3), 207–216. [https://doi.org/10.1016/S2468-1253\(16\)30014-0](https://doi.org/10.1016/S2468-1253(16)30014-0).
- (106) Auman, J. T.; McLeod, H. L. Colorectal Cancer Cell Lines Lack the Molecular Heterogeneity of Clinical Colorectal Tumors. *Clin Colorectal Cancer* **2010**, *9* (1), 40–47. <https://doi.org/10.3816/CCC.2010.n.005>.
- (107) Kapałczyńska, M.; Kolenda, T.; Przybyła, W.; Zajączkowska, M.; Teresiak, A.; Filas, V.; Ibbs, M.; Bliźniak, R.; Łuczewski, Ł.; Lamperska, K. 2D and 3D Cell Cultures - a Comparison of Different Types of Cancer Cell Cultures. *Arch Med Sci* **2018**, *14* (4), 910–919. <https://doi.org/10.5114/aoms.2016.63743>.
- (108) Wong, C. H.; Siah, K. W.; Lo, A. W. Estimation of Clinical Trial Success Rates and Related Parameters. *Biostatistics* **2019**, *20* (2), 273–286. <https://doi.org/10.1093/biostatistics/kxx069>.
- (109) Mak, I. W.; Evaniew, N.; Ghert, M. Lost in Translation: Animal Models and Clinical Trials in Cancer Treatment. *Am J Transl Res* **2014**, *6* (2), 114–118.
- (110) Bhimani, J.; Ball, K.; Stebbing, J. Patient-Derived Xenograft Models-the Future of Personalised Cancer Treatment. *Br J Cancer* **2020**, *122* (5), 601–602. <https://doi.org/10.1038/s41416-019-0678-0>.
- (111) van de Wetering, M.; Francies, H. E.; Francis, J. M.; Bounova, G.; Iorio, F.; Pronk, A.; van Houdt, W.; van Gorp, J.; Taylor-Weiner, A.; Kester, L.; McLaren-Douglas, A.; Blokker, J.; Jaksani, S.; Bartfeld, S.; Volckman, R.; van Sluis, P.; Li, V. S. W.; Seepo, S.; Sekhar Pedamallu, C.; Cibulskis, K.; Carter, S. L.; McKenna, A.; Lawrence, M. S.; Lichtenstein, L.; Stewart, C.; Koster, J.; Versteeg,

- R.; van Oudenaarden, A.; Saez-Rodriguez, J.; Vries, R. G. J.; Getz, G.; Wessels, L.; Stratton, M. R.; McDermott, U.; Meyerson, M.; Garnett, M. J.; Clevers, H. Prospective Derivation of a Living Organoid Biobank of Colorectal Cancer Patients. *Cell* **2015**, *161* (4), 933–945. <https://doi.org/10.1016/j.cell.2015.03.053>.
- (112) Weeber, F.; van de Wetering, M.; Hoogstraat, M.; Dijkstra, K. K.; Krijgsman, O.; Kuilman, T.; Gadellaa-van Hooijdonk, C. G. M.; van der Velden, D. L.; Peeper, D. S.; Cuppen, E. P. J. G.; Vries, R. G.; Clevers, H.; Voest, E. E. Preserved Genetic Diversity in Organoids Cultured from Biopsies of Human Colorectal Cancer Metastases. *Proc Natl Acad Sci U S A* **2015**, *112* (43), 13308–13311. <https://doi.org/10.1073/pnas.1516689112>.
- (113) Kondo, J.; Ekawa, T.; Endo, H.; Yamazaki, K.; Tanaka, N.; Kukita, Y.; Okuyama, H.; Okami, J.; Imamura, F.; Ohue, M.; Kato, K.; Nomura, T.; Kohara, A.; Mori, S.; Dan, S.; Inoue, M. High-Throughput Screening in Colorectal Cancer Tissue-Originated Spheroids. *Cancer Sci* **2019**, *110* (1), 345–355. <https://doi.org/10.1111/cas.13843>.
- (114) Vlachogiannis, G.; Hedayat, S.; Vatsiou, A.; Jamin, Y.; Fernández-Mateos, J.; Khan, K.; Lampis, A.; Eason, K.; Huntingford, I.; Burke, R.; Rata, M.; Koh, D.-M.; Tunariu, N.; Collins, D.; Hulkki-Wilson, S.; Ragulan, C.; Spiteri, I.; Moorcraft, S. Y.; Chau, I.; Rao, S.; Watkins, D.; Fotiadis, N.; Bali, M.; Darvish-Damavandi, M.; Lote, H.; Eltahir, Z.; Smyth, E. C.; Begum, R.; Clarke, P. A.; Hahne, J. C.; Dowsett, M.; de Bono, J.; Workman, P.; Sadanandam, A.; Fassan, M.; Sansom, O. J.; Eccles, S.; Starling, N.; Braconi, C.; Sottoriva, A.; Robinson, S. P.; Cunningham, D.; Valeri, N. Patient-Derived Organoids Model Treatment Response of Metastatic Gastrointestinal Cancers. *Science* **2018**, *359* (6378), 920–926. <https://doi.org/10.1126/science.aao2774>.
- (115) Ooft, S. N.; Weeber, F.; Dijkstra, K. K.; McLean, C. M.; Kaing, S.; van Werkhoven, E.; Schipper, L.; Hoes, L.; Vis, D. J.; van de Haar, J.; Prevoo, W.; Snaebjornsson, P.; van der Velden, D.; Klein, M.; Chalabi, M.; Boot, H.; van Leerdam, M.; Bloemendal, H. J.; Beerepoot, L. V.; Wessels, L.; Cuppen, E.; Clevers, H.; Voest, E. E. Patient-Derived Organoids Can Predict Response to Chemotherapy in Metastatic Colorectal Cancer Patients. *Sci Transl Med* **2019**, *11* (513), eaay2574. <https://doi.org/10.1126/scitranslmed.aay2574>.
- (116) Klempner, S. J.; Fabrizio, D.; Bane, S.; Reinhart, M.; Peoples, T.; Ali, S. M.; Sokol, E. S.; Frampton, G.; Schrock, A. B.; Anhorn, R.; Reddy, P. Tumor Mutational Burden as a Predictive Biomarker for Response to Immune Checkpoint Inhibitors: A Review of Current Evidence. *Oncologist* **2020**, *25* (1), e147–e159. <https://doi.org/10.1634/theoncologist.2019-0244>.
- (117) Chae, Y. K.; Anker, J. F.; Carneiro, B. A.; Chandra, S.; Kaplan, J.; Kalyan, A.; Santa-Maria, C. A.; Plataniias, L. C.; Giles, F. J. Genomic Landscape of DNA Repair Genes in Cancer. *Oncotarget* **2016**, *7* (17), 23312–23321. <https://doi.org/10.18632/oncotarget.8196>.
- (118) Gargiulo, P.; Della Pepa, C.; Berardi, S.; Califano, D.; Scala, S.; Buonaguro, L.; Ciliberto, G.; Brauchli, P.; Pignata, S. Tumor Genotype and Immune Microenvironment in POLE-Ultramutated and MSI-Hypermuted Endometrial Cancers: New Candidates for Checkpoint Blockade Immunotherapy? *Cancer Treat Rev* **2016**, *48*, 61–68. <https://doi.org/10.1016/j.ctrv.2016.06.008>.



- (119) Stadler, Z. K.; Battaglin, F.; Middha, S.; Hechtman, J. F.; Tran, C.; Cercek, A.; Yaeger, R.; Segal, N. H.; Varghese, A. M.; Reidy-Lagunes, D. L.; Kemeny, N. E.; Salo-Mullen, E. E.; Ashraf, A.; Weiser, M. R.; Garcia-Aguilar, J.; Robson, M. E.; Offit, K.; Arcila, M. E.; Berger, M. F.; Shia, J.; Solit, D. B.; Saltz, L. B. Reliable Detection of Mismatch Repair Deficiency in Colorectal Cancers Using Mutational Load in Next-Generation Sequencing Panels. *J Clin Oncol* **2016**, *34* (18), 2141–2147. <https://doi.org/10.1200/JCO.2015.65.1067>.
- (120) Budinska, E.; Popovici, V.; Tejpar, S.; D'Ario, G.; Lapique, N.; Sikora, K. O.; Di Narzo, A. F.; Yan, P.; Hodgson, J. G.; Weinrich, S.; Bosman, F.; Roth, A.; Delorenzi, M. Gene Expression Patterns Unveil a New Level of Molecular Heterogeneity in Colorectal Cancer. *J Pathol* **2013**, *231* (1), 63–76. <https://doi.org/10.1002/path.4212>.
- (121) Marisa, L.; de Reyniès, A.; Duval, A.; Selves, J.; Gaub, M. P.; Vescovo, L.; Etienne-Grimaldi, M.-C.; Schiappa, R.; Guenot, D.; Ayadi, M.; Kirzin, S.; Chazal, M.; Fléjou, J.-F.; Benchimol, D.; Berger, A.; Lagarde, A.; Pencreach, E.; Piard, F.; Elias, D.; Parc, Y.; Olschwang, S.; Milano, G.; Laurent-Puig, P.; Boige, V. Gene Expression Classification of Colon Cancer into Molecular Subtypes: Characterization, Validation, and Prognostic Value. *PLoS Med* **2013**, *10* (5), e1001453. <https://doi.org/10.1371/journal.pmed.1001453>.
- (122) Sadanandam, A.; Lyssiotis, C. A.; Homicsko, K.; Collisson, E. A.; Gibb, W. J.; Wullschleger, S.; Ostos, L. C. G.; Lannon, W. A.; Grotzinger, C.; Del Rio, M.; Lhermitte, B.; Olshen, A. B.; Wiedenmann, B.; Cantley, L. C.; Gray, J. W.; Hanahan, D. A Colorectal Cancer Classification System That Associates Cellular Phenotype and Responses to Therapy. *Nat Med* **2013**, *19* (5), 619–625. <https://doi.org/10.1038/nm.3175>.
- (123) De Sousa E Melo, F.; Wang, X.; Jansen, M.; Fessler, E.; Trinh, A.; de Rooij, L. P. M. H.; de Jong, J. H.; de Boer, O. J.; van Leersum, R.; Bijlsma, M. F.; Rodermond, H.; van der Heijden, M.; van Noesel, C. J. M.; Tuynman, J. B.; Dekker, E.; Markowitz, F.; Medema, J. P.; Vermeulen, L. Poor-Prognosis Colon Cancer Is Defined by a Molecularly Distinct Subtype and Develops from Serrated Precursor Lesions. *Nat Med* **2013**, *19* (5), 614–618. <https://doi.org/10.1038/nm.3174>.
- (124) Roepman, P.; Schlicker, A.; Tabernero, J.; Majewski, I.; Tian, S.; Moreno, V.; Snel, M. H.; Chresta, C. M.; Rosenberg, R.; Nitsche, U.; Macarulla, T.; Capella, G.; Salazar, R.; Orphanides, G.; Wessels, L. F. A.; Bernards, R.; Simon, I. M. Colorectal Cancer Intrinsic Subtypes Predict Chemotherapy Benefit, Deficient Mismatch Repair and Epithelial-to-Mesenchymal Transition. *Int J Cancer* **2014**, *134* (3), 552–562. <https://doi.org/10.1002/ijc.28387>.
- (125) Schlicker, A.; Beran, G.; Chresta, C. M.; McWalter, G.; Pritchard, A.; Weston, S.; Runswick, S.; Davenport, S.; Heathcote, K.; Castro, D. A.; Orphanides, G.; French, T.; Wessels, L. F. A. Subtypes of Primary Colorectal Tumors Correlate with Response to Targeted Treatment in Colorectal Cell Lines. *BMC Med Genomics* **2012**, *5*, 66. <https://doi.org/10.1186/1755-8794-5-66>.
- (126) Eide, P. W.; Bruun, J.; Lothe, R. A.; Sveen, A. CMScaller: An R Package for Consensus Molecular Subtyping of Colorectal Cancer Pre-Clinical Models. *Sci Rep* **2017**, *7* (1), 16618. <https://doi.org/10.1038/s41598-017-16747-x>.

- (127) Masud, S. N.; Chandrashekhar, M.; Aregger, M.; Tan, G.; Zhang, X.; Mero, P.; Pirman, D. A.; Zaslaver, O.; Smolen, G. A.; Lin, Z.-Y.; Wong, C. J.; Boone, C.; Gingras, A.-C.; Montenegro-Burke, J. R.; Moffat, J. Chemical Genomics with Pyrvinium Identifies C1orf115 as a Regulator of Drug Efflux. *Nat Chem Biol* **2022**, *18* (12), 1370–1379. <https://doi.org/10.1038/s41589-022-01109-0>.
- (128) Jiang, J.; Xu, Y.; Ren, H.; Wudu, M.; Wang, Q.; Song, X.; Su, H.; Jiang, X.; Jiang, L.; Qiu, X. MKRN2 Inhibits Migration and Invasion of Non-Small-Cell Lung Cancer by Negatively Regulating the PI3K/Akt Pathway. *J Exp Clin Cancer Res* **2018**, *37* (1), 189. <https://doi.org/10.1186/s13046-018-0855-7>.
- (129) Jia, C.; Tang, H.; Yang, Y.; Yuan, S.; Han, T.; Fang, M.; Huang, S.; Hu, R.; Li, C.; Geng, W. Ubiquitination of IGF2BP3 by E3 Ligase MKRN2 Regulates the Proliferation and Migration of Human Neuroblastoma SHSY5Y Cells. *Biochem Biophys Res Commun* **2020**, *529* (1), 43–50. <https://doi.org/10.1016/j.bbrc.2020.05.112>.
- (130) Schatoff, E. M.; Leach, B. I.; Dow, L. E. Wnt Signaling and Colorectal Cancer. *Curr Colorectal Cancer Rep* **2017**, *13* (2), 101–110. <https://doi.org/10.1007/s11888-017-0354-9>.
- (131) Po, A.; Citarella, A.; Catanzaro, G.; Besharat, Z. M.; Trocchianesi, S.; Gianno, F.; Sabato, C.; Moretti, M.; De Smaele, E.; Vacca, A.; Fiori, M. E.; Ferretti, E. Hedgehog-GLI Signalling Promotes Chemoresistance through the Regulation of ABC Transporters in Colorectal Cancer Cells. *Sci Rep* **2020**, *10* (1), 13988. <https://doi.org/10.1038/s41598-020-70871-9>.
- (132) Wang, Q.; Shi, Y.-L.; Zhou, K.; Wang, L.-L.; Yan, Z.-X.; Liu, Y.-L.; Xu, L.-L.; Zhao, S.-W.; Chu, H.-L.; Shi, T.-T.; Ma, Q.-H.; Bi, J. PIK3CA Mutations Confer Resistance to First-Line Chemotherapy in Colorectal Cancer. *Cell Death Dis* **2018**, *9* (7), 739. <https://doi.org/10.1038/s41419-018-0776-6>.
- (1) Aravind, L.; Koonin, E. V. The HORMA Domain: A Common Structural Denominator in Mitotic Checkpoints, Chromosome Synapsis and DNA Repair. *Trends in Biochemical Sciences* **1998**, *23* (8), 284–286. [https://doi.org/10.1016/S0968-0004\(98\)01257-2](https://doi.org/10.1016/S0968-0004(98)01257-2).
- (2) Rosenberg, S. C.; Corbett, K. D. The Multifaceted Roles of the HORMA Domain in Cellular Signaling. *Journal of Cell Biology* **2015**, *211* (4), 745–755. <https://doi.org/10.1083/jcb.201509076>.
- (3) Clairmont, C. S.; Sarangi, P.; PonnienSelvan, K.; Galli, L. D.; Csete, I.; Moreau, L.; Adelmant, G.; Chowdhury, D.; Marto, J. A.; D'Andrea, A. D. TRIP13 Regulates DNA Repair Pathway Choice through REV7 Conformational Change. *Nat Cell Biol* **2020**, *22* (1), 87–96. <https://doi.org/10.1038/s41556-019-0442-y>.
- (4) Wojtasz, L.; Daniel, K.; Roig, I.; Bolcun-Filas, E.; Xu, H.; Boonsanay, V.; Eckmann, C. R.; Cooke, H. J.; Jasin, M.; Keeney, S.; McKay, M. J.; Toth, A. Mouse HORMAD1 and HORMAD2, Two Conserved Meiotic Chromosomal Proteins, Are Depleted from Synapsed Chromosome Axes with the Help of TRIP13 AAA-ATPase. *PLoS Genet* **2009**, *5* (10), e1000702. <https://doi.org/10.1371/journal.pgen.1000702>.
- (5) Musacchio, A. The Molecular Biology of Spindle Assembly Checkpoint Signaling Dynamics.

- Curr Biol* **2015**, 25 (20), R1002-1018. <https://doi.org/10.1016/j.cub.2015.08.051>.
- (6) Yost, S.; de Wolf, B.; Hanks, S.; Zachariou, A.; Marcozzi, C.; Clarke, M.; de Voer, R. M.; Etemad, B.; Uijttewaal, E.; Ramsay, E.; Wylie, H.; Elliott, A.; Picton, S.; Smith, A.; Smithson, S.; Seal, S.; Ruark, E.; Houge, G.; Pines, J.; Kops, G. J. P. L.; Rahman, N. Biallelic TRIP13 Mutations Predispose to Wilms Tumor and Chromosome Missegregation. *Nat Genet* **2017**, 49 (7), 1148–1151. <https://doi.org/10.1038/ng.3883>.
  - (7) Zhang, G.; Zhu, Q.; Fu, G.; Hou, J.; Hu, X.; Cao, J.; Peng, W.; Wang, X.; Chen, F.; Cui, H. TRIP13 Promotes the Cell Proliferation, Migration and Invasion of Glioblastoma through the FBXW7/c-MYC Axis. *Br J Cancer* **2019**, 121 (12), 1069–1078. <https://doi.org/10.1038/s41416-019-0633-0>.
  - (8) Banerjee, R.; Russo, N.; Liu, M.; Basrur, V.; Bellile, E.; Palanisamy, N.; Scanlon, C. S.; van Tubergen, E.; Inglehart, R. C.; Metwally, T.; Mani, R.-S.; Yocum, A.; Nyati, M. K.; Castilho, R. M.; Varambally, S.; Chinnaiyan, A. M.; D'Silva, N. J. TRIP13 Promotes Error-Prone Nonhomologous End Joining and Induces Chemoresistance in Head and Neck Cancer. *Nat Commun* **2014**, 5, 4527. <https://doi.org/10.1038/ncomms5527>.
  - (9) Sarangi, P.; Clairmont, C. S.; Galli, L. D.; Moreau, L. A.; D'Andrea, A. D. P31comet Promotes Homologous Recombination by Inactivating REV7 through the TRIP13 ATPase. *Proc Natl Acad Sci U S A* **2020**, 117 (43), 26795–26803. <https://doi.org/10.1073/pnas.2008830117>.
  - (10) Ho, H.-C.; Burgess, S. M. Pch2 Acts through Xrs2 and Tel1/ATM to Modulate Interhomolog Bias and Checkpoint Function during Meiosis. *PLOS Genetics* **2011**, 7 (11), e1002351. <https://doi.org/10.1371/journal.pgen.1002351>.
  - (11) Villar-Fernández, M. A.; Silva, R. C. da; Firlej, M.; Pan, D.; Weir, E.; Sarembe, A.; Raina, V. B.; Bange, T.; Weir, J. R.; Vader, G. Biochemical and Functional Characterization of a Meiosis-Specific Pch2/ORC AAA+ Assembly. *Life Science Alliance* **2020**, 3 (11). <https://doi.org/10.26508/lsa.201900630>.
  - (12) Zhou, Y.; Caron, P.; Legube, G.; Paull, T. T. Quantitation of DNA Double-Strand Break Resection Intermediates in Human Cells. *Nucleic Acids Res* **2014**, 42 (3), e19. <https://doi.org/10.1093/nar/gkt1309>.
  - (13) Kim, D. H.; Han, J. S.; Ly, P.; Ye, Q.; McMahon, M. A.; Myung, K.; Corbett, K. D.; Cleveland, D. W. TRIP13 and APC15 Drive Mitotic Exit by Turnover of Interphase- and Unattached Kinetochore-Produced MCC. *Nat Commun* **2018**, 9 (1), 4354. <https://doi.org/10.1038/s41467-018-06774-1>.
  - (14) Lee, S.-G.; Kim, N.; Kim, S.-M.; Park, I. B.; Kim, H.; Kim, S.; Kim, B.-G.; Hwang, J. M.; Baek, I.-J.; Gartner, A.; Park, J. H.; Myung, K. Ewing Sarcoma Protein Promotes Dissociation of Poly(ADP-Ribose) Polymerase 1 from Chromatin. *EMBO Rep* **2020**, 21 (11), e48676. <https://doi.org/10.15252/embr.201948676>.
  - (15) Schneider, C. A.; Rasband, W. S.; Eliceiri, K. W. NIH Image to ImageJ: 25 Years of Image Analysis. *Nat Methods* **2012**, 9 (7), 671–675. <https://doi.org/10.1038/nmeth.2089>.
  - (16) Paull, T. T.; Gellert, M. The 3' to 5' Exonuclease Activity of Mre11 Facilitates Repair of DNA

- Double-Strand Breaks. *Molecular Cell* **1998**, *1* (7), 969–979. [https://doi.org/10.1016/S1097-2765\(00\)80097-0](https://doi.org/10.1016/S1097-2765(00)80097-0).
- (17) Howard, S. M.; Yanez, D. A.; Stark, J. M. DNA Damage Response Factors from Diverse Pathways, Including DNA Crosslink Repair, Mediate Alternative End Joining. *PLoS Genet* **2015**, *11* (1), e1004943. <https://doi.org/10.1371/journal.pgen.1004943>.
  - (18) Kochan, J. A.; Desclos, E. C. B.; Bosch, R.; Meister, L.; Vriend, L. E. M.; van Attikum, H.; Krawczyk, P. M. Meta-Analysis of DNA Double-Strand Break Response Kinetics. *Nucleic Acids Res* **2017**, *45* (22), 12625–12637. <https://doi.org/10.1093/nar/gkx1128>.
  - (19) Natsume, T.; Kiyomitsu, T.; Saga, Y.; Kanemaki, M. T. Rapid Protein Depletion in Human Cells by Auxin-Inducible Degron Tagging with Short Homology Donors. *Cell Rep* **2016**, *15* (1), 210–218. <https://doi.org/10.1016/j.celrep.2016.03.001>.
  - (20) Kim, D. I.; Jensen, S. C.; Noble, K. A.; Kc, B.; Roux, K. H.; Motamedchaboki, K.; Roux, K. J. An Improved Smaller Biotin Ligase for BioID Proximity Labeling. *Mol Biol Cell* **2016**, *27* (8), 1188–1196. <https://doi.org/10.1091/mbc.E15-12-0844>.
  - (21) Ong, S.-E.; Blagoev, B.; Kratchmarova, I.; Kristensen, D. B.; Steen, H.; Pandey, A.; Mann, M. Stable Isotope Labeling by Amino Acids in Cell Culture, SILAC, as a Simple and Accurate Approach to Expression Proteomics. *Mol Cell Proteomics* **2002**, *1* (5), 376–386. <https://doi.org/10.1074/mcp.m200025-mcp200>.
  - (22) Ong, S.-E.; Mann, M. A Practical Recipe for Stable Isotope Labeling by Amino Acids in Cell Culture (SILAC). *Nat Protoc* **2006**, *1* (6), 2650–2660. <https://doi.org/10.1038/nprot.2006.427>.
  - (23) Lee, J.-H.; Paull, T. T. Activation and Regulation of ATM Kinase Activity in Response to DNA Double-Strand Breaks. *Oncogene* **2007**, *26* (56), 7741–7748. <https://doi.org/10.1038/sj.onc.1210872>.
  - (24) Wang, Y.; Cortez, D.; Yazdi, P.; Neff, N.; Elledge, S. J.; Qin, J. BASC, a Super Complex of BRCA1-Associated Proteins Involved in the Recognition and Repair of Aberrant DNA Structures. *Genes Dev* **2000**, *14* (8), 927–939.
  - (25) Haber, J. E. The Many Interfaces of Mre11. *Cell* **1998**, *95* (5), 583–586. [https://doi.org/10.1016/S0092-8674\(00\)81626-8](https://doi.org/10.1016/S0092-8674(00)81626-8).
  - (26) Stucki, M.; Clapperton, J. A.; Mohammad, D.; Yaffe, M. B.; Smerdon, S. J.; Jackson, S. P. MDC1 Directly Binds Phosphorylated Histone H2AX to Regulate Cellular Responses to DNA Double-Strand Breaks. *Cell* **2005**, *123* (7), 1213–1226. <https://doi.org/10.1016/j.cell.2005.09.038>.
  - (27) Chapman, J. R.; Jackson, S. P. Phospho-Dependent Interactions between NBS1 and MDC1 Mediate Chromatin Retention of the MRN Complex at Sites of DNA Damage. *EMBO Rep* **2008**, *9* (8), 795–801. <https://doi.org/10.1038/embor.2008.103>.
  - (28) Spycher, C.; Miller, E. S.; Townsend, K.; Pavic, L.; Morrice, N. A.; Janscak, P.; Stewart, G. S.; Stucki, M. Constitutive Phosphorylation of MDC1 Physically Links the MRE11-RAD50-NBS1 Complex to Damaged Chromatin. *J Cell Biol* **2008**, *181* (2), 227–240. <https://doi.org/10.1083/jcb.200709008>.

- (29) Wu, L.; Luo, K.; Lou, Z.; Chen, J. MDC1 Regulates Intra-S-Phase Checkpoint by Targeting NBS1 to DNA Double-Strand Breaks. *Proc Natl Acad Sci U S A* **2008**, *105* (32), 11200–11205. <https://doi.org/10.1073/pnas.0802885105>.
- (30) Lee, M. S.; Edwards, R. A.; Thede, G. L.; Glover, J. N. M. Structure of the BRCT Repeat Domain of MDC1 and Its Specificity for the Free COOH-Terminal End of the Gamma-H2AX Histone Tail. *J Biol Chem* **2005**, *280* (37), 32053–32056. <https://doi.org/10.1074/jbc.C500273200>.
- (31) Stewart, G. S.; Wang, B.; Bignell, C. R.; Taylor, A. M. R.; Elledge, S. J. MDC1 Is a Mediator of the Mammalian DNA Damage Checkpoint. *Nature* **2003**, *421* (6926), 961–966. <https://doi.org/10.1038/nature01446>.
- (32) Lee, J.-H.; Mand, M. R.; Deshpande, R. A.; Kinoshita, E.; Yang, S.-H.; Wyman, C.; Paull, T. T. Ataxia Telangiectasia-Mutated (ATM) Kinase Activity Is Regulated by ATP-Driven Conformational Changes in the Mre11/Rad50/Nbs1 (MRN) Complex. *J Biol Chem* **2013**, *288* (18), 12840–12851. <https://doi.org/10.1074/jbc.M113.460378>.
- (33) Zhou, Y.; Paull, T. T. Direct Measurement of Single-Stranded DNA Intermediates in Mammalian Cells by Quantitative Polymerase Chain Reaction. *Anal Biochem* **2015**, *479*, 48–50. <https://doi.org/10.1016/j.ab.2015.03.025>.
- (34) Crossen, P. E.; Drets, M. E.; Arrighi, F. E.; Johnston, D. A. Analysis of the Frequency and Distribution of Sister Chromatid Exchanges in Cultured Human Lymphocytes. *Hum Genet* **1977**, *35* (3), 345–352. <https://doi.org/10.1007/BF00446625>.
- (35) Galloway, S. M.; Evans, H. J. Sister Chromatid Exchange in Human Chromosomes from Normal Individuals and Patients with Ataxia Telangiectasia. *Cytogenet Cell Genet* **1975**, *15* (1), 17–29. <https://doi.org/10.1159/000130495>.
- (36) Sonoda, E.; Sasaki, M. S.; Morrison, C.; Yamaguchi-Iwai, Y.; Takata, M.; Takeda, S. Sister Chromatid Exchanges Are Mediated by Homologous Recombination in Vertebrate Cells. *Mol Cell Biol* **1999**, *19* (7), 5166–5169.
- (37) Kieffer, S. R.; Lowndes, N. F. Immediate-Early, Early, and Late Responses to DNA Double Stranded Breaks. *Frontiers in Genetics* **2022**, *13*.
- (38) Lee, J.-H.; Paull, T. T. Direct Activation of the ATM Protein Kinase by the Mre11/Rad50/Nbs1 Complex. *Science* **2004**, *304* (5667), 93–96. <https://doi.org/10.1126/science.1091496>.
- (39) Paull, T. T.; Lee, J.-H. The Mre11/Rad50/Nbs1 Complex and Its Role as a DNA Double-Strand Break Sensor for ATM. *Cell Cycle* **2005**, *4* (6), 737–740. <https://doi.org/10.4161/cc.4.6.1715>.
- (40) Lee, J.-H.; Paull, T. T. ATM Activation by DNA Double-Strand Breaks through the Mre11-Rad50-Nbs1 Complex. *Science* **2005**, *308* (5721), 551–554. <https://doi.org/10.1126/science.1108297>.
- (41) Limbo, O.; Yamada, Y.; Russell, P. Mre11-Rad50-Dependent Activity of ATM/Tel1 at DNA Breaks and Telomeres in the Absence of Nbs1. *Mol Biol Cell* **2018**, *29* (11), 1389–1399. <https://doi.org/10.1091/mbc.E17-07-0470>.
- (42) Drew, K.; Wallingford, J. B.; Marcotte, E. M. Hu.MAP 2.0: Integration of over 15,000 Proteomic Experiments Builds a Global Compendium of Human Multiprotein Assemblies. *Mol Syst Biol*



- 2021**, 17 (5), e10016. <https://doi.org/10.15252/msb.202010016>.
- (43) Yasugi, T.; Vidal, M.; Sakai, H.; Howley, P. M.; Benson, J. D. Two Classes of Human Papillomavirus Type 16 E1 Mutants Suggest Pleiotropic Conformational Constraints Affecting E1 Multimerization, E2 Interaction, and Interaction with Cellular Proteins. *J Virol* **1997**, 71 (8), 5942–5951. <https://doi.org/10.1128/JVI.71.8.5942-5951.1997>.
  - (44) Eytan, E.; Wang, K.; Miniowitz-Shemtov, S.; Sitry-Shevah, D.; Kaisari, S.; Yen, T. J.; Liu, S.-T.; Herskho, A. Disassembly of Mitotic Checkpoint Complexes by the Joint Action of the AAA-ATPase TRIP13 and P31(Comet). *Proc Natl Acad Sci U S A* **2014**, 111 (33), 12019–12024. <https://doi.org/10.1073/pnas.1412901111>.
  - (45) Kolas, N. K.; Chapman, J. R.; Nakada, S.; Ylanko, J.; Chahwan, R.; Sweeney, F. D.; Panier, S.; Mendez, M.; Wildenhain, J.; Thomson, T. M.; Pelletier, L.; Jackson, S. P.; Durocher, D. Orchestration of the DNA-Damage Response by the RNF8 Ubiquitin Ligase. *Science* **2007**, 318 (5856), 1637–1640. <https://doi.org/10.1126/science.1150034>.
  - (46) Nowsheen, S.; Aziz, K.; Aziz, A.; Deng, M.; Qin, B.; Luo, K.; Jeganathan, K. B.; Zhang, H.; Liu, T.; Yu, J.; Deng, Y.; Yuan, J.; Ding, W.; van Deursen, J. M.; Lou, Z. L3MBTL2 Orchestrates Ubiquitin Signalling by Dictating the Sequential Recruitment of RNF8 and RNF168 after DNA Damage. *Nat Cell Biol* **2018**, 20 (4), 455–464. <https://doi.org/10.1038/s41556-018-0071-x>.
  - (47) Thorslund, T.; Ripplinger, A.; Hoffmann, S.; Wild, T.; Uckelmann, M.; Villumsen, B.; Narita, T.; Sixma, T. K.; Choudhary, C.; Bekker-Jensen, S.; Mailand, N. Histone H1 Couples Initiation and Amplification of Ubiquitin Signalling after DNA Damage. *Nature* **2015**, 527 (7578), 389–393. <https://doi.org/10.1038/nature15401>.
  - (48) Chapman, J. R.; Barral, P.; Vannier, J.-B.; Borel, V.; Steger, M.; Tomas-Loba, A.; Sartori, A. A.; Adams, I. R.; Batista, F. D.; Boulton, S. J. RIF1 Is Essential for 53BP1-Dependent Nonhomologous End Joining and Suppression of DNA Double-Strand Break Resection. *Mol Cell* **2013**, 49 (5), 858–871. <https://doi.org/10.1016/j.molcel.2013.01.002>.
  - (49) Escribano-Díaz, C.; Orthwein, A.; Fradet-Turcotte, A.; Xing, M.; Young, J. T. F.; Tkáč, J.; Cook, M. A.; Rosebrock, A. P.; Munro, M.; Canny, M. D.; Xu, D.; Durocher, D. A Cell Cycle-Dependent Regulatory Circuit Composed of 53BP1-RIF1 and BRCA1-CtIP Controls DNA Repair Pathway Choice. *Mol Cell* **2013**, 49 (5), 872–883. <https://doi.org/10.1016/j.molcel.2013.01.001>.
  - (50) Zimmermann, M.; Lottersberger, F.; Buonomo, S. B.; Sfeir, A.; de Lange, T. 53BP1 Regulates DSB Repair Using Rif1 to Control 5' End Resection. *Science* **2013**, 339 (6120), 700–704. <https://doi.org/10.1126/science.1231573>.
  - (51) Munoz, I. M.; Jowsey, P. A.; Toth, R.; Rouse, J. Phospho-Epitope Binding by the BRCT Domains of HPTIP Controls Multiple Aspects of the Cellular Response to DNA Damage. *Nucleic Acids Res* **2007**, 35 (16), 5312–5322. <https://doi.org/10.1093/nar/gkm493>.
  - (52) Noordermeer, S. M.; Adam, S.; Setiawati, D.; Barazas, M.; Pettitt, S. J.; Ling, A. K.; Olivieri, M.; Álvarez-Quilón, A.; Moatti, N.; Zimmermann, M.; Annunziato, S.; Krastev, D. B.; Song, F.; Brandsma, I.; Frankum, J.; Brough, R.; Sherker, A.; Landry, S.; Szilard, R. K.; Munro, M. M.;

- McEwan, A.; Goullet de Rugy, T.; Lin, Z.-Y.; Hart, T.; Moffat, J.; Gingras, A.-C.; Martin, A.; van Attikum, H.; Jonkers, J.; Lord, C. J.; Rottenberg, S.; Durocher, D. The Shieldin Complex Mediates 53BP1-Dependent DNA Repair. *Nature* **2018**, *560* (7716), 117–121. <https://doi.org/10.1038/s41586-018-0340-7>.
- (53) Xu, G.; Chapman, J. R.; Brandsma, I.; Yuan, J.; Mistrik, M.; Bouwman, P.; Bartkova, J.; Gogola, E.; Warmerdam, D.; Barazas, M.; Jaspers, J. E.; Watanabe, K.; Pieterse, M.; Kersbergen, A.; Sol, W.; Celie, P. H. N.; Schouten, P. C.; van den Broek, B.; Salman, A.; Nieuwland, M.; de Rink, I.; de Ronde, J.; Jalink, K.; Boulton, S. J.; Chen, J.; van Gent, D. C.; Bartek, J.; Jonkers, J.; Borst, P.; Rottenberg, S. REV7 Counteracts DNA Double-Strand Break Resection and Affects PARP Inhibition. *Nature* **2015**, *521* (7553), 541–544. <https://doi.org/10.1038/nature14328>.
- (54) Boersma, V.; Moatti, N.; Segura-Bayona, S.; Peuscher, M. H.; van der Torre, J.; Wevers, B. A.; Orthwein, A.; Durocher, D.; Jacobs, J. J. L. MAD2L2 Controls DNA Repair at Telomeres and DNA Breaks by Inhibiting 5' End Resection. *Nature* **2015**, *521* (7553), 537–540. <https://doi.org/10.1038/nature14216>.
- (55) Lapointe, S.; Perry, A.; Butowski, N. A. Primary Brain Tumours in Adults. *Lancet* **2018**, *392* (10145), 432–446. [https://doi.org/10.1016/S0140-6736\(18\)30990-5](https://doi.org/10.1016/S0140-6736(18)30990-5).
- (56) Wen, P. Y.; Huse, J. T. 2016 World Health Organization Classification of Central Nervous System Tumors. *Continuum (Minneap Minn)* **2017**, *23* (6, Neuro-oncology), 1531–1547. <https://doi.org/10.1212/CON.0000000000000536>.
- (57) Louis, D. N.; Perry, A.; Wesseling, P.; Brat, D. J.; Cree, I. A.; Figarella-Branger, D.; Hawkins, C.; Ng, H. K.; Pfister, S. M.; Reifenberger, G.; Soffietti, R.; von Deimling, A.; Ellison, D. W. The 2021 WHO Classification of Tumors of the Central Nervous System: A Summary. *Neuro-Oncology* **2021**, *23* (8), 1231–1251. <https://doi.org/10.1093/neuonc/noab106>.
- (58) Brennan, C. W.; Verhaak, R. G. W.; McKenna, A.; Campos, B.; Noushmehr, H.; Salama, S. R.; Zheng, S.; Chakravarty, D.; Sanborn, J. Z.; Berman, S. H.; Beroukhi, R.; Bernard, B.; Wu, C.-J.; Genovese, G.; Shmulevich, I.; Barnholtz-Sloan, J.; Zou, L.; Vegesna, R.; Shukla, S. A.; Ciriello, G.; Yung, W. K.; Zhang, W.; Sougnez, C.; Mikkelsen, T.; Aldape, K.; Bigner, D. D.; Van Meir, E. G.; Prados, M.; Sloan, A.; Black, K. L.; Eschbacher, J.; Finocchiaro, G.; Friedman, W.; Andrews, D. W.; Guha, A.; Iacocca, M.; O'Neill, B. P.; Foltz, G.; Myers, J.; Weisenberger, D. J.; Penny, R.; Kucherlapati, R.; Perou, C. M.; Hayes, D. N.; Gibbs, R.; Marra, M.; Mills, G. B.; Lander, E.; Spellman, P.; Wilson, R.; Sander, C.; Weinstein, J.; Meyerson, M.; Gabriel, S.; Laird, P. W.; Haussler, D.; Getz, G.; Chin, L.; TCGA Research Network. The Somatic Genomic Landscape of Glioblastoma. *Cell* **2013**, *155* (2), 462–477. <https://doi.org/10.1016/j.cell.2013.09.034>.
- (59) Phillips, H. S.; Kharbanda, S.; Chen, R.; Forrest, W. F.; Soriano, R. H.; Wu, T. D.; Misra, A.; Nigro, J. M.; Colman, H.; Soroceanu, L.; Williams, P. M.; Modrusan, Z.; Feuerstein, B. G.; Aldape, K. Molecular Subclasses of High-Grade Glioma Predict Prognosis, Delineate a Pattern of Disease Progression, and Resemble Stages in Neurogenesis. *Cancer Cell* **2006**, *9* (3), 157–173. <https://doi.org/10.1016/j.ccr.2006.02.019>.
- (60) Verhaak, R. G. W.; Hoadley, K. A.; Purdom, E.; Wang, V.; Qi, Y.; Wilkerson, M. D.; Miller, C. R.;



- Ding, L.; Golub, T.; Mesirov, J. P.; Alexe, G.; Lawrence, M.; O'Kelly, M.; Tamayo, P.; Weir, B. A.; Gabriel, S.; Winckler, W.; Gupta, S.; Jakkula, L.; Feiler, H. S.; Hodgson, J. G.; James, C. D.; Sarkaria, J. N.; Brennan, C.; Kahn, A.; Spellman, P. T.; Wilson, R. K.; Speed, T. P.; Gray, J. W.; Meyerson, M.; Getz, G.; Perou, C. M.; Hayes, D. N.; Cancer Genome Atlas Research Network. Integrated Genomic Analysis Identifies Clinically Relevant Subtypes of Glioblastoma Characterized by Abnormalities in PDGFRA, IDH1, EGFR, and NF1. *Cancer Cell* **2010**, *17* (1), 98–110. <https://doi.org/10.1016/j.ccr.2009.12.020>.
- (61) Brat, D. J.; Aldape, K.; Colman, H.; Holland, E. C.; Louis, D. N.; Jenkins, R. B.; Kleinschmidt-DeMasters, B. K.; Perry, A.; Reifenberger, G.; Stupp, R.; von Deimling, A.; Weller, M. CIMPACT-NOW Update 3: Recommended Diagnostic Criteria for "Diffuse Astrocytic Glioma, IDH-Wildtype, with Molecular Features of Glioblastoma, WHO Grade IV." *Acta Neuropathol* **2018**, *136* (5), 805–810. <https://doi.org/10.1007/s00401-018-1913-0>.
- (62) Ellison, D. W.; Hawkins, C.; Jones, D. T. W.; Onar-Thomas, A.; Pfister, S. M.; Reifenberger, G.; Louis, D. N. CIMPACT-NOW Update 4: Diffuse Gliomas Characterized by MYB, MYBL1, or FGFR1 Alterations or BRAFV600E Mutation. *Acta Neuropathol* **2019**, *137* (4), 683–687. <https://doi.org/10.1007/s00401-019-01987-0>.
- (63) Louis, D. N.; Wesseling, P.; Aldape, K.; Brat, D. J.; Capper, D.; Cree, I. A.; Eberhart, C.; Figarella-Branger, D.; Fouladi, M.; Fuller, G. N.; Giannini, C.; Haberler, C.; Hawkins, C.; Komori, T.; Kros, J. M.; Ng, H. K.; Orr, B. A.; Park, S.-H.; Paulus, W.; Perry, A.; Pietsch, T.; Reifenberger, G.; Rosenblum, M.; Rous, B.; Sahm, F.; Sarkar, C.; Solomon, D. A.; Tabori, U.; van den Bent, M. J.; von Deimling, A.; Weller, M.; White, V. A.; Ellison, D. W. CIMPACT-NOW Update 6: New Entity and Diagnostic Principle Recommendations of the CIMPACT-Utrecht Meeting on Future CNS Tumor Classification and Grading. *Brain Pathol* **2020**, *30* (4), 844–856. <https://doi.org/10.1111/bpa.12832>.
- (64) Louis, D. N.; Wesseling, P.; Paulus, W.; Giannini, C.; Batchelor, T. T.; Cairncross, J. G.; Capper, D.; Figarella-Branger, D.; Lopes, M. B.; Wick, W.; van den Bent, M. CIMPACT-NOW Update 1: Not Otherwise Specified (NOS) and Not Elsewhere Classified (NEC). *Acta Neuropathol* **2018**, *135* (3), 481–484. <https://doi.org/10.1007/s00401-018-1808-0>.
- (65) Louis, D. N.; Aldape, K.; Brat, D. J.; Capper, D.; Ellison, D. W.; Hawkins, C.; Paulus, W.; Perry, A.; Reifenberger, G.; Figarella-Branger, D.; Wesseling, P.; Batchelor, T. T.; Gregory Cairncross, J.; Pfister, S. M.; Rutkowski, S.; Weller, M.; Wick, W.; von Deimling, A. CIMPACT-NOW (the Consortium to Inform Molecular and Practical Approaches to CNS Tumor Taxonomy): A New Initiative in Advancing Nervous System Tumor Classification. *Brain Pathol* **2017**, *27* (6), 851–852. <https://doi.org/10.1111/bpa.12457>.
- (66) Louis, D. N.; Aldape, K.; Brat, D. J.; Capper, D.; Ellison, D. W.; Hawkins, C.; Paulus, W.; Perry, A.; Reifenberger, G.; Figarella-Branger, D.; Wesseling, P.; Batchelor, T. T.; Gregory Cairncross, J.; Pfister, S. M.; Rutkowski, S.; Weller, M.; Wick, W.; von Deimling, A. CIMPACT-NOW (the Consortium to Inform Molecular and Practical Approaches to CNS Tumor Taxonomy): A New Initiative in Advancing Nervous System Tumor Classification. *Brain Pathol* **2016**, *27* (6), 851–

852. <https://doi.org/10.1111/bpa.12457>.
- (67) Friedmann-Morvinski, D. Glioblastoma Heterogeneity and Cancer Cell Plasticity. *Crit Rev Oncog* **2014**, *19* (5), 327–336. <https://doi.org/10.1615/critrevoncog.2014011777>.
- (68) Parker, N. R.; Khong, P.; Parkinson, J. F.; Howell, V. M.; Wheeler, H. R. Molecular Heterogeneity in Glioblastoma: Potential Clinical Implications. *Front Oncol* **2015**, *5*, 55. <https://doi.org/10.3389/fonc.2015.00055>.
- (69) Shen, Y.; Grisdale, C. J.; Islam, S. A.; Bose, P.; Lever, J.; Zhao, E. Y.; Grinshtein, N.; Ma, Y.; Mungall, A. J.; Moore, R. A.; Lun, X.; Senger, D. L.; Robbins, S. M.; Wang, A. Y.; MacIsaac, J. L.; Kobor, M. S.; Luchman, H. A.; Weiss, S.; Chan, J. A.; Blough, M. D.; Kaplan, D. R.; Cairncross, J. G.; Marra, M. A.; Jones, S. J. M. Comprehensive Genomic Profiling of Glioblastoma Tumors, BTICs, and Xenografts Reveals Stability and Adaptation to Growth Environments. *Proc. Natl. Acad. Sci. U.S.A.* **2019**, *116* (38), 19098–19108. <https://doi.org/10.1073/pnas.1813495116>.
- (70) Vaubel, R. A.; Tian, S.; Remonde, D.; Schroeder, M. A.; Mladek, A. C.; Kitange, G. J.; Caron, A.; Kollmeyer, T. M.; Grove, R.; Peng, S.; Carlson, B. L.; Ma, D. J.; Sarkar, G.; Evers, L.; Decker, P. A.; Yan, H.; Dhruv, H. D.; Berens, M. E.; Wang, Q.; Marin, B. M.; Klee, E. W.; Califano, A.; LaChance, D. H.; Eckel-Passow, J. E.; Verhaak, R. G.; Sulman, E. P.; Burns, T. C.; Meyer, F. B.; O'Neill, B. P.; Tran, N. L.; Giannini, C.; Jenkins, R. B.; Parney, I. F.; Sarkaria, J. N. Genomic and Phenotypic Characterization of a Broad Panel of Patient-Derived Xenografts Reflects the Diversity of Glioblastoma. *Clin Cancer Res* **2020**, *26* (5), 1094–1104. <https://doi.org/10.1158/1078-0432.CCR-19-0909>.
- (71) Ben-David, U.; Ha, G.; Tseng, Y.-Y.; Greenwald, N. F.; Oh, C.; Shih, J.; McFarland, J. M.; Wong, B.; Boehm, J. S.; Beroukhi, R.; Golub, T. R. Patient-Derived Xenografts Undergo Mouse-Specific Tumor Evolution. *Nat Genet* **2017**, *49* (11), 1567–1575. <https://doi.org/10.1038/ng.3967>.
- (72) Bolger, A. M.; Lohse, M.; Usadel, B. Trimmomatic: A Flexible Trimmer for Illumina Sequence Data. *Bioinformatics* **2014**, *30* (15), 2114–2120. <https://doi.org/10.1093/bioinformatics/btu170>.
- (73) Li, H. Aligning Sequence Reads, Clone Sequences and Assembly Contigs with BWA-MEM. *arXiv:1303.3997 [q-bio]* **2013**.
- (74) Kim, S.; Scheffler, K.; Halpern, A. L.; Bekritsky, M. A.; Noh, E.; Källberg, M.; Chen, X.; Kim, Y.; Beyter, D.; Krusche, P.; Saunders, C. T. Strelka2: Fast and Accurate Calling of Germline and Somatic Variants. *Nat Methods* **2018**, *15* (8), 591–594. <https://doi.org/10.1038/s41592-018-0051-x>.
- (75) McLaren, W.; Gil, L.; Hunt, S. E.; Riat, H. S.; Ritchie, G. R. S.; Thormann, A.; Flicek, P.; Cunningham, F. The Ensembl Variant Effect Predictor. *Genome Biol* **2016**, *17* (1), 122. <https://doi.org/10.1186/s13059-016-0974-4>.
- (76) Tate, J. G.; Bamford, S.; Jubb, H. C.; Sondka, Z.; Beare, D. M.; Bindal, N.; Boutselakis, H.; Cole, C. G.; Creatore, C.; Dawson, E.; Fish, P.; Harsha, B.; Hathaway, C.; Jupe, S. C.; Kok, C. Y.; Noble, K.; Ponting, L.; Ramshaw, C. C.; Rye, C. E.; Speedy, H. E.; Stefancsik, R.; Thompson, S. L.; Wang,

- S.; Ward, S.; Campbell, P. J.; Forbes, S. A. COSMIC: The Catalogue Of Somatic Mutations In Cancer. *Nucleic Acids Research* **2019**, *47* (D1), D941–D947. <https://doi.org/10.1093/nar/gky1015>.
- (77) PCAWG Mutational Signatures Working Group; PCAWG Consortium; Alexandrov, L. B.; Kim, J.; Haradhvala, N. J.; Huang, M. N.; Tian Ng, A. W.; Wu, Y.; Boot, A.; Covington, K. R.; Gordenin, D. A.; Bergstrom, E. N.; Islam, S. M. A.; Lopez-Bigas, N.; Klimczak, L. J.; McPherson, J. R.; Morganella, S.; Sabarinathan, R.; Wheeler, D. A.; Mustonen, V.; Getz, G.; Rozen, S. G.; Stratton, M. R. The Repertoire of Mutational Signatures in Human Cancer. *Nature* **2020**, *578* (7793), 94–101. <https://doi.org/10.1038/s41586-020-1943-3>.
- (78) Bergstrom, E. N.; Huang, M. N.; Mahto, U.; Barnes, M.; Stratton, M. R.; Rozen, S. G.; Alexandrov, L. B. SigProfilerMatrixGenerator: A Tool for Visualizing and Exploring Patterns of Small Mutational Events. *BMC Genomics* **2019**, *20* (1), 685. <https://doi.org/10.1186/s12864-019-6041-2>.
- (79) Mi, H.; Muruganujan, A.; Huang, X.; Ebert, D.; Mills, C.; Guo, X.; Thomas, P. D. Protocol Update for Large-Scale Genome and Gene Function Analysis with the PANTHER Classification System (v.14.0). *Nat Protoc* **2019**, *14* (3), 703–721. <https://doi.org/10.1038/s41596-019-0128-8>.
- (80) Moore, L.; Cagan, A.; Coorens, T. H. H.; Neville, M. D. C.; Sanghvi, R.; Sanders, M. A.; Oliver, T. R. W.; Leongamornlert, D.; Ellis, P.; Noorani, A.; Mitchell, T. J.; Butler, T. M.; Hooks, Y.; Warren, A. Y.; Jorgensen, M.; Dawson, K. J.; Menzies, A.; O'Neill, L.; Latimer, C.; Teng, M.; van Bostel, R.; Iacobuzio-Donahue, C. A.; Martincorena, I.; Heer, R.; Campbell, P. J.; Fitzgerald, R. C.; Stratton, M. R.; Rahbari, R. The Mutational Landscape of Human Somatic and Germline Cells. *Nature* **2021**, *597* (7876), 381–386. <https://doi.org/10.1038/s41586-021-03822-7>.
- (81) Rouhani, F. J.; Nik-Zainal, S.; Wuster, A.; Li, Y.; Conte, N.; Koike-Yusa, H.; Kumasaka, N.; Vallier, L.; Yusa, K.; Bradley, A. Mutational History of a Human Cell Lineage from Somatic to Induced Pluripotent Stem Cells. *PLoS Genet* **2016**, *12* (4), e1005932. <https://doi.org/10.1371/journal.pgen.1005932>.
- (82) Pich, O.; Muiños, F.; Lolkema, M. P.; Steeghs, N.; Gonzalez-Perez, A.; Lopez-Bigas, N. The Mutational Footprints of Cancer Therapies. *Nat Genet* **2019**, *51* (12), 1732–1740. <https://doi.org/10.1038/s41588-019-0525-5>.
- (83) Wang, J.; Cazzato, E.; Ladewig, E.; Frattini, V.; Rosenbloom, D. I. S.; Zairis, S.; Abate, F.; Liu, Z.; Elliott, O.; Shin, Y.-J.; Lee, J.-K.; Lee, I.-H.; Park, W.-Y.; Eoli, M.; Blumberg, A. J.; Lasorella, A.; Nam, D.-H.; Finocchiaro, G.; Iavarone, A.; Rabadan, R. Clonal Evolution of Glioblastoma under Therapy. *Nat Genet* **2016**, *48* (7), 768–776. <https://doi.org/10.1038/ng.3590>.
- (84) LeBlanc, V. G.; Trinh, D. L.; Aslanpour, S.; Hughes, M.; Livingstone, D.; Jin, D.; Ahn, B. Y.; Blough, M. D.; Cairncross, J. G.; Chan, J. A.; Kelly, J. J. P.; Marra, M. A. Single-Cell Landscapes of Primary Glioblastomas and Matched Explants and Cell Lines Show Variable Retention of Inter- and Intratumor Heterogeneity. *Cancer Cell* **2022**, *40* (4), 379–392.e9. <https://doi.org/10.1016/j.ccell.2022.02.016>.

- (85) Nigro, J. M.; Baker, S. J.; Preisinger, A. C.; Jessup, J. M.; Hostetter, R.; Cleary, K.; Bigner, S. H.; Davidson, N.; Baylin, S.; Devilee, P. Mutations in the P53 Gene Occur in Diverse Human Tumour Types. *Nature* **1989**, *342* (6250), 705–708. <https://doi.org/10.1038/342705a0>.
- (86) Wong, A. J.; Bigner, S. H.; Bigner, D. D.; Kinzler, K. W.; Hamilton, S. R.; Vogelstein, B. Increased Expression of the Epidermal Growth Factor Receptor Gene in Malignant Gliomas Is Invariably Associated with Gene Amplification. *Proc Natl Acad Sci U S A* **1987**, *84* (19), 6899–6903. <https://doi.org/10.1073/pnas.84.19.6899>.
- (87) Hernández Borrero, L. J.; El-Deiry, W. S. Tumor Suppressor P53: Biology, Signaling Pathways, and Therapeutic Targeting. *Biochimica et Biophysica Acta (BBA) - Reviews on Cancer* **2021**, *1876* (1), 188556. <https://doi.org/10.1016/j.bbcan.2021.188556>.
- (88) Furnari, F. B.; Fenton, T.; Bachoo, R. M.; Mukasa, A.; Stommel, J. M.; Stegh, A.; Hahn, W. C.; Ligon, K. L.; Louis, D. N.; Brennan, C.; Chin, L.; DePinho, R. A.; Cavenee, W. K. Malignant Astrocytic Glioma: Genetics, Biology, and Paths to Treatment. *Genes Dev* **2007**, *21* (21), 2683–2710. <https://doi.org/10.1101/gad.1596707>.
- (89) AACR Project GENIE Consortium. AACR Project GENIE: Powering Precision Medicine through an International Consortium. *Cancer Discov* **2017**, *7* (8), 818–831. <https://doi.org/10.1158/2159-8290.CD-17-0151>.
- (90) Goranci-Buzhala, G.; Mariappan, A.; Ricci-Vitiani, L.; Josipovic, N.; Pacioni, S.; Gottardo, M.; Ptok, J.; Schaal, H.; Callaini, G.; Rajalingam, K.; Dynlacht, B.; Hadian, K.; Papantonis, A.; Pallini, R.; Gopalakrishnan, J. Cilium Induction Triggers Differentiation of Glioma Stem Cells. *Cell Rep* **2021**, *36* (10), 109656. <https://doi.org/10.1016/j.celrep.2021.109656>.
- (91) Mallm, J.-P.; Windisch, P.; Biran, A.; Gal, Z.; Schumacher, S.; Glass, R.; Herold-Mende, C.; Meshorer, E.; Barbus, M.; Rippe, K. Glioblastoma Initiating Cells Are Sensitive to Histone Demethylase Inhibition Due to Epigenetic Dereglulation. *Int J Cancer* **2020**, *146* (5), 1281–1292. <https://doi.org/10.1002/ijc.32649>.
- (92) Global Burden of Disease Cancer Collaboration; Fitzmaurice, C.; Allen, C.; Barber, R. M.; Barregard, L.; Bhutta, Z. A.; Brenner, H.; Dicker, D. J.; Chimed-Orchir, O.; Dandona, R.; Dandona, L.; Fleming, T.; Forouzanfar, M. H.; Hancock, J.; Hay, R. J.; Hunter-Merrill, R.; Huynh, C.; Hosgood, H. D.; Johnson, C. O.; Jonas, J. B.; Khubchandani, J.; Kumar, G. A.; Kutz, M.; Lan, Q.; Larson, H. J.; Liang, X.; Lim, S. S.; Lopez, A. D.; MacIntyre, M. F.; Marczak, L.; Marquez, N.; Mokdad, A. H.; Pinho, C.; Pourmalek, F.; Salomon, J. A.; Sanabria, J. R.; Sandar, L.; Sartorius, B.; Schwartz, S. M.; Shackelford, K. A.; Shibuya, K.; Stanaway, J.; Steiner, C.; Sun, J.; Takahashi, K.; Vollset, S. E.; Vos, T.; Wagner, J. A.; Wang, H.; Westerman, R.; Zeeb, H.; Zoeckler, L.; Abd-Allah, F.; Ahmed, M. B.; Alabed, S.; Alam, N. K.; Aldhahri, S. F.; Alem, G.; Alemayohu, M. A.; Ali, R.; Al-Raddadi, R.; Amare, A.; Amoako, Y.; Artaman, A.; Asayesh, H.; Atnafu, N.; Awasthi, A.; Saleem, H. B.; Barac, A.; Bedi, N.; Bensenor, I.; Berhane, A.; Bernabé, E.; Betsu, B.; Binagwaho, A.; Boneya, D.; Campos-Nonato, I.; Castañeda-Orjuela, C.; Catalá-López, F.; Chiang, P.; Chibueze, C.; Chitheer, A.; Choi, J.-Y.; Cowie, B.; Damtew, S.; das Neves, J.; Dey, S.; Dharmaratne, S.; Dhillon, P.; Ding, E.; Driscoll, T.; Ekwueme, D.; Endries, A. Y.; Farvid, M.;

- Farzadfar, F.; Fernandes, J.; Fischer, F.; G/Hiwot, T. T.; Gebru, A.; Gopalani, S.; Hailu, A.; Horino, M.; Horita, N.; Husseini, A.; Huybrechts, I.; Inoue, M.; Islami, F.; Jakovljevic, M.; James, S.; Javanbakht, M.; Jee, S. H.; Kasaeian, A.; Kadir, M. S.; Khader, Y. S.; Khang, Y.-H.; Kim, D.; Leigh, J.; Linn, S.; Lunevicius, R.; El Razek, H. M. A.; Malekzadeh, R.; Malta, D. C.; Marcenes, W.; Markos, D.; Melaku, Y. A.; Meles, K. G.; Mendoza, W.; Mengiste, D. T.; Meretoja, T. J.; Miller, T. R.; Mohammad, K. A.; Mohammadi, A.; Mohammed, S.; Moradi-Lakeh, M.; Nagel, G.; Nand, D.; Le Nguyen, Q.; Nolte, S.; Ogbo, F. A.; Oladimeji, K. E.; Oren, E.; Pa, M.; Park, E.-K.; Pereira, D. M.; Plass, D.; Qorbani, M.; Radfar, A.; Rafay, A.; Rahman, M.; Rana, S. M.; Søreide, K.; Satpathy, M.; Sawhney, M.; Sepanlou, S. G.; Shaikh, M. A.; She, J.; Shiue, I.; Shore, H. R.; Shrim, M. G.; So, S.; Soneji, S.; Stathopoulou, V.; Stroumpoulis, K.; Sufiyan, M. B.; Sykes, B. L.; Tabarés-Seisdedos, R.; Tadese, F.; Tedla, B. A.; Tessema, G. A.; Thakur, J. S.; Tran, B. X.; Ukwaja, K. N.; Uzochukwu, B. S. C.; Vlassov, V. V.; Weiderpass, E.; Wubshet Terefe, M.; Yebyo, H. G.; Yimam, H. H.; Yonemoto, N.; Younis, M. Z.; Yu, C.; Zaidi, Z.; Zaki, M. E. S.; Zenebe, Z. M.; Murray, C. J. L.; Naghavi, M. Global, Regional, and National Cancer Incidence, Mortality, Years of Life Lost, Years Lived With Disability, and Disability-Adjusted Life-Years for 32 Cancer Groups, 1990 to 2015: A Systematic Analysis for the Global Burden of Disease Study. *JAMA Oncol* **2017**, *3* (4), 524–548. <https://doi.org/10.1001/jamaoncol.2016.5688>.
- (93) Prossomariti, A.; Piazz, G.; Alquati, C.; Ricciardiello, L. Are Wnt/ $\beta$ -Catenin and PI3K/AKT/MTORC1 Distinct Pathways in Colorectal Cancer? *Cell Mol Gastroenterol Hepatol* **2020**, *10* (3), 491–506. <https://doi.org/10.1016/j.jcmgh.2020.04.007>.
- (94) Naeem, A.; Tun, A. M.; Guevara, E. Molecular Genetics and the Role of Molecularly Targeted Agents in Metastatic Colorectal Carcinoma. *J Gastrointest Cancer* **2020**, *51* (2), 387–400. <https://doi.org/10.1007/s12029-019-00272-3>.
- (95) Jung, G.; Hernández-Illán, E.; Moreira, L.; Balaguer, F.; Goel, A. Epigenetics of Colorectal Cancer: Biomarker and Therapeutic Potential. *Nat Rev Gastroenterol Hepatol* **2020**, *17* (2), 111–130. <https://doi.org/10.1038/s41575-019-0230-y>.
- (96) Boland, C. R.; Goel, A. Microsatellite Instability in Colorectal Cancer. *Gastroenterology* **2010**, *138* (6), 2073–2087.e3. <https://doi.org/10.1053/j.gastro.2009.12.064>.
- (97) Elshazli, R. M.; Toraih, E. A.; Elgaml, A.; Kandil, E.; Fawzy, M. S. Genetic Polymorphisms of TP53 (Rs1042522) and MDM2 (Rs2279744) and Colorectal Cancer Risk: An Updated Meta-Analysis Based on 59 Case-Control Studies. *Gene* **2020**, *734*, 144391. <https://doi.org/10.1016/j.gene.2020.144391>.
- (98) Overman, M. J.; McDermott, R.; Leach, J. L.; Lonardi, S.; Lenz, H.-J.; Morse, M. A.; Desai, J.; Hill, A.; Axelson, M.; Moss, R. A.; Goldberg, M. V.; Cao, Z. A.; Ledine, J.-M.; Maglinte, G. A.; Kopetz, S.; André, T. Nivolumab in Patients with Metastatic DNA Mismatch Repair-Deficient or Microsatellite Instability-High Colorectal Cancer (CheckMate 142): An Open-Label, Multicentre, Phase 2 Study. *Lancet Oncol* **2017**, *18* (9), 1182–1191. [https://doi.org/10.1016/S1470-2045\(17\)30422-9](https://doi.org/10.1016/S1470-2045(17)30422-9).
- (99) Le, D. T.; Durham, J. N.; Smith, K. N.; Wang, H.; Bartlett, B. R.; Aulakh, L. K.; Lu, S.; Kemberling,



- H.; Wilt, C.; Lubner, B. S.; Wong, F.; Azad, N. S.; Rucki, A. A.; Laheru, D.; Donehower, R.; Zaheer, A.; Fisher, G. A.; Crocenzi, T. S.; Lee, J. J.; Greten, T. F.; Duffy, A. G.; Ciombor, K. K.; Eyring, A. D.; Lam, B. H.; Joe, A.; Kang, S. P.; Holdhoff, M.; Danilova, L.; Cope, L.; Meyer, C.; Zhou, S.; Goldberg, R. M.; Armstrong, D. K.; Bever, K. M.; Fader, A. N.; Taube, J.; Housseau, F.; Spetzler, D.; Xiao, N.; Pardoll, D. M.; Papadopoulos, N.; Kinzler, K. W.; Eshleman, J. R.; Vogelstein, B.; Anders, R. A.; Diaz, L. A. Mismatch Repair Deficiency Predicts Response of Solid Tumors to PD-1 Blockade. *Science* **2017**, *357* (6349), 409–413. <https://doi.org/10.1126/science.aan6733>.
- (100) Dudley, J. C.; Lin, M.-T.; Le, D. T.; Eshleman, J. R. Microsatellite Instability as a Biomarker for PD-1 Blockade. *Clin Cancer Res* **2016**, *22* (4), 813–820. <https://doi.org/10.1158/1078-0432.CCR-15-1678>.
- (101) Fabrizio, D. A.; George, T. J.; Dunne, R. F.; Frampton, G.; Sun, J.; Gowen, K.; Kennedy, M.; Greenbowe, J.; Schrock, A. B.; Hezel, A. F.; Ross, J. S.; Stephens, P. J.; Ali, S. M.; Miller, V. A.; Fakih, M.; Klemperer, S. J. Beyond Microsatellite Testing: Assessment of Tumor Mutational Burden Identifies Subsets of Colorectal Cancer Who May Respond to Immune Checkpoint Inhibition. *J Gastrointest Oncol* **2018**, *9* (4), 610–617. <https://doi.org/10.21037/jgo.2018.05.06>.
- (102) Kong, J. C.; Guerra, G. R.; Pham, T.; Mitchell, C.; Lynch, A. C.; Warriar, S. K.; Ramsay, R. G.; Heriot, A. G. Prognostic Impact of Tumor-Infiltrating Lymphocytes in Primary and Metastatic Colorectal Cancer: A Systematic Review and Meta-Analysis. *Dis Colon Rectum* **2019**, *62* (4), 498–508. <https://doi.org/10.1097/DCR.0000000000001332>.
- (103) Havel, J. J.; Chowell, D.; Chan, T. A. The Evolving Landscape of Biomarkers for Checkpoint Inhibitor Immunotherapy. *Nat Rev Cancer* **2019**, *19* (3), 133–150. <https://doi.org/10.1038/s41568-019-0116-x>.
- (104) Samstein, R. M.; Lee, C.-H.; Shoushtari, A. N.; Hellmann, M. D.; Shen, R.; Janjigian, Y. Y.; Barron, D. A.; Zehir, A.; Jordan, E. J.; Omuro, A.; Kaley, T. J.; Kendall, S. M.; Motzer, R. J.; Hakimi, A. A.; Voss, M. H.; Russo, P.; Rosenberg, J.; Iyer, G.; Bochner, B. H.; Bajorin, D. F.; Al-Ahmadie, H. A.; Chaft, J. E.; Rudin, C. M.; Riely, G. J.; Baxi, S.; Ho, A. L.; Wong, R. J.; Pfister, D. G.; Wolchok, J. D.; Barker, C. A.; Gutin, P. H.; Brennan, C. W.; Tabar, V.; Mellinghoff, I. K.; DeAngelis, L. M.; Ariyan, C. E.; Lee, N.; Tap, W. D.; Gounder, M. M.; D'Angelo, S. P.; Saltz, L.; Stadler, Z. K.; Scher, H. I.; Baselga, J.; Razavi, P.; Klebanoff, C. A.; Yaeger, R.; Segal, N. H.; Ku, G. Y.; DeMatteo, R. P.; Ladanyi, M.; Rizvi, N. A.; Berger, M. F.; Riaz, N.; Solit, D. B.; Chan, T. A.; Morris, L. G. Tumor Mutational Load Predicts Survival after Immunotherapy across Multiple Cancer Types. *Nat Genet* **2019**, *51* (2), 202–206. <https://doi.org/10.1038/s41588-018-0312-8>.
- (105) Domingo, E.; Freeman-Mills, L.; Rayner, E.; Glaire, M.; Briggs, S.; Vermeulen, L.; Fessler, E.; Medema, J. P.; Boot, A.; Morreau, H.; van Wezel, T.; Liefers, G.-J.; Lothe, R. A.; Danielsen, S. A.; Sveen, A.; Nesbakken, A.; Zlobec, I.; Lugli, A.; Koelzer, V. H.; Berger, M. D.; Castellví-Bel, S.; Muñoz, J.; Epicolon consortium; de Bruyn, M.; Nijman, H. W.; Novelli, M.; Lawson, K.; Ouakrif, D.; Frangou, E.; Dutton, P.; Tejpar, S.; Delorenzi, M.; Kerr, R.; Kerr, D.; Tomlinson, I.; Church, D. N. Somatic POLE Proofreading Domain Mutation, Immune Response, and Prognosis in

- Colorectal Cancer: A Retrospective, Pooled Biomarker Study. *Lancet Gastroenterol Hepatol* **2016**, *1* (3), 207–216. [https://doi.org/10.1016/S2468-1253\(16\)30014-0](https://doi.org/10.1016/S2468-1253(16)30014-0).
- (106) Auman, J. T.; McLeod, H. L. Colorectal Cancer Cell Lines Lack the Molecular Heterogeneity of Clinical Colorectal Tumors. *Clin Colorectal Cancer* **2010**, *9* (1), 40–47. <https://doi.org/10.3816/CCC.2010.n.005>.
- (107) Kapałczyńska, M.; Kolenda, T.; Przybyła, W.; Zajączkowska, M.; Teresiak, A.; Filas, V.; Ibbs, M.; Bliźniak, R.; Łuczewski, Ł.; Lamperska, K. 2D and 3D Cell Cultures - a Comparison of Different Types of Cancer Cell Cultures. *Arch Med Sci* **2018**, *14* (4), 910–919. <https://doi.org/10.5114/aoms.2016.63743>.
- (108) Wong, C. H.; Siah, K. W.; Lo, A. W. Estimation of Clinical Trial Success Rates and Related Parameters. *Biostatistics* **2019**, *20* (2), 273–286. <https://doi.org/10.1093/biostatistics/kxx069>.
- (109) Mak, I. W.; Evaniew, N.; Ghert, M. Lost in Translation: Animal Models and Clinical Trials in Cancer Treatment. *Am J Transl Res* **2014**, *6* (2), 114–118.
- (110) Bhimani, J.; Ball, K.; Stebbing, J. Patient-Derived Xenograft Models-the Future of Personalised Cancer Treatment. *Br J Cancer* **2020**, *122* (5), 601–602. <https://doi.org/10.1038/s41416-019-0678-0>.
- (111) van de Wetering, M.; Francies, H. E.; Francis, J. M.; Bounova, G.; Iorio, F.; Pronk, A.; van Houdt, W.; van Gorp, J.; Taylor-Weiner, A.; Kester, L.; McLaren-Douglas, A.; Blokker, J.; Jaksani, S.; Bartfeld, S.; Volckman, R.; van Sluis, P.; Li, V. S. W.; Seepo, S.; Sekhar Pedomallu, C.; Cibulskis, K.; Carter, S. L.; McKenna, A.; Lawrence, M. S.; Lichtenstein, L.; Stewart, C.; Koster, J.; Versteeg, R.; van Oudenaarden, A.; Saez-Rodriguez, J.; Vries, R. G. J.; Getz, G.; Wessels, L.; Stratton, M. R.; McDermott, U.; Meyerson, M.; Garnett, M. J.; Clevers, H. Prospective Derivation of a Living Organoid Biobank of Colorectal Cancer Patients. *Cell* **2015**, *161* (4), 933–945. <https://doi.org/10.1016/j.cell.2015.03.053>.
- (112) Weeber, F.; van de Wetering, M.; Hoogstraat, M.; Dijkstra, K. K.; Krijgsman, O.; Kuilman, T.; Gadellaa-van Hooijdonk, C. G. M.; van der Velden, D. L.; Peeper, D. S.; Cuppen, E. P. J. G.; Vries, R. G.; Clevers, H.; Voest, E. E. Preserved Genetic Diversity in Organoids Cultured from Biopsies of Human Colorectal Cancer Metastases. *Proc Natl Acad Sci U S A* **2015**, *112* (43), 13308–13311. <https://doi.org/10.1073/pnas.1516689112>.
- (113) Kondo, J.; Ekawa, T.; Endo, H.; Yamazaki, K.; Tanaka, N.; Kukita, Y.; Okuyama, H.; Okami, J.; Imamura, F.; Ohue, M.; Kato, K.; Nomura, T.; Kohara, A.; Mori, S.; Dan, S.; Inoue, M. High-Throughput Screening in Colorectal Cancer Tissue-Originated Spheroids. *Cancer Sci* **2019**, *110* (1), 345–355. <https://doi.org/10.1111/cas.13843>.
- (114) Vlachogiannis, G.; Hedayat, S.; Vatsiou, A.; Jamin, Y.; Fernández-Mateos, J.; Khan, K.; Lampis, A.; Eason, K.; Huntingford, I.; Burke, R.; Rata, M.; Koh, D.-M.; Tunariu, N.; Collins, D.; Hulkki-Wilson, S.; Ragulan, C.; Spiteri, I.; Moorcraft, S. Y.; Chau, I.; Rao, S.; Watkins, D.; Fotiadis, N.; Bali, M.; Darvish-Damavandi, M.; Lote, H.; Eltahir, Z.; Smyth, E. C.; Begum, R.; Clarke, P. A.; Hahne, J. C.; Dowsett, M.; de Bono, J.; Workman, P.; Sadanandam, A.; Fassan, M.; Sansom, O. J.; Eccles, S.; Starling, N.; Braconi, C.; Sottoriva, A.; Robinson, S. P.; Cunningham, D.; Valeri, N.



- Patient-Derived Organoids Model Treatment Response of Metastatic Gastrointestinal Cancers. *Science* **2018**, 359 (6378), 920–926. <https://doi.org/10.1126/science.aao2774>.
- (115) Ooft, S. N.; Weeber, F.; Dijkstra, K. K.; McLean, C. M.; Kaing, S.; van Werkhoven, E.; Schipper, L.; Hoes, L.; Vis, D. J.; van de Haar, J.; Prevoo, W.; Snaebjornsson, P.; van der Velden, D.; Klein, M.; Chalabi, M.; Boot, H.; van Leerdam, M.; Bloemendal, H. J.; Beerepoot, L. V.; Wessels, L.; Cuppen, E.; Clevers, H.; Voest, E. E. Patient-Derived Organoids Can Predict Response to Chemotherapy in Metastatic Colorectal Cancer Patients. *Sci Transl Med* **2019**, 11 (513), eaay2574. <https://doi.org/10.1126/scitranslmed.aay2574>.
- (116) Klempner, S. J.; Fabrizio, D.; Bane, S.; Reinhart, M.; Peoples, T.; Ali, S. M.; Sokol, E. S.; Frampton, G.; Schrock, A. B.; Anhorn, R.; Reddy, P. Tumor Mutational Burden as a Predictive Biomarker for Response to Immune Checkpoint Inhibitors: A Review of Current Evidence. *Oncologist* **2020**, 25 (1), e147–e159. <https://doi.org/10.1634/theoncologist.2019-0244>.
- (117) Chae, Y. K.; Anker, J. F.; Carneiro, B. A.; Chandra, S.; Kaplan, J.; Kalyan, A.; Santa-Maria, C. A.; Plataniias, L. C.; Giles, F. J. Genomic Landscape of DNA Repair Genes in Cancer. *Oncotarget* **2016**, 7 (17), 23312–23321. <https://doi.org/10.18632/oncotarget.8196>.
- (118) Gargiulo, P.; Della Pepa, C.; Berardi, S.; Califano, D.; Scala, S.; Buonaguro, L.; Ciliberto, G.; Brauchli, P.; Pignata, S. Tumor Genotype and Immune Microenvironment in POLE-Ultramutated and MSI-Hypermethylated Endometrial Cancers: New Candidates for Checkpoint Blockade Immunotherapy? *Cancer Treat Rev* **2016**, 48, 61–68. <https://doi.org/10.1016/j.ctrv.2016.06.008>.
- (119) Stadler, Z. K.; Battaglin, F.; Middha, S.; Hechtman, J. F.; Tran, C.; Cercek, A.; Yaeger, R.; Segal, N. H.; Varghese, A. M.; Reidy-Lagunes, D. L.; Kemeny, N. E.; Salo-Mullen, E. E.; Ashraf, A.; Weiser, M. R.; Garcia-Aguilar, J.; Robson, M. E.; Offit, K.; Arcila, M. E.; Berger, M. F.; Shia, J.; Solit, D. B.; Saltz, L. B. Reliable Detection of Mismatch Repair Deficiency in Colorectal Cancers Using Mutational Load in Next-Generation Sequencing Panels. *J Clin Oncol* **2016**, 34 (18), 2141–2147. <https://doi.org/10.1200/JCO.2015.65.1067>.
- (120) Budinska, E.; Popovici, V.; Tejpar, S.; D'Ario, G.; Lapique, N.; Sikora, K. O.; Di Narzo, A. F.; Yan, P.; Hodgson, J. G.; Weinrich, S.; Bosman, F.; Roth, A.; Delorenzi, M. Gene Expression Patterns Unveil a New Level of Molecular Heterogeneity in Colorectal Cancer. *J Pathol* **2013**, 231 (1), 63–76. <https://doi.org/10.1002/path.4212>.
- (121) Marisa, L.; de Reyniès, A.; Duval, A.; Selves, J.; Gaub, M. P.; Vescovo, L.; Etienne-Grimaldi, M.-C.; Schiappa, R.; Guenot, D.; Ayadi, M.; Kirzin, S.; Chazal, M.; Fléjou, J.-F.; Benchimol, D.; Berger, A.; Lagarde, A.; Pencreach, E.; Piard, F.; Elias, D.; Parc, Y.; Olschwang, S.; Milano, G.; Laurent-Puig, P.; Boige, V. Gene Expression Classification of Colon Cancer into Molecular Subtypes: Characterization, Validation, and Prognostic Value. *PLoS Med* **2013**, 10 (5), e1001453. <https://doi.org/10.1371/journal.pmed.1001453>.
- (122) Sadanandam, A.; Lyssiotis, C. A.; Homicsko, K.; Collisson, E. A.; Gibb, W. J.; Wullschlegel, S.; Ostos, L. C. G.; Lannon, W. A.; Grotzinger, C.; Del Rio, M.; Lhermitte, B.; Olshen, A. B.; Wiedenmann, B.; Cantley, L. C.; Gray, J. W.; Hanahan, D. A Colorectal Cancer Classification

- System That Associates Cellular Phenotype and Responses to Therapy. *Nat Med* **2013**, *19* (5), 619–625. <https://doi.org/10.1038/nm.3175>.
- (123) De Sousa E Melo, F.; Wang, X.; Jansen, M.; Fessler, E.; Trinh, A.; de Rooij, L. P. M. H.; de Jong, J. H.; de Boer, O. J.; van Leersum, R.; Bijlsma, M. F.; Rodermond, H.; van der Heijden, M.; van Noesel, C. J. M.; Tuynman, J. B.; Dekker, E.; Markowitz, F.; Medema, J. P.; Vermeulen, L. Poor-Prognosis Colon Cancer Is Defined by a Molecularly Distinct Subtype and Develops from Serrated Precursor Lesions. *Nat Med* **2013**, *19* (5), 614–618. <https://doi.org/10.1038/nm.3174>.
- (124) Roepman, P.; Schlicker, A.; Tabernero, J.; Majewski, I.; Tian, S.; Moreno, V.; Snel, M. H.; Chresta, C. M.; Rosenberg, R.; Nitsche, U.; Macarulla, T.; Capella, G.; Salazar, R.; Orphanides, G.; Wessels, L. F. A.; Bernards, R.; Simon, I. M. Colorectal Cancer Intrinsic Subtypes Predict Chemotherapy Benefit, Deficient Mismatch Repair and Epithelial-to-Mesenchymal Transition. *Int J Cancer* **2014**, *134* (3), 552–562. <https://doi.org/10.1002/ijc.28387>.
- (125) Schlicker, A.; Beran, G.; Chresta, C. M.; McWalter, G.; Pritchard, A.; Weston, S.; Runswick, S.; Davenport, S.; Heathcote, K.; Castro, D. A.; Orphanides, G.; French, T.; Wessels, L. F. A. Subtypes of Primary Colorectal Tumors Correlate with Response to Targeted Treatment in Colorectal Cell Lines. *BMC Med Genomics* **2012**, *5*, 66. <https://doi.org/10.1186/1755-8794-5-66>.
- (126) Eide, P. W.; Bruun, J.; Lothe, R. A.; Sveen, A. CMScaller: An R Package for Consensus Molecular Subtyping of Colorectal Cancer Pre-Clinical Models. *Sci Rep* **2017**, *7* (1), 16618. <https://doi.org/10.1038/s41598-017-16747-x>.
- (127) Masud, S. N.; Chandrashekar, M.; Aregger, M.; Tan, G.; Zhang, X.; Mero, P.; Pirman, D. A.; Zaslaver, O.; Smolen, G. A.; Lin, Z.-Y.; Wong, C. J.; Boone, C.; Gingras, A.-C.; Montenegro-Burke, J. R.; Moffat, J. Chemical Genomics with Pyrvinium Identifies C1orf115 as a Regulator of Drug Efflux. *Nat Chem Biol* **2022**, *18* (12), 1370–1379. <https://doi.org/10.1038/s41589-022-01109-0>.
- (128) Jiang, J.; Xu, Y.; Ren, H.; Wudu, M.; Wang, Q.; Song, X.; Su, H.; Jiang, X.; Jiang, L.; Qiu, X. MKRN2 Inhibits Migration and Invasion of Non-Small-Cell Lung Cancer by Negatively Regulating the PI3K/Akt Pathway. *J Exp Clin Cancer Res* **2018**, *37* (1), 189. <https://doi.org/10.1186/s13046-018-0855-7>.
- (129) Jia, C.; Tang, H.; Yang, Y.; Yuan, S.; Han, T.; Fang, M.; Huang, S.; Hu, R.; Li, C.; Geng, W. Ubiquitination of IGF2BP3 by E3 Ligase MKRN2 Regulates the Proliferation and Migration of Human Neuroblastoma SHSY5Y Cells. *Biochem Biophys Res Commun* **2020**, *529* (1), 43–50. <https://doi.org/10.1016/j.bbrc.2020.05.112>.
- (130) Schatoff, E. M.; Leach, B. I.; Dow, L. E. Wnt Signaling and Colorectal Cancer. *Curr Colorectal Cancer Rep* **2017**, *13* (2), 101–110. <https://doi.org/10.1007/s11888-017-0354-9>.
- (131) Po, A.; Citarella, A.; Catanzaro, G.; Besharat, Z. M.; Trocchianesi, S.; Gianno, F.; Sabato, C.; Moretti, M.; De Smaele, E.; Vacca, A.; Fiori, M. E.; Ferretti, E. Hedgehog-GLI Signalling Promotes Chemoresistance through the Regulation of ABC Transporters in Colorectal Cancer Cells. *Sci Rep* **2020**, *10* (1), 13988. <https://doi.org/10.1038/s41598-020-70871-9>.

- (132) Wang, Q.; Shi, Y.-L.; Zhou, K.; Wang, L.-L.; Yan, Z.-X.; Liu, Y.-L.; Xu, L.-L.; Zhao, S.-W.; Chu, H.-L.; Shi, T.-T.; Ma, Q.-H.; Bi, J. PIK3CA Mutations Confer Resistance to First-Line Chemotherapy in Colorectal Cancer. *Cell Death Dis* **2018**, *9* (7), 739. <https://doi.org/10.1038/s41419-018-0776-6>.

## Thanks to

박사과정과 학위논문을 마무리하면서 저의 논문이 잘 마무리 될 수 있게 많은 분들의 도움이 있었습니다. 이 글을 통해서 감사를 전하려합니다.

먼저, 권태준 지도교수님께 감사의 말씀을 드립니다. 바이오인포매틱스 전반적인 분야에서 넓고 깊은 이해를 갖고 계시고 열정적이고 성실하신 교수님을 만났기 때문에 제 박사졸업이 가능하지않았나 생각합니다. 학위과정동안 데이터를 다루는 인사이트와 논문작성 및 발표스킬들을 꼼꼼하게 지도해주셨고 제가 원하는 프로젝트를 할수있도록 배려해주시고 하고싶은 공부를 할 수 있도록 지지해주셨던 점들 감사함을 담아 이 지면에 표현하고자 합니다.

실험을 하다 인포매틱스 연구실에 뒤늦게 합류했는데 처음 해보는 코딩이나 개구리관리, 행정업무 등에서 어려움이 많았는데 잘 적응하고 지낼수있게 도와준 연구실 동생들 휘, 신혁, 구진, 경하, 성민이한테도 고마움을 표합니다. 꼼꼼한 편이 아니라 놓치고 넘어간게 많았을텐데 알게모르게 뒤에서 많이 도와준 동생들 덕분에 졸업까지 잘 마무리했다고 생각합니다. 그리고 매주 같이 밥먹는 시간을 가지면서 이런저런 연구아이디어도 공유하고 도움을 많이 주셨던 김병규 박사님 덕분에 대학원생활중에서도 폭넓은 사고를 할 수 있었습니다. 질량분석장비로 단백질데이터도 많이 만들어주셨고 관련분야로 진로를 결정하는데도 많은 도움을 주셔서 앞으로도 자주 뵙게 될 것 같습니다. 항상 감사드리고 저도 박사님께 앞으로 많은 도움드릴수있길 바랍니다.

토요일마다 모여서 스터디하고 놀러도 다녔던 우재, 혜진이, 승규도 기억에 많이 남는다. 졸업준비할때는 너무 바빠져서 많이 못보고 올라와버려서 아쉬운데 승규는 미국가서 졸업준비 잘하고 적응잘하길 바래. 오가노이드 프로젝트 같이 진행하면서 고생 많이 한 혜진이도 이제 혼자서 프로젝트 마무리지어야할텐데 혼자 두고 먼저 졸업해버려서 미안하고 고마워. 어려운 프로젝트였지만 같이 연구할 수 있어서 다행이고 고마운 시간이었던거같아. 우재도 IBS 에서 같이 보낸 시간은 짧지만 서로 잘 맞아서 친하게 지냈는데 즉흥적으로 행동할때마다 잔소리도 많이 하면서 잘 따라줘서 고맙고 멀리 떨어져있어도 계속 연락하며 잘 지내자. 유니스트와서 가장 오랫동안 자주 보고 많이 엮인 후배인 민우도 이사때마다 꼭 도와주러와주고 마지막에 리비전도 잘 마무리해줘서 이번학기 졸업 해내게 됐네. 다음학기 졸업 꼭 잘되길바라고 진로도 고민많을텐데 잘 결정하길바래. 이외에도 연구실은 떠났지만 계속 연락하고 졸업도 축하해준 윤범이, 남우, 상인이도 고마워 다들 학위 얼마안남았을텐데 잘 마무리했으면 좋겠다.

혜영이랑 태형이도 졸업하고 동탄으로 올라오고나서 다시 자주보게 돼서 고마운 사람들이야. 같이 울산에서 홈파티하고 여행다녔던 추억덕분에 대학원생활 잘 지냈던거같아. 앞으로도 계속 자주 봤으면 좋겠다. 계비가 이제 한 4~500 쌍인 경관, 지수, 명우, 숙, 태양, 지웅, 지율, 용환, 준호, 인솔, 효은, 현아, 세훈이 몇몇은 아직 울산이고 몇몇은 해외에 있지만 수도권에 있는 사람들끼리 조만간 대게먹으러 얼굴봅시다. 동기지만 먼저 졸업해서 회사애기도 많이해주고 조언도 해준 규민이랑 학위과정 걱정도 많이 해주고 지지도 많이해준 혜림이도 학부생때 같이 놀던 기억들이 많은데 이제 나도 올라왔으니 자주 보자. 전문연하는동안 제일 많이 같이 놀았던 민지랑 현진이, 찬호도 울산 떠난 지금도 여전히 연락해주고 그리워해줘서 너무 고맙고 앞으로 울산에 내가 간다면 너네보러가는 일뿐일거야. 특히 졸업남겨뒀을때 바쁜와중에도 1 일 1 민지할정도로 자주 봤는데 졸업하면서 선물로 윤영이랑 형준이 남겨두고왔는데 같이 잘지냈으면 좋겠다. 몸은 멀어졌지만 종종 시간내서 같이 놀자. 윤영이도 졸업막바지에 너무 늦게 친해져서 아쉽네. 얼른 졸업하고 올라와 그전에도 놀러오고 나도 많이 놀러가볼게. 이외에도 언급해야할 사람이 너무 많지만 자칫하면 논문보다 길어질거 같아서 줄이겠습니다. 항상 잘되라고 기도해주시는 우리 고모랑 할머니 누나한테 고맙고 마지막으로 항상 믿어주고 지지해주시고 키워주신 부모님 사랑하고 앞으로 효도 많이 하는 아들이 될게.